Discussion Of Momentum Theory For Windmills

UNIVERSITY OF MASSACHUSETTS/AMHERST

ENERGY ALTERNATIVES PROGRAM

DISCUSSION OF MOMENTUM THEORY FOR WINDMILLS

by

Forrest S. Stoddard

U.Mass. Wind Furnace
Energy Alternatives Program
University of Massachusetts
Amherst, Massachusetts 01002

TR/76/ 2
Appendix IV

DISCUSSION OF MOMENTUM THEORY FOR WINDMILLS

Momentum theory has been extensively used to predict the relative performance of lifting propellers and rotors.[1,2,3,4] The performance equations are analytically and conceptually simple; this leads to quick ideal predictions and comparisons. Often a physical "feeling" or understanding of the system can be gained by exercising this simple approach first, before more complex blade element and strip theories are used.

This discussion concerns the ramifications and interpretation of the momentum theory expressions for a thrusting windmill in the light of observed windmill behavior. It should be kept in mind that the (idealized) analytical formulation depends on the following strict assumptions:

a) definite streamlines exist in the flow field;

b) no frictional losses are present;

c) the induced velocity imparted to the free stream is constant over the area of the idealized rotor, or actuator.

The following well-known expressions are thus developed for the actuator shown:[4,5]

$$T = \text{thrust} = 2\rho\ A\ [V_o - v]v \qquad (1)$$

$$P = \text{power} = T(V_o - v) = 2\rho\ A\ [V_o - v]^2 v \qquad (2)$$

In non-dimensional form:

$$C_T = \begin{matrix}\text{thrust}\\ \text{coefficient}\end{matrix} = \frac{T}{1/2\rho A V_o^{\ 2}} \qquad (3)$$

$$C_P = \begin{matrix}\text{power}\\ \text{coefficient}\end{matrix} = \frac{P}{1/2\rho A V_o^{\ 3}} \qquad (4)$$

and

$$a = \begin{matrix}\text{axial}\\ \text{interference}\\ \text{factor}\end{matrix} = \frac{v}{V_o} \qquad \left(\begin{matrix}v \text{ positive in}\\ \text{the direction}\\ \text{shown}\end{matrix}\right)$$

The flow field for the normal windmill state is:

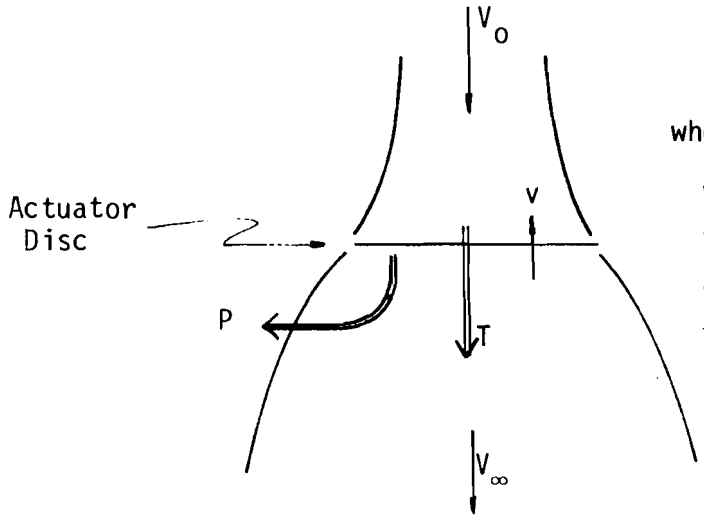

where:

V_o = free stream velocity
V_∞ = far wake velocity
v = induced velocity
T = thrust (down wind)
P = power (out of system)

FIGURE 1

This is also called the windmill brake state for rotors since the thrust is in the same direction as the free stream; thus, this state represents a rotor in autorotation or vertical descent. In windmill terminology, as shown above, thrust coefficient, C_T, and power coefficient, C_P, are positive, indicating thrust (or drag) in the downwind direction and power out of the system.

As shown by Wilson & Lissaman, Reference 1, there are two other important flow states determined by the value of induced velocity, v, written non-dimensionally as axial interference factor, $a = v/V_o$:

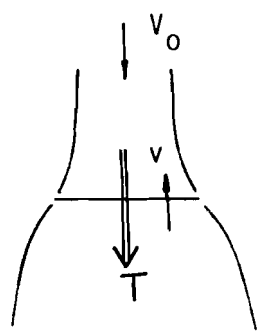	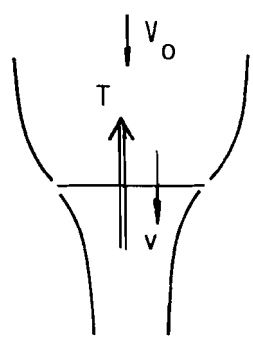	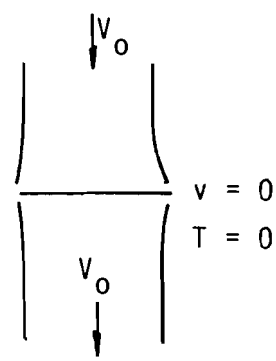
Normal Working State (Windmill Brake State)	Propeller State	Zero Slip Case
$0 \leq a \leq 0.5$	$a < 0$	$a = 0$
C_p, C_T positive	C_p, C_T negative	$C_p = C_T = 0$

FIGURE 2

For a = 1/2, the developed wake velocity is:

$$V_{\infty} = \begin{matrix}\text{far}\\ \text{wake}\\ \text{velocity}\end{matrix} = V_o(1 - 2a) = 0$$

This condition represents a point at which streamlines no longer exist. Hence, the momentum theory assumption has been violated, and this state cannot exist as a momentum theory solution.

Writing C_T and C_p in terms of a:

$$C_T = 4a\,|1-a|$$
$$C_p = 4a\,|1-a|\,(1-a) \qquad (5)$$

Wilson & Lissaman get the following plot (Reference 1):

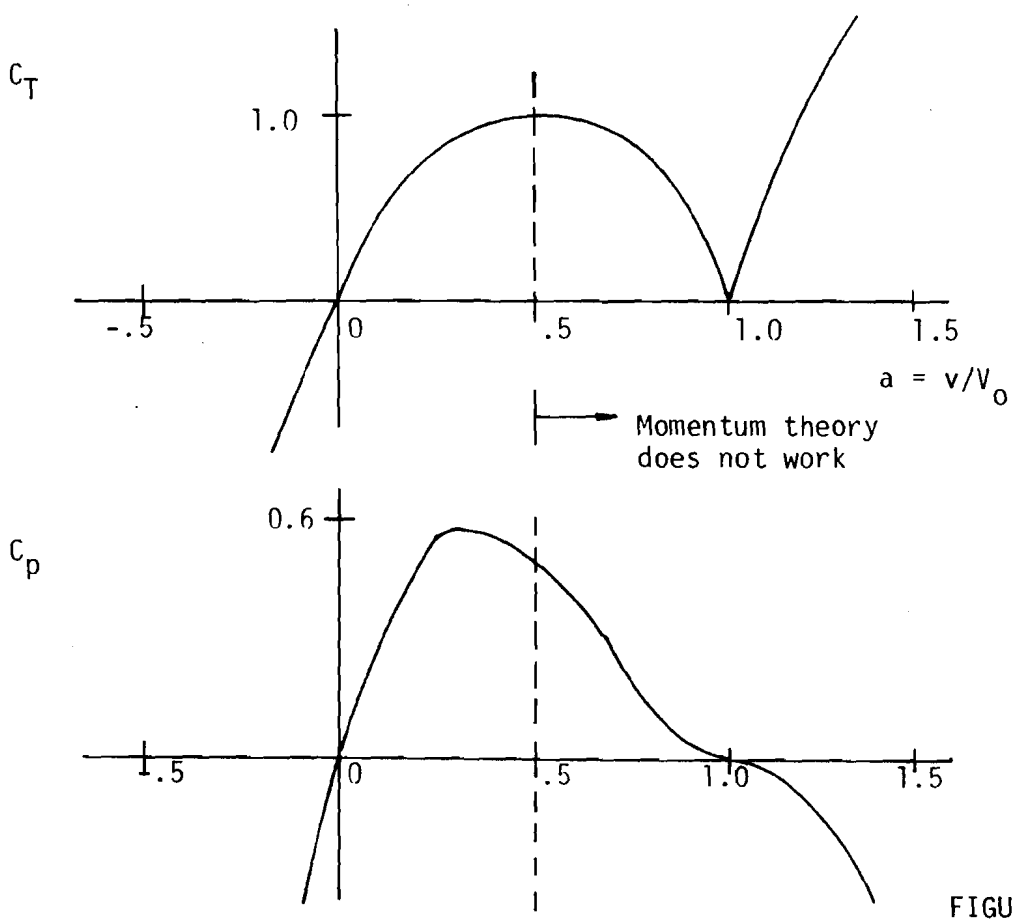

FIGURE 3

For a >1.0, the far wake velocity, V_∞, is still not defined by momentum theory; but this state can also be seen to be the propeller acting as a brake. That is, power is being added to the flow to create high C_T, or high thrust downwind. This would be the case of reversing propeller thrust on landing.

These flow states represent a series of gradual changes which occur on the rotor as induced velocity is changed uniformly. Unfortunately, because a definite slipstream does not exist for a $\geq$-1/2, momentum theory cannot be used to predict the rotor performance in this region. However, from helicopter autorotative data, empirical curves have been drawn, and the flow states have been documented.[2,6,7] Expanding the curve from the preceding page, the rotor behavior can be described in more detail:

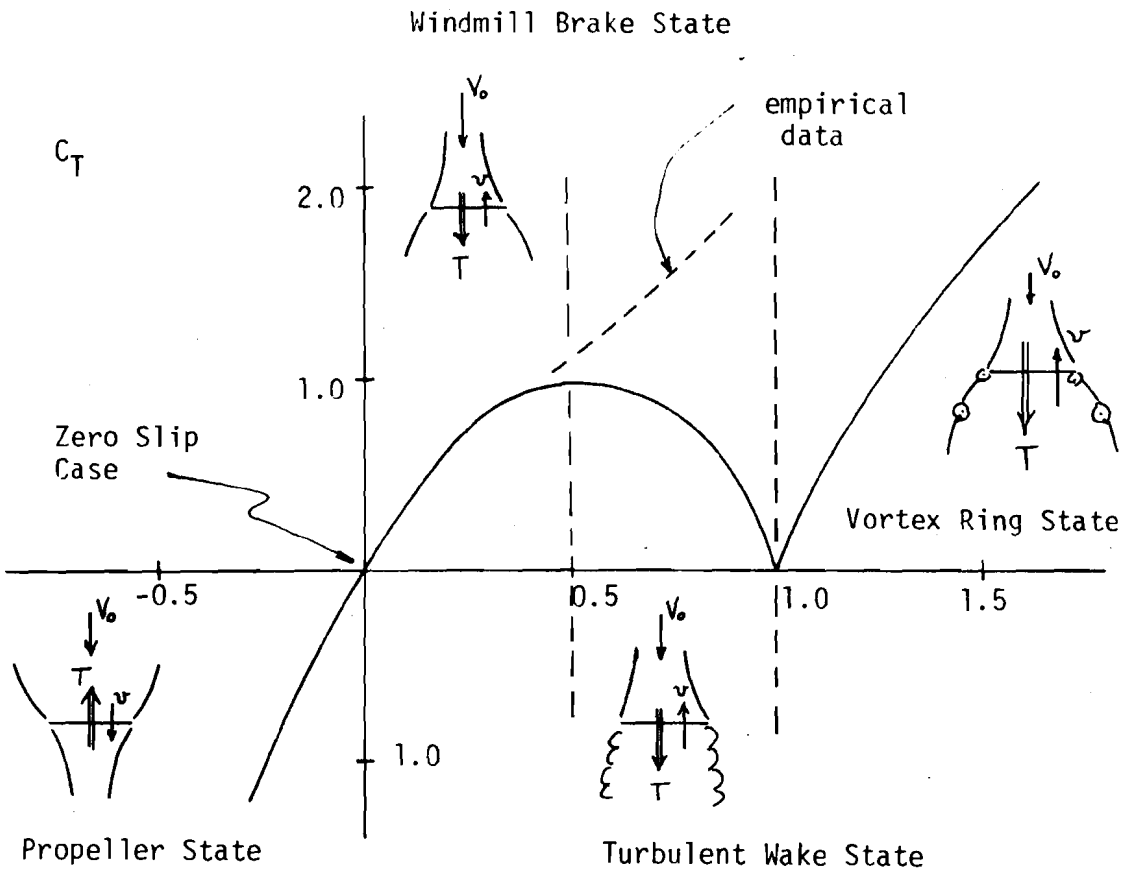

FIGURE 4

The empirical state boundaries are found from typical helicopter descent (autorotative) performance data plotted as follows. The abscissa is non-dimensional rate of climb, $\bar{V}_o$, and the ordinate is non-dimensional induced velocity, $\bar{v}$, as defined below:

with
$$\bar{v} = \frac{v}{\sqrt{T/2\rho A}} \quad ; \quad \bar{V}_o = \frac{V_o}{\sqrt{T/2\rho A}} \tag{6}$$

[Note: Here the sign of the free stream velocity, V_o, is opposite to that used for windmill theory]

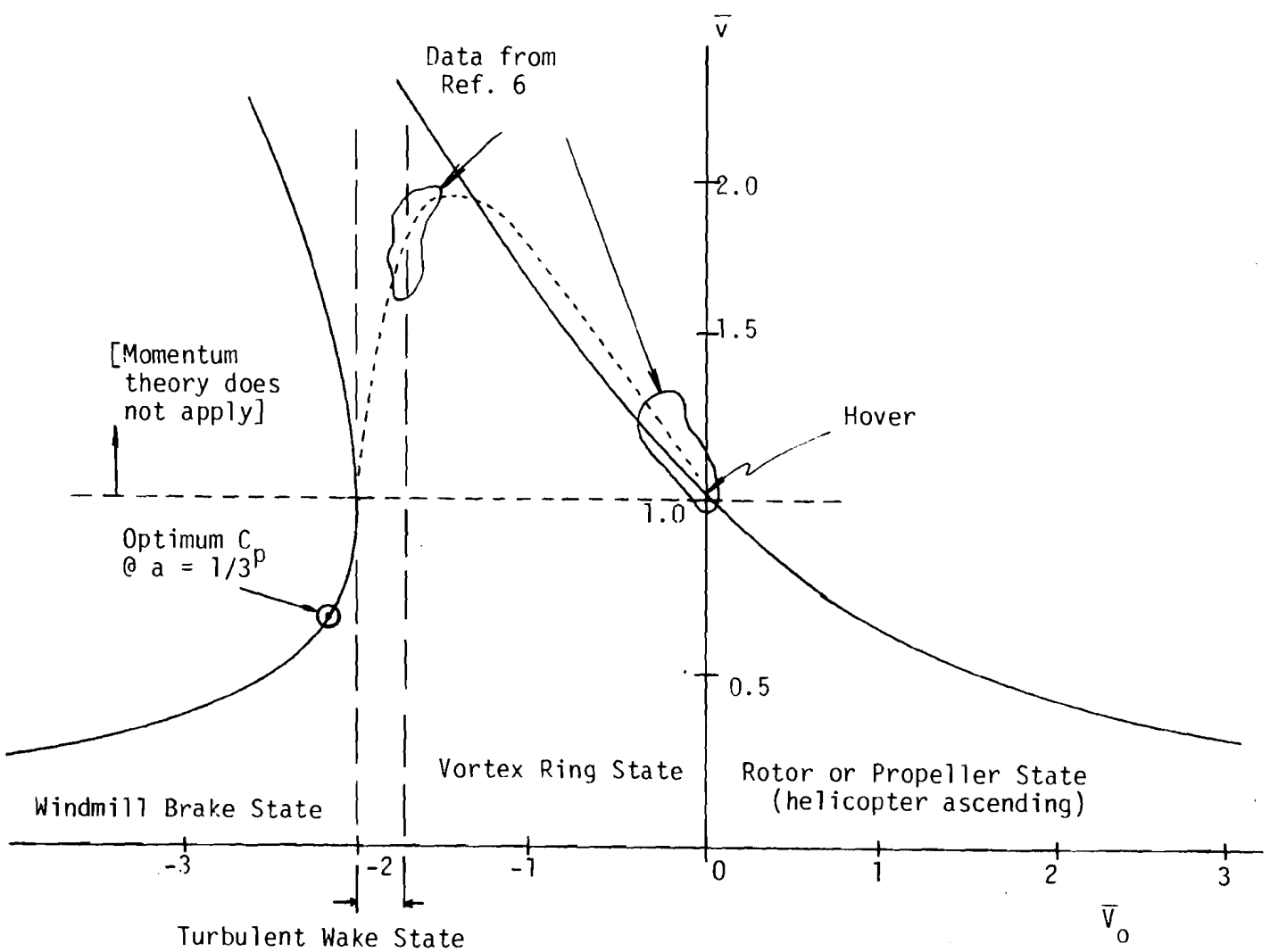

FIGURE 5

The momentum equations (shown here in solid lines) for the helicopter performance case are:[2,8]

Propeller or Rotor State: $\bar{V}_o = \frac{1}{\bar{v}} - \bar{v}$

Windmill Brake State: $V_o = -\frac{1}{\bar{v}} - \bar{v}$ (7)

It is also seen that any point on the curve represents a value of a:

$$a = \frac{v}{V_o} = \frac{\bar{v}}{\bar{V}_o}$$

Thus, the Turbulent Wake State limiting case occurs at:

$$\bar{v} = 1.0, \ (-)\bar{V}_o = 2.0, \ a = 1/2$$

And the Vortex Ring State:

$(-)\bar{V}_o \simeq 1.73$, $\bar{v} = 1.3$, $a \simeq .75$ (Ref. 7)

$\bar{v} = 1.75$, $a \simeq 1.0$ (Ref. 6)

The actual values of thrust cannot be found from Figure 5, since the original data were lost in the non-dimensionalizing process. However, the existing test data could be used to generate C_T and C_P vs v/V_o empirical plots to appear in Figure 4.

The test data referred to appear in two distinct groupings; one is at $\bar{V}_o = -1.75$ and the other is just below hover (just descending). The cluster around hover indicates the part-power descent of (rotary wing) flight vehicles; the left cluster is from free-wheeling rotors (i.e., $C_P = 0$ neglecting profile drag losses), and occurs at $\bar{v}/\bar{V}_o \simeq 1.0$. This verifies the momentum theory prediction that $C_P = 0$ at $v/V_o = 1.0$ (see Figure 3).

In the Turbulent Wake State, the slipstream expansion is very large, and considerable turbulence and recirculation exist (Reference 2). In fact, the rotor acts as a large disc perpendicular to the flow. Thus, the thrust coefficient is synonymous with the drag coefficient of a solid disc: $C_D \simeq 1.5 - 2.0$. As a result we would expect the C_T to go up sharply as $a = v/V_0$ (synonymous with porosity of the disc) increases. Hence, we would expect higher values of C_T than those predicted by momentum theory.

The Vortex Ring State boundary is not well established, but has been observed for a number of different NACA rotors (see Reference 6) and earlier tests (see Reference 7). This boundary also marks the change from positive to negative power; that is, the vortex ring state represents helicopter rotors in powered autorotation (for which significant test data exist) as well as reverse thrusting propellers (the same flow field). Momentum theory cannot be believed in the range, $1/2 < a \lesssim 1.0$, but the power equation (Equation 5) does predict the change in C_P (see Figure 3).

References

1. Wilson & Lissaman "Applied Aerodynamics of Wind Power Machines," Oregon State University, July 1974.

2. Gessow & Myers, Aerodynamics of the Helicopter, Frederick Ungar Publishing, 1952.

3. Prandtl & Tietjens, Applied Hydro & Aeromechanics, Dover Publications, 1934.

4. Glauert, Elements of Aerofoil & Airscrew Theory, Cambridge University Press, 1959.

5. Glauert, "Windmills and Fans," Aerodynamic Theory, Vol IV, Durand, ed., Dover Publications, 1963, pp. 324-332.

6. Gessow, "Flight Investigation of Effects of Rotor Blade Twist on Helicopter Performance in the High Speed and Vertical-Autorotative Decsent Conditions," NACA TN 1666, 1948.

7. Lock, Bateman, Townend, "An Extension of the Vortex Theory of Airscrews with Applications to Airscrews of Small Pitch and Including Experimental Results," British Aeronautical Research Comm. Reports & Memoranda, No. 1014, 1924.

8. Ham, "V/STOL Vehicle Aerodynamics and Dynamics," Course 16.50 class notes, MIT, 1963.

UNIVERSITY OF MASSACHUSETTS/AMHERST

ENERGY ALTERNATIVES PROGRAM

AN APPROACH TO PRELIMINARY SYSTEMS OPTIMIZATION OF THE NEW ENGLAND WIND FURNACE

by

Forrest S. Stoddard

U.Mass. Wind Furnace
Energy Alternatives Program
University of Massachusetts
Amherst, Massachusetts 01002

TR/76/3
Appendix V

AN APPROACH TO PRELIMINARY SYSTEMS OPTIMIZATION OF THE NEW ENGLAND WIND FURNACE

1. General Approach

The Wind Furnace system is represented in Figure 1. The diagram illustrates the three independent control variables: pitch (β_o), field excitation (P_{exc}), and load resistance (R_L). That is, for each set of input conditions ($V_o, \beta_o, P_{exc}, R_L$) there will be an output energy, $I_o^2 R_L$. The optimization task consists of finding the right combinations of these variables which yield the highest output for given wind speed, V_o. Later, the analysis can be refined to give dynamic and stability improvements given $V_o(t)$ (subject to the quasi-static assumptions used in deriving the analytical models for the propeller and generator). Transient behavior of the system may be attempted for certain equilibrium cases, as is done with stability derivatives for flight systems.

Preliminary, or "static," systems optimization uses analytic and/or semi-empirical performance characteristics of the two subsystems, and simply matches operating points to determine equilibrium conditions. Parametric torque-speed plots will be used in this analysis; hence the interpretation of "matching the characteristics," is to equate the output torque of the mechanical (windmill) shaft, to the input torque of the generator.

The parametric performance of the generator has been measured in laboratory tests[9] (Figure 2). For each point on this plot an output load current, I_o, will determine the output power, $I_o^2 R_L$. Work is continuing, to develop an analytical model for the generator and for other types of generators. It is understood that laboratory tests are important for the comprehension and verification of the general analytical theory.

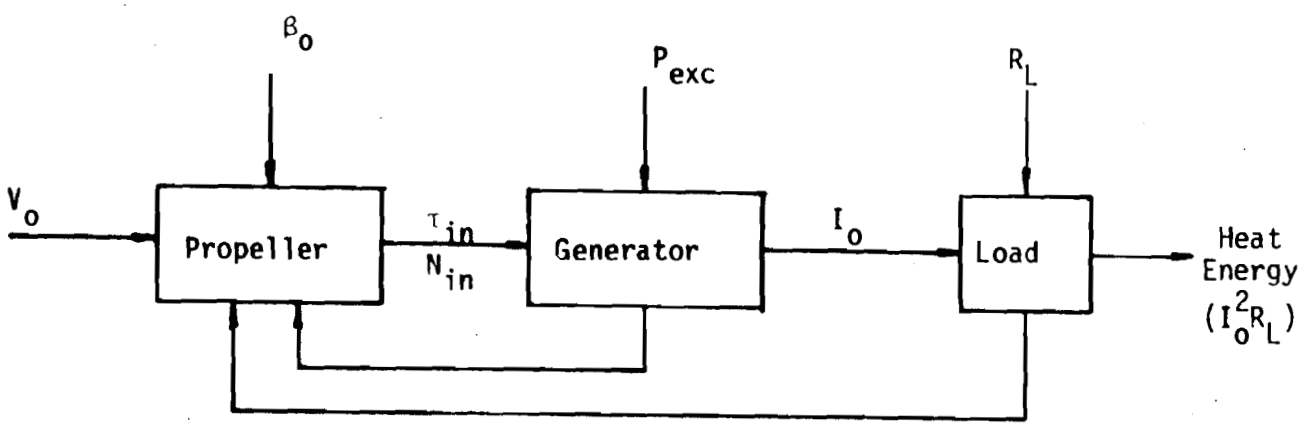

FIGURE 1

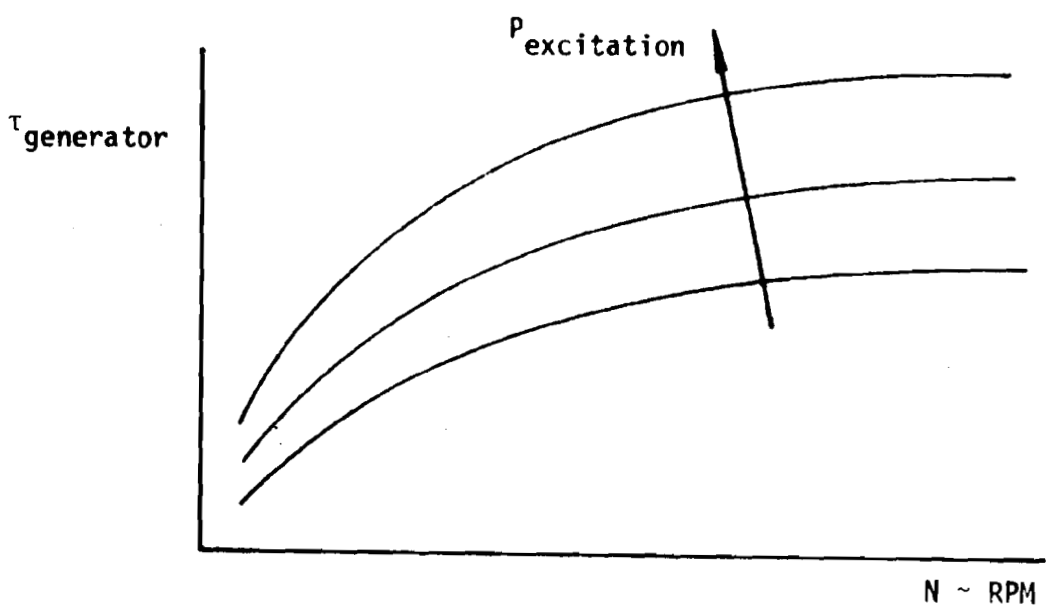

FIGURE 2

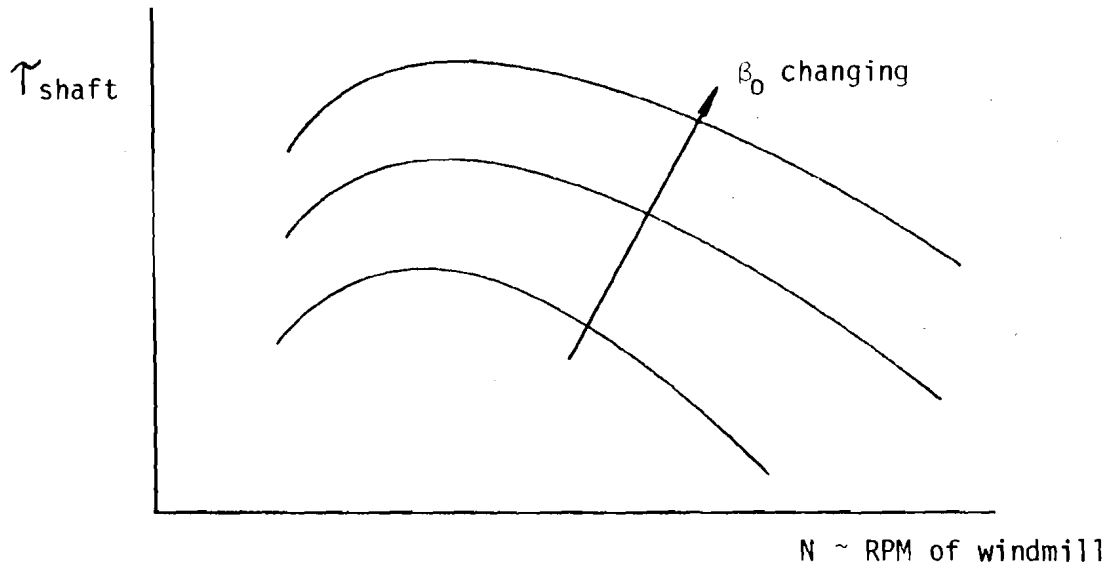

FIGURE 3

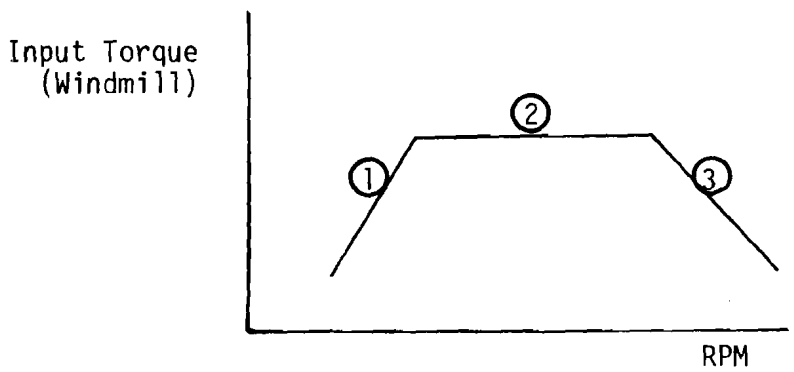

FIGURE 4

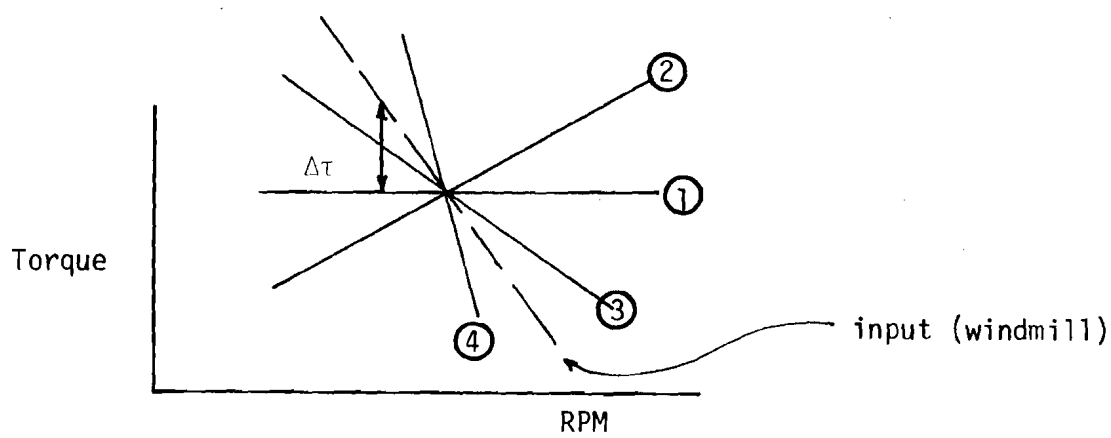

FIGURE 5

The task remaining is to derive a representation of the propeller torque/speed characteristic for various wind speeds (V_0) and pitch angles (β_0) (Figure 3). The characteristics can then be superposed, e.g. $\tau_{shaft} = \tau_{generator}$, and intersection points will determine the parametric operating points of the system. [Note that the shaft torque, τ_{shaft}, must include a penalty due to mechanical losses in the step up gearing and bearings, typically 25%.]

The system performance computation will establish output power (or energy) for various points along the intersection locus of these torque characteristics. This will yield the combination of variables which gives highest output; e.g. which combination of R_L, P_{exc}, and β_0 gives ($I_0^2 R_L$) maximum. These (quasi static) solutions are for equilibrium conditions and for constant wind speed. It is understood that dynamic factors such as gust amplitude and frequency may dictate other operating conditions than the "highest output" determined by this simple model.

II. Stability Considerations

The superimposed curves will give a qualitative indication of the first order "tightness" or sensitivity of the system to small perturbations from equilibrium. As an example consider the plot in Figure 4.

For this example assume the generator torque characteristic is flat (insensitive to RPM). If the operating equilibrium point (intersection with generator characteristic) occurs at ②, it can be seen that output will be insensitive to a wide variation in RPM. That is, the first order system is neutrally stable, and will establish equilibrium for any RPM setting in the flat range. At ①, as windmill RPM decreases (due to overloading or

gusts) the generator characteristic must be changed to keep from stalling the system; likewise, an increase in input RPM will cause the system to diverge. This condition is statically unstable. In region 3, the system is statically stable, since a perturbation in windmill RPM will cause an opposite change in excess torque. The slope of the characteristic is analogous to spring rate, and if other dynamic (higher order) influences are important, the slope will be analogous to the natural frequency of vibration in that mode.

Now reexamine the assumption of flat generator torque; consider Figure 5. We have established that condition 1 is stable; if input RPM decreases the torque increment $\Delta\tau$ is positive, and reaccelerates the system to equilibrium. It is evident that this torque increment also depends on the slope of the generator characteristic: viz., for line 2 the $\Delta\tau$ is larger and the system that much "tighter"; and for line 3 the $\Delta\tau$ has decreased to a small restorative quantity. Thus, for line 4, the system is statically unstable; i.e. the slope of the output characteristic is larger than the slope of the input characteristic.

III. Approach to Propeller Solution

The approach for solutions of the propeller problem is to develop power-speed and torque-speed characteristics using nondimensional quantities torque and power coefficients and tip speed ratio; this eliminates the dependence on V_0 or on RPM. The nondimensional plot can then be used to develop any desired cross-plot at any desired V_0 to be used in matching the system.

One of the existing computational results is a plot of the power coefficient maxima, for various tip speed ratios, for the machine, see Figure 6. This curve represents the locus of all maxima of individual C_p curves

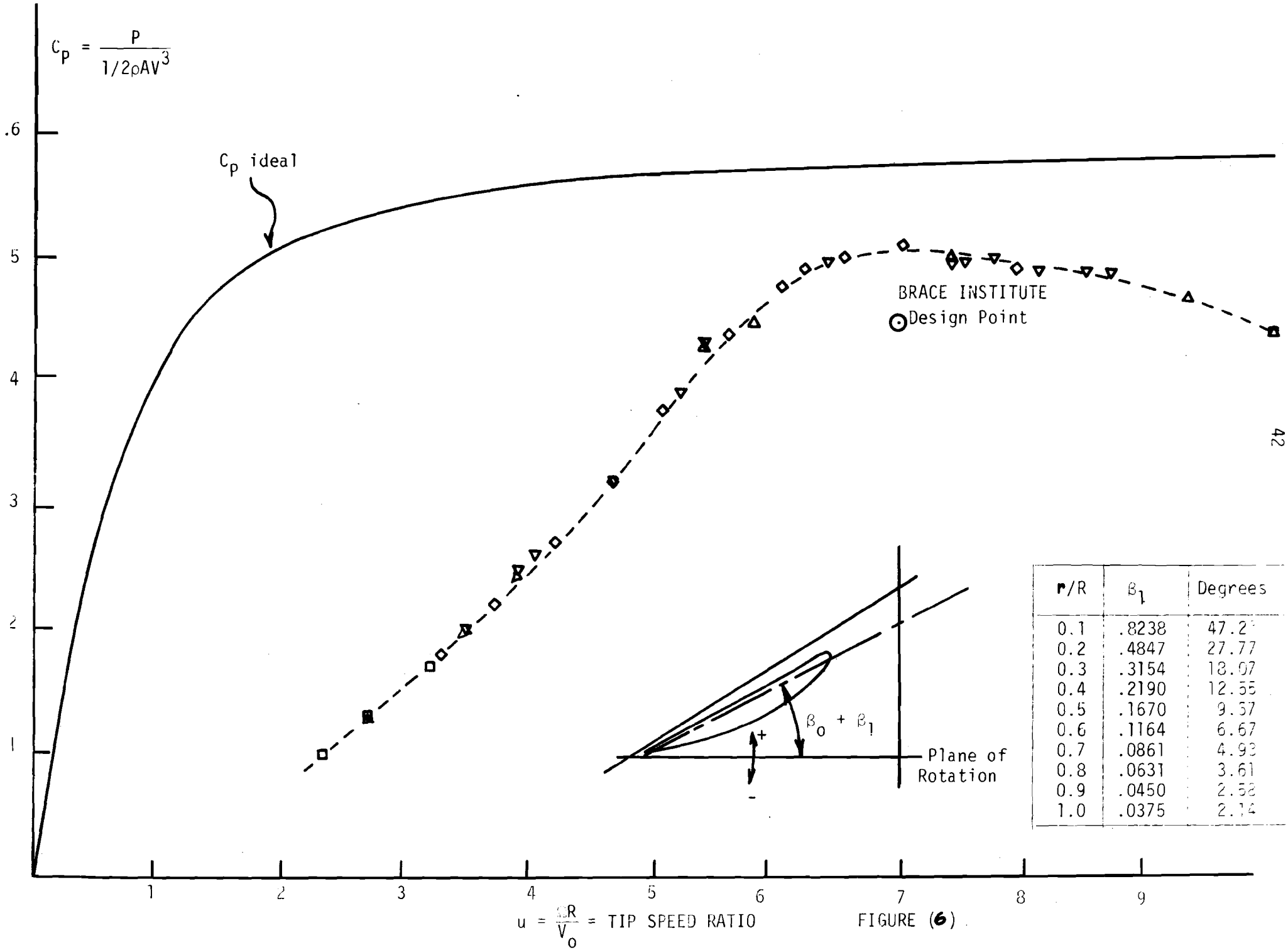

r/R	β_1	Degrees
0.1	.8238	47.2[illegible]
0.2	.4847	27.77
0.3	.3154	18.07
0.4	.2190	12.55
0.5	.1670	9.57
0.6	.1164	6.67
0.7	.0861	4.93
0.8	.0631	3.61
0.9	.0450	2.58
1.0	.0375	2.14

FIGURE (6)

for various values of β_0, as shown. For a fixed pitch machine, the performance characteristic would be as shown on the dotted line. For synchronous (constant speed) windmill systems, the power coefficient variation with increasing wind speed is determined from this plot (2).

The torque can be derived from this curve using the following approach. The definitions are:

$$C_p = \text{power coefficient} = \frac{P}{\frac{1}{2}\rho A V_0^3}$$

ρ = density of air @ sea level

A = propeller disc area

V_0 = wind speed

$$C_\tau = \text{torque coefficient} = \frac{\tau}{\frac{1}{2}\rho A V_0^2 R}$$

with:

$$\mu = \text{tip speed ratio} = \frac{\Omega R}{V_0}$$

Ω = rotational speed

R = radius of propeller

Also:

$$P = \tau\Omega$$

This gives:

$$C_p = \mu C_\tau \qquad \text{or} \qquad C_\tau = \frac{C_p}{\mu}$$

Thus the torque coefficient can be found directly from the C_p simulation results. The C_τ dependence on pitch will likewise be shown (Figure 7).

When this relationship is found, a map of points (parametric plot) will be calculated for each wind speed of interest, and actual torque vs. RPM curves can be generated (see Figure 8). There will be regions on these plots which will indicate aerodynamic non-linear phenomena, and will probably not be important equilibrium conditions:

a) <u>stall</u> - occurs where angle of attack is higher than the maximum value for maintaining streamlines for the particular airfoil of

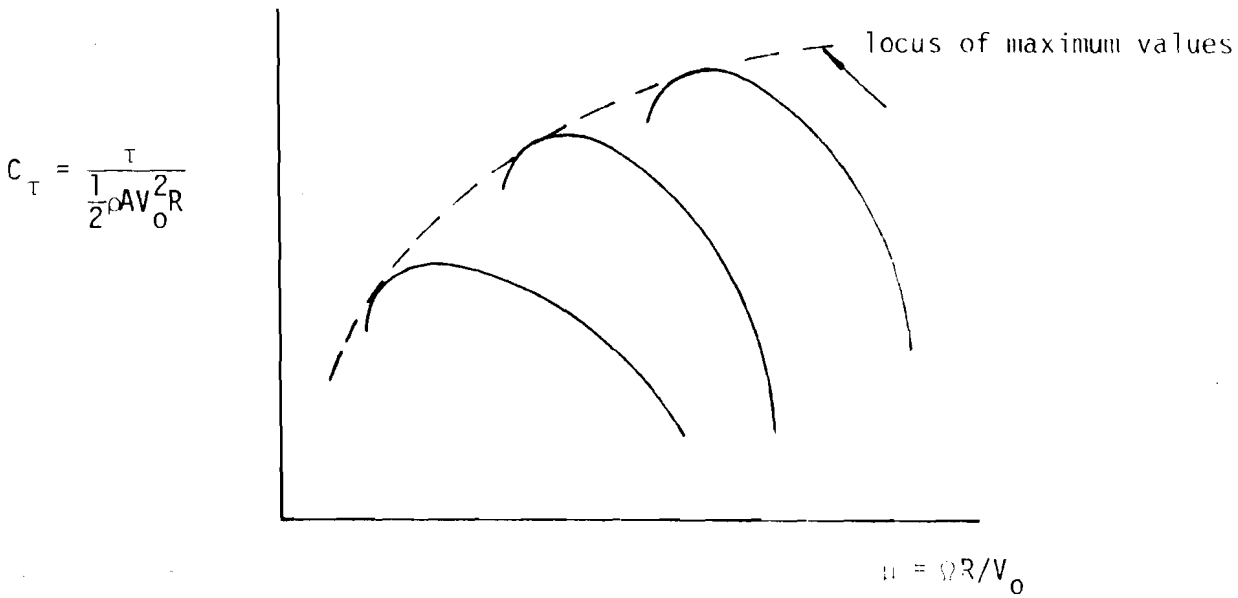

FIGURE 7

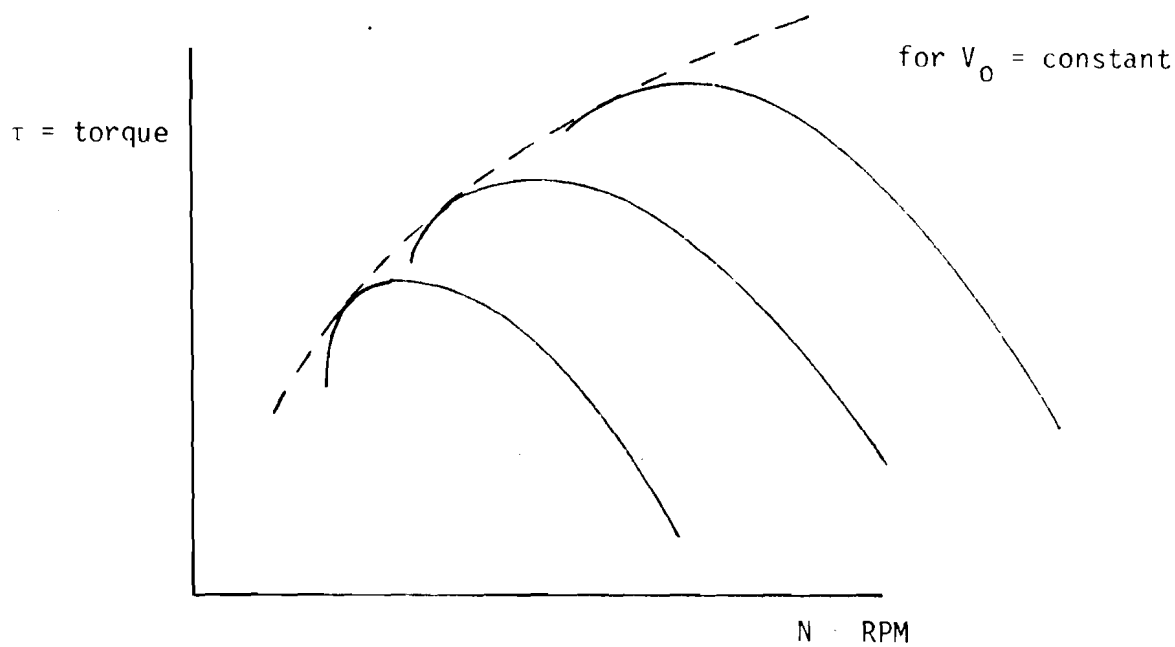

FIGURE 8

interest; performance is sharply degraded.

b) reverse flow - where local velocity over blade is from the trailing edge forward; thus will probably not occur except in small portions of the blade and for unusual conditions; this condition will not show up except as a rapid decrease in C_p with μ.

c) negative lift - the windmill acts as a propeller as angles of attack, lift, and torque, become negative.

IV. Results of Propeller Simulation

The computational results of the performance (strip) theory are shown in Figures 9 and 10. In Figure 9 can be seen the constant pitch curves used to generate the locus of C_p maxima shown in Figure 6. As pitch angle (β_0) is decreased (e.g. angle of attack of blade elements increased as shown in the inset), the rotor is loaded more and more. As the angle changes, the tip speed ratio for highest power increases to about 9 (@ $\beta_0 = -2°$) and then decreases to the design tip speed ratio of 7. The decrease in power with increased pitch angle represents the control philosophy advanced for $V_0 > V_{rated}$ (26.1 MPH); that is, shaft speed is kept constant and C_p decreases with increasing free stream velocity. This philosophy is also discussed by Hutter,[1] Golding,[2] Rohrback,[3] and Deutsch,[4] among others. A similar curve in terms of power (watts) vs. RPM, is shown in Figure 11. These results were obtained from wind tunnel tests of a fixed pitch, constant chord blade (Reference 7). The corresponding power coefficient characteristic is included in Figure 9.

In Figure 9, as pitch angle is decreased, the power characteristic becomes more and more sensitive. The left margin of each curve is a stall boundary; a phenomenon which occurs first at the tip of the blade, since the NEWF design is close to optimum twist and taper. The induced velocity

FIXED PITCH BEHAVIOR - WIND FURNACE

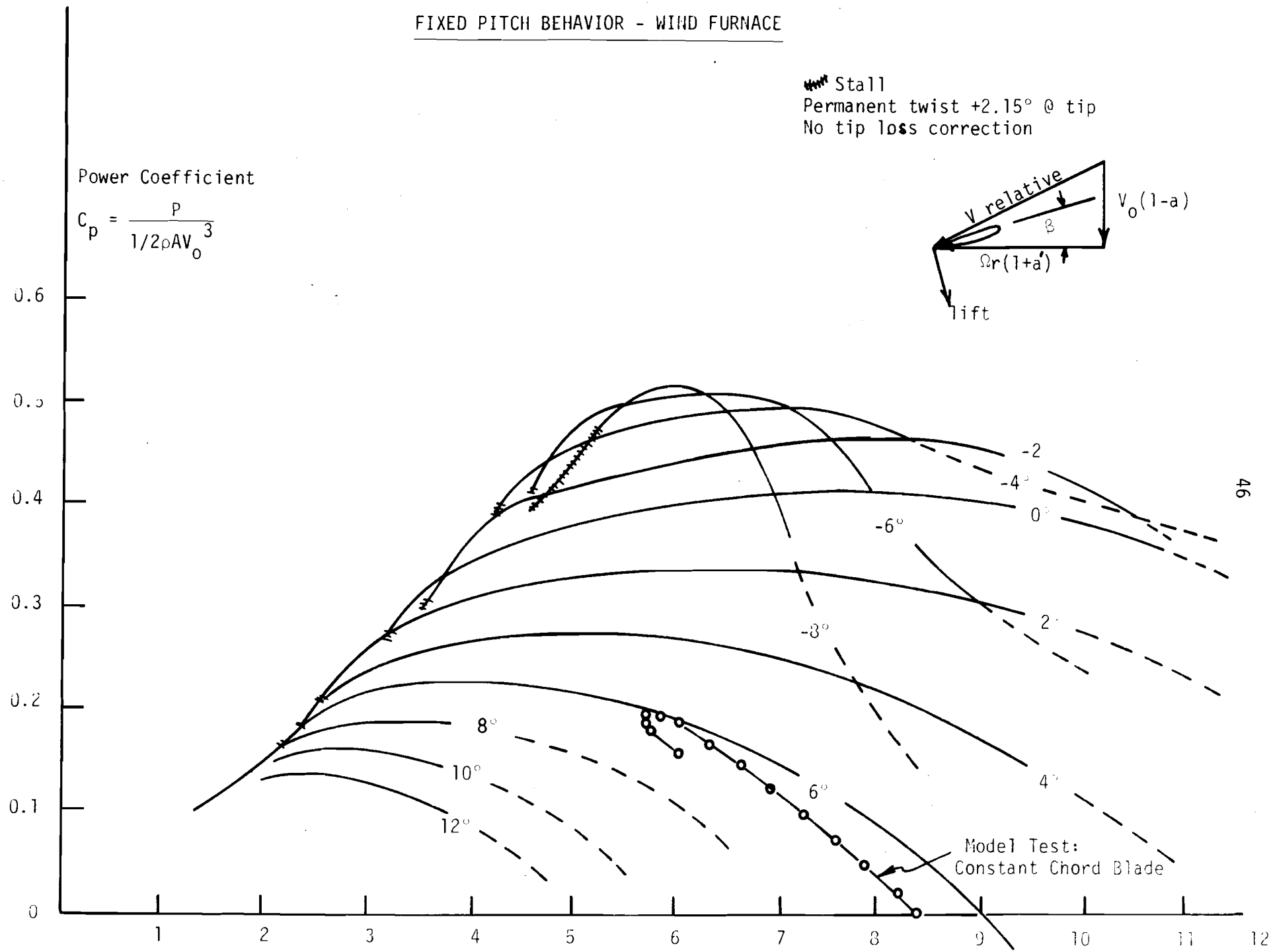

TIP SPEED RATIO $\frac{\Omega R}{V_o}$ = μ FIGURE (9)

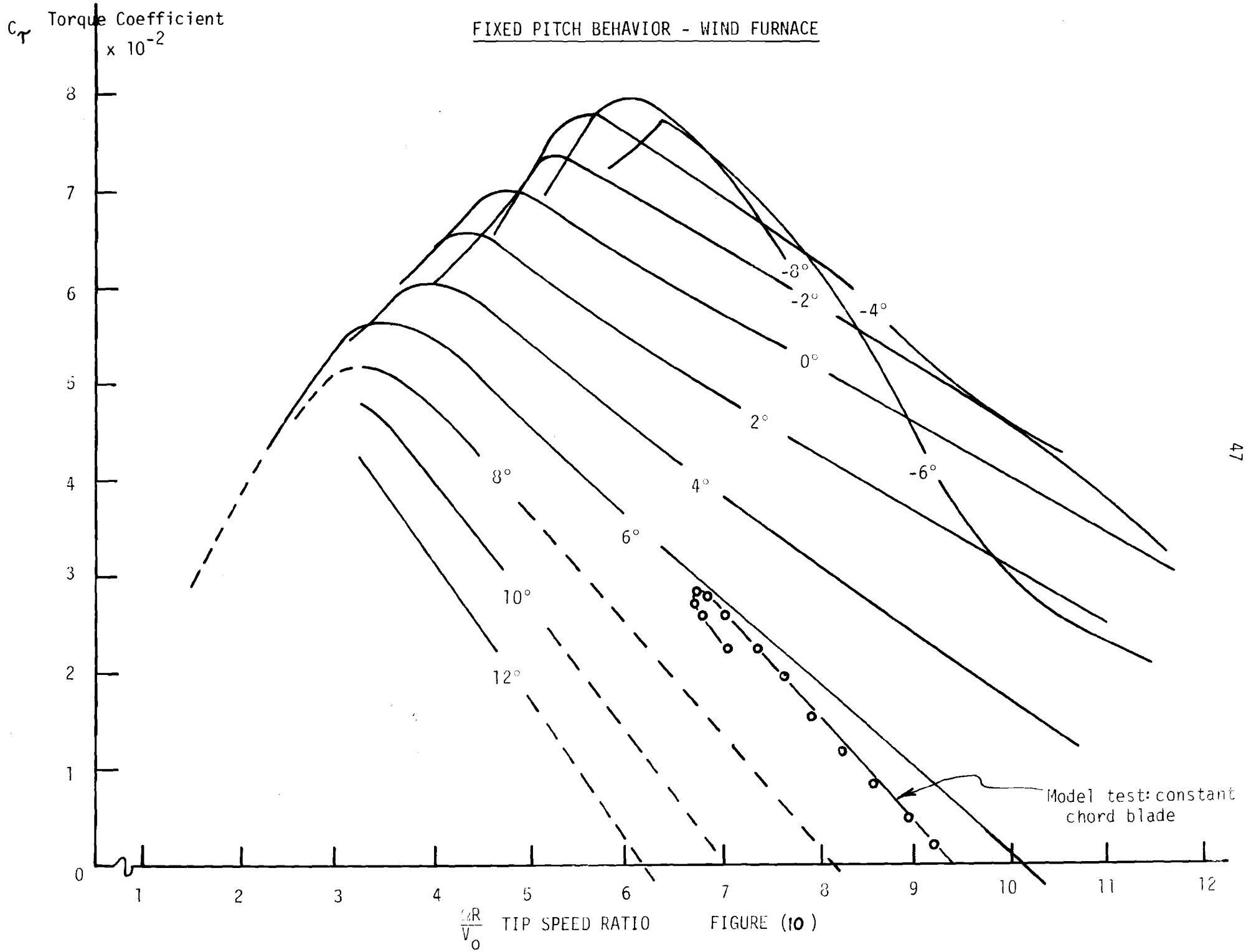
FIXED PITCH BEHAVIOR - WIND FURNACE
C_T Torque Coefficient
x 10^{-2}
8
7
6
5
4
3
2
1
0
1
2
3
4
5
6
7
8
9
10
11
12
-8°
-2°
-4°
0°
2°
-6°
8°
4°
6°
10°
12°
Model test: constant chord blade
$\frac{\omega R}{V_o}$ TIP SPEED RATIO

FIGURE (10)

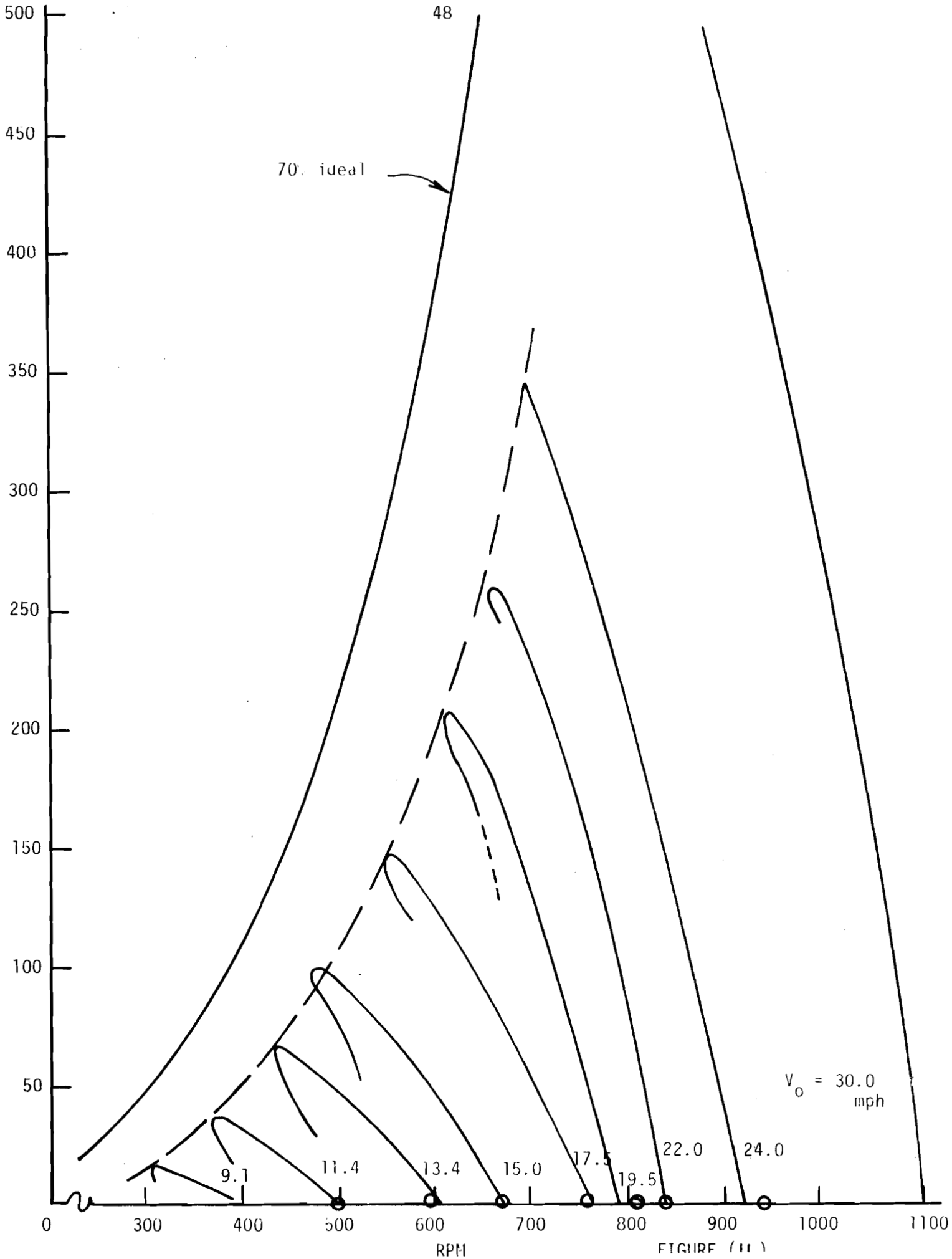
500
450
400
350
300
250
200
150
100
50
0
300
400
500
600
700
800
900
1000
1100
RPM
48
70% ideal
9.1
11.4
13.4
15.0
17.5
19.5
22.0
24.0
V_o = 30.0 mph

FIGURE (11)

(downwash) distribution along the blade is characteristic of optimum designs (see Figure 12). Untwisted, and constant chord, blades show a much less sensitive stall that starts at the root at much smaller pitch angles[5,6]; thus, the power characteristic of an off-design blade will be flatter and have smaller C_p than the NEWF blade (see Figures 9 and 11). This points out the need for thorough stability analysis of the optimum momentum exchanger system philosophy adopted for the NEWF design.

Also, from Figure 9, the power characteristic is seen to become higher order as stall is approached; that is, at pitch angles less than 0°, the drop in power with increasing tip speed ratio (or RPM for constant V_o) is much more severe. This is also believed to be a function of blade design, characterized by increased drag and highly twisted sections becoming negative lift.

In Figure 10 is plotted the corresponding torque characteristic, discussed earlier. The non-linear behavior at pitch angles less than 0° is also seen. But the striking characteristic is the linearity of the torque curves over the unstalled region. This represents system static stability for each constant pitch setting (in the linear range).

Near maximum torque, the curves are very peaky, and may constitute a catastrophic stall for small RPM perturbations. Typically, these RPM variations will be caused by gusts; an increase in wind speed momentarily decreasing tip speed ratio, and vice-versa. However, when μ is decreased far enough to push the propeller into stall, there is also a balancing effect caused by the increase in torque available in the free stream (e.g. due to increased wind velocity). Therefore, the dynamic behavior is important, and must be considered for a realistic stability and control solution.

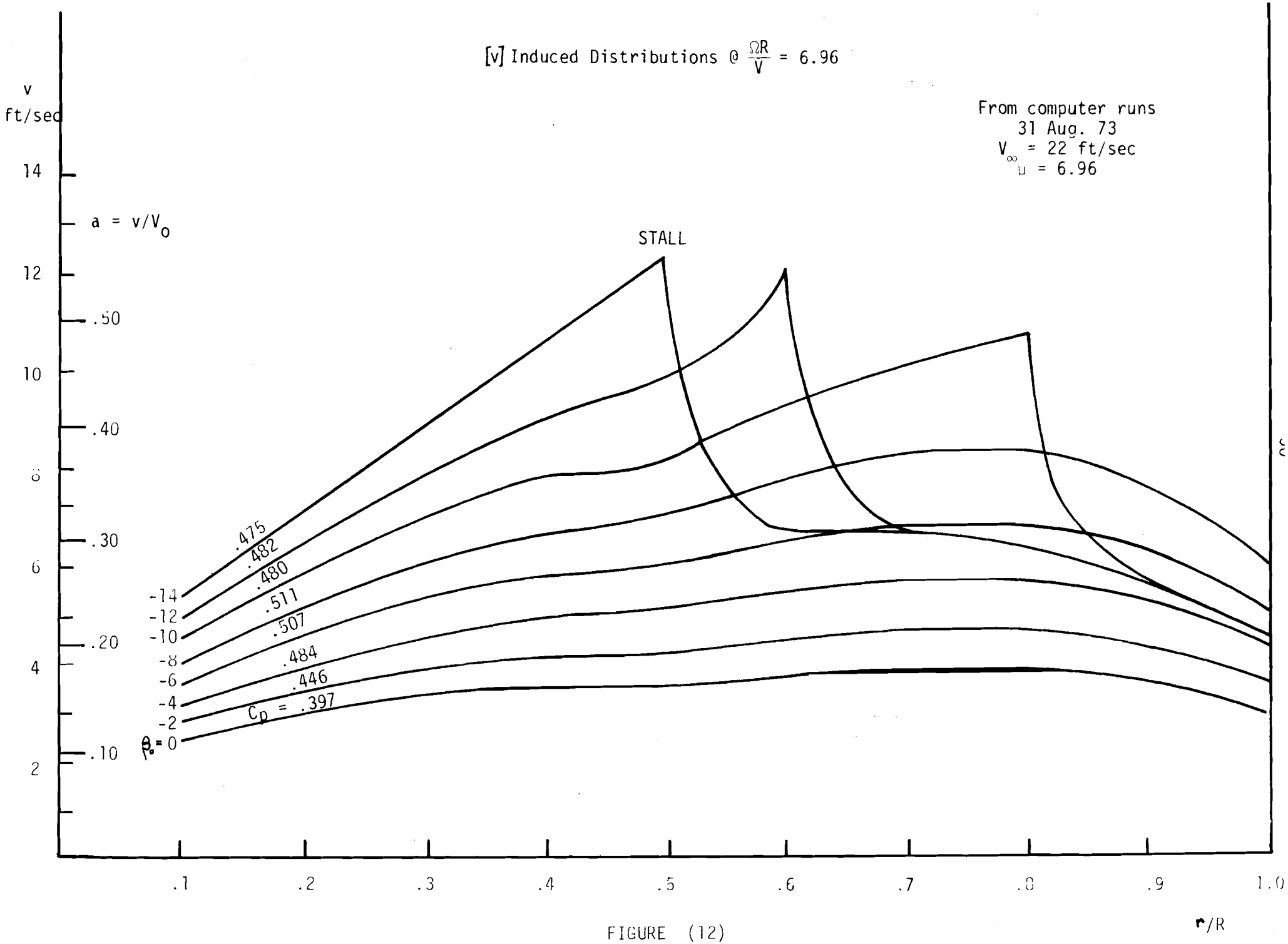
[v] Induced Distributions @ $\frac{\Omega R}{V}$ = 6.96
From computer runs
31 Aug. 73
V_∞ = 22 ft/sec
μ = 6.96
v
ft/sec
14
12
10
8
6
4
2
a = v/V_o
.50
.40
.30
.20
.10
STALL
.475
.482
.480
.511
.507
.484
.446
C_D = .397
-14
-12
-10
-8
-6
-4
-2
β_o = 0
.1
.2
.3
.4
.5
.6
.7
.8
.9
1.0
r/R

FIGURE (12)

More analytical and experimental data are needed to establish the slopes of the torque curves at the abscissa intersection (e.g. rotor unloaded). This is the condition which would be reached in the event of a shaft or generator failure. The wind generator will speed up to the point at which shaft torque input just balances friction torque, and classical "windmilling" is achieved.[7] [This is not the same as feathering, which is represented by the origin, or zero RPM.]

V. Rotor Flow States

The various rotor flow states can be identified on this characteristic.[5,8] The Zero Slip Case is represented by $C_\tau = 0$ just discussed; and the Propeller State is below the abscissa, where C_τ is negative (power goes into the system). As the constant pitch propeller is loaded more and more, the output power (and thrust) increases to the point where (torque x RPM) = power is a maximum (torque alone is not a maximum). This point occurs, according to momentum theory, where the average inflow is 1/3; and the ideal $C_p = .5926$.[2] If loading is increased beyond this, the inflow increases on the blade until the airfoil stalls; power falls off and thrust (not shown) increases, as verified by helicopter autorotative tests.[6] This is called the Turbulent Wake State, and is characterized by the absence of streamlines, severe buffeting, and the quick fall-off in developed power. The task of the control system will be to prevent entrance into this operating state, even for transient conditions. It should be understood that for high values of β_0 (e.g. 12°) the angles of attack are small to begin with, and it is unlikely that a significant portion of the (highly twisted) blade could ever be stalled. And the blade may never really enter Turbulent Wake State. Hence a positive output torque could be expected for extremely low RPM (or μ). However, our discussion will focus

on pitch angles closer to the torque and power peaks, where most running is done.

It is instructive to examine the blade element diagrams for these flow states. From Wilson and Lissman, Reference 5, Figure 13 is reproduced.

From examination of Figure 13, the "average" blade element situation can be described for regions of the power characteristic, Figure 9, as discussed. In the Turbulent Wake State, power decreases rapidly as most of the blade is stalled, and thrust increases rapidly. If the blade is allowed to reach stalled equilibrium, the resting point is again the zero torque abscissa. That is, a fixed pitch windmill can be driven into the stalled, or Turbulent Wake State, and this will cause the propeller-generator system to become statically unstable; a slight increase in generator torque (or load) will cause a rapid decrease in propeller RPM and the torque will drop to zero. Most generators have "residual" torque when unloaded at low RPM. The constant field in a permanent magnet generator, and the residual magnetism in separately excited field machines, will be a large residual torque. The stalled equilibrium, then, will be the point at which the Turbulent Wake State shaft torque (slightly positive) will just be enough to balance the generator "residual" torque. If the residual magnetism or permanent field is too high even for very low RPM's, the windmill can actually come to rest. In practice, a machine such as this is seldom seen because it would not be self-starting (without pitch control). This condition, however, does exist for certain high efficiency vertical axis wind generators.[10] It is not expected that the Turbulent Wake State operation will be useful for wind generator speed control since the blade loadings and thrust increase with rapidly decreasing power. Also, the flow conditions are unstable; high

Blade Elements for Various Rotor States (from Ref. 5)

V_o = free stream velocity

v = induced velocity (axial)

α = local angle of attack

β_o = pitch angle at blade element (includes local twist angle)

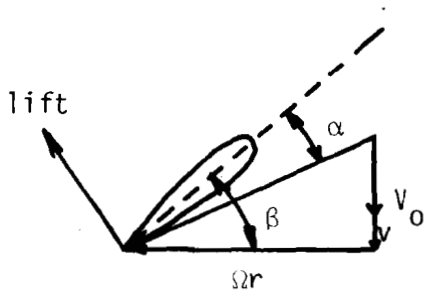

Propeller State

(C_p and C_T are negative)

$a < 0$

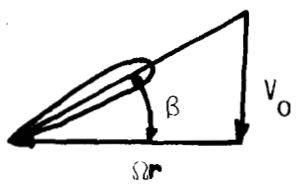

Zero Slip Case

($C_p = C_T = 0$)

$a = 0$

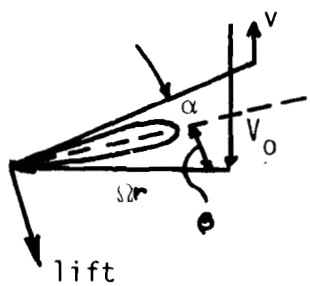

Windmill State

(C_p and C_T are positive)

$0 < a \leq 1/2$

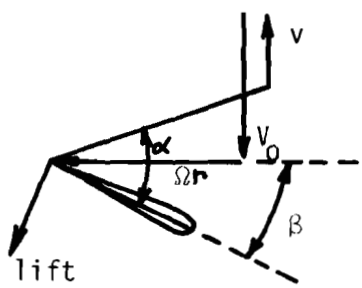

Turbulent Wake State

(C_p is negative; C_T is positive)

$a \geq 1/2$

vibration and buffetting can occur, as with helicopter rotors.

It is interesting to also consider the low RPM behavior of high solidity propellers, such as the American fan mill. As RPM is decreased, the corresponding change in downwash and angle of attack is much smaller for these machines; hence, large positive torque is still produced at very low RPM, and the machines can literally never be stalled by conventional loads. Also, it points out the non-necessity of variable pitch on these machines (static torque is already high). However, these machines are generally not important for electricity generation since the overall power coefficients are small, and optimum tip speed ratios are close to unity.[2]

A rough idea of the Turbulent Wake State boundary (for low solidity, high speed wind generator propellers) can be gained from simple theory.

From blade element theory (neglecting slip stream rotation) the tip section is:

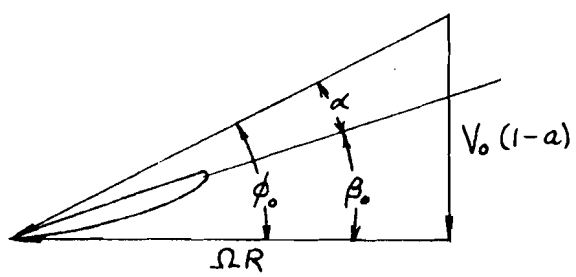

where

ϕ_o = blade element angle

The Turbulent Wake State boundary is the point at which streamlines are no longer well-defined; this occurs at values of $a = v/V_o = 1/2$.[5,6,8] Hence:

$$\phi_o \Big|_{\substack{\text{Turbulent}\\ \text{Wake State}\\ \text{Boundary}}} = \tan^{-1}\left[\frac{V_o(1-a)}{\Omega R}\right] = \tan^{-1}\left[\frac{1-a}{\mu}\right] = \tan^{-1}\left[\frac{1}{2\mu}\right]$$

Thus, the blade element angle (or inflow angle) at the tip for Turbulent Wake State to occur depends on tip speed ratio:

Tip Speed Ratio $\Omega R/V_o$	Turbulent Wake Boundary ϕ_o at blade tip
1	26.6°
2	14.0
3	9.5
4	7.1
5	5.7
6	4.8
7	4.1
8	3.6
9	3.2
10	2.9

TABLE 1

Most airfoils approach stall at angles of attack about 12°. Thus, the approximate pitch angle to produce turbulent wake state is simply:

$$\beta_o \Big|_{\substack{\text{Turbulent}\\ \text{Wake State}}} = \phi_o \Big|_{TWS} - \alpha_{stall}$$

where $\phi \Big|_{TWS}$ is given in Table 1 above, and $\alpha_{stall} \simeq 12°$.

References

1. Hutter, "Operating Experience Obtained with a 100-kW Wind Power Plant," NASA TTF-15, 068, August 1973.

2. Golding, The Generation of Electricity by Wind Power, Philosophical Library, 1955.

3. Rohrback and Worobel, "Performance Characteristics of Aerodynamically Optimum Turbines for Wind Energy Generators," 31st Annual National Forum, American Helicopter Society, May 1975.

4. Deutsch, L., Grumman Aerospace Corporation, personal communication, 19 March 1976.

5. Wilson and Lissman, "Applied Aerodynamics of Wind Power Machines," Oregon State University, July 1974.

6. Gessow and Myers, Aerodynamics of the Helicopter, Frederick Ungar Publishers, 1952.

7. Stoddard, Edds, "Final Report on Wind Tunnel Test Program of Model Blades on a 200 watt, 12 volt Wind Generator," University of Massachusetts, Civil Engineering Department In-House Report, May 1974.

8. Stoddard, "Discussion of Momentum Theory for Windmills," (this report).

9. Edds, M., "Optimization of Output Power of an AC Synchronous Machine by Varying Excitation and Load," M.S. Ocean Engineering Thesis, to be published, June 1976.

10. Blackwell, "The Vertical Axis Wind Turbine; How it Works," Sandia Laboratories, Albuquerque, New Mexico, SLA-74-0160, April 1974.

UNIVERSITY OF MASSACHUSETTS/AMHERST
ENERGY ALTERNATIVES PROGRAM

UNIVERSITY OF MASSACHUSETTS/AMHERST

ENERGY ALTERNATIVES PROGRAM

Preliminary Report on

OPTIMIZING THE WINDMILL ROTOR

by

Paul Lefebvre
and
Duane E. Cromack

U.Mass Wind Furnace
Energy Alternatives Program
University of Massachusetts
Amherst, Massachusetts 01002

TR/76/4
Appendix VI

OPTIMIZING THE WINDMILL ROTOR

abstract

Twelve horizontal axis wind rotor systems are analyzed by means of computer simulation. The purpose of this analysis is to develop a method of designing optimized blades of different rotor configurations. The results of the simulation are then compared with wind tunnel test results.

introduction

One of the principal components of any windmill is the momentum exchange device, or rotor. This device converts the kinetic energy of a moving air stream to a more usable form of power. There are two basic classifications for windmills: vertical axis machines and horizontal axis machines. This report deals only with horizontal axis rotors. Within this category all rotors take the form of an airscrew with the difference between designs being in the chord and twist distribution of each blade, and the number of blades employed for any given rotor. The functional relationship of these variables determines how efficiently a rotor performs. Four different rotor systems are studied and their performance capabilities optimized. The rotor types considered are: (1) constant chord, zero twist (CCZT); (2) linear tapered chord, zero twist (LCZT); (3) linear tapered chord, linear twist (LCLT); and (4) aerodynamically optimum chord and taper (OPT). The optimum blade is taken to be that air screw configuration which will extract the highest percentage of the power available. It has been shown that the maximum power coefficient obtainable is .5926, and in practice C_p will invariably be less than this value. To

determine the most advantageous chord and twist distribution, it is necessary to combine momentum and annulus theory.[2] The following equations are obtained and the optimum blade can be designed accordingly.

$$X = \sin\phi(2\cos\phi - 1)/((1+2\cos\phi)(1-\cos\phi))$$

$$BcC_L\ \Omega/2\pi\ Vo=4\sin\phi\ (2\cos\phi - 1)/(1+2\cos\phi)$$

A simple computer program was written to facilitate this design specification process and is listed in Appendix A. The program is written in Fortran for use on the Kronos time sharing system in use at the University of Massachusetts, and should be readily adaptable to any other system. The input is limited to five lines containing the rotor radius, the number of blades, the tip speed ratio and the C_L and α that correspond to C_L/C_D maximum for the airfoil data being used. The format in each case is F7.3.

The performance characteristics of each of these four airscrew configurations are determined for two, three, and four bladed systems. The power coefficients cited were obtained using a NACA 4415 standard roughness airfoil profile and a design tip speed ratio of 7. Each value represents the maximum power obtainable for that given rotor type under these conditions.

Computer Simulation: The computer model used to predict performance capabilities is one developed by Wilson and Lissaman,[3] and modified for our purposes. This model uses blade element theory to calculate the operating characreristics at each radial station. These characteristics are then numerically integrated along the blade to oobtain the calculated rotor performance. Refering to Figure 1, the following equations may be obtained:

$$\alpha = \phi - \theta \tag{3}$$

$$\tan \phi = (1-a)(Vo/((1+a')\,\Omega r) \tag{4}$$

$$C_Y = C_L \cos\phi + C_D \sin\phi \tag{5}$$

$$C_X = C_L \sin\phi - C_D \cos\phi \tag{6}$$

From aerodynamic strip theory, the thrust and torque on a differential blade element are given as

$$dT_a = .5Bc\,\rho V r^2\, C_Y dr \tag{7}$$

$$dQ_a = .5Bc\,\rho V r^2\, C_X dr \tag{8}$$

From momentum theory, the thrust and torque become

$$dT_m = (2\,\pi r dr)\,\rho u(Vo-u_1) \tag{9}$$

$$dQ_m = (2\,\pi r dr)\,\rho u r(2a'\Omega) \tag{10}$$

Defining the downstream axial interference factor, a_w, as twice the axial interference factor at the rotor, equations (7) and (9) may then be equated to yield a relation between a and other known rotor parameters such that

$$a = (BcC_Y/8\pi r)/(\sin^2\phi + (BcC_Y/8\pi\, r)) \tag{11}$$

In a similar manner, if the angular velocity downstream is assumed to be twice that found at the rotor, equations (8) and (10) may be equated to obtain the angular interference factor in terms of known variables. Thus:

$$a' = (BcC_X/4\pi r)/(\sin 2\phi - (BcC_X/4\pi r)) \tag{12}$$

Enough information is now available so that the flow characteristics for any given blade element can be found. If initial values for a and a' are assumed (a=.05 and a'=0) equation (4) can be used to calculate ϕ. Once ϕ is

known equation (3) is used to find α. For a given value of α, C_L and C_D can be obtained from polynomial curvefits of the aerodynamic data. Knowing the lift and drag coefficients, and ϕ, equations (5) and (6) are then used to find Cy and Cx. This allows for the calculation of a new value of a and a' which are then used to repeat the entire process. The iteration continues until convergence on a and a' occurs.

In practice it was found that at low local speed ratios the iteration loop would sometimes fail to converge. This is due to the non-linear relationship between a and a', and the local speed ratio (Figure 2). Because of this convergence problem, it was necessary to further modify the original program so that each successive iteration used the mean value of a and a' found in the two previous passes. A correction factor was also introduced in which at local speed ratios of .75 or below, a' was multiplied by one quarter of the local speed ratio, and this new value of a' used for the next pass. This facilitates the convergence procedure.

The constraints used in the computer simulation are as follows:

(1) Hub radius of 10 percent the blade radius,

(2) A standard axial interference model,

(3) Altitude above sea level of 200 feet,

(4) No coning angle used,

(5) Tip losses modeled by Prandtl's method,

(6) No nub loss model used,

(7) A NACA 4415 Standard roughness airfoil profile was used,

(8) A tip speed ratio of 7 was used.

Computer Simulation Results: The power coefficients obtained with optimum rotors of two, three and four blades are listed in Table 1. These rotors were designed for a tip speed ratio of 7, a C_L of .914, at an angle of attack of 5.57 degrees. The last two figures represent the point at which C_L/C_D is maximum for an NACA 4415 standard roughness profile.

The next two blade types to be considered are linear chord zero twist and linear chord linear twist. In both cases the final design configuration was found by making a series of computer runs in which chord and twist were systematically changed in a series of approximations, as were β_0 and X, until a maximum power output at a tip speed ratio of 7 was reached. The chord and twist approximations that were tried are shown in Figure 3. In order to obtain a consistent method of designing blades of this type, their chord and twist distributions are listed in Table 2 in terms of the optimum blade of similar design constraints.

For example, if an LCZT 3-bladed rotor with a radius of 10 feet and a tip speed ratio of 7 is desired, the blade configuration is found as follows. The optimum blade for these conditions is laid out. The chord of the LCZT blade at 100 percent of the radius is taken as 90 percent of the chord of the optimum blade at that point. The chord of the LCZT blade at 10 percent of the radius is taken as 67 percent of the chord of the optimum blade at that point. As the chord distribution is linear, the dimensions of the blade are now fixed. All that remains is to set the β_0 to that specified in Table 2.

The power coefficients obtained for LCZT and LCLT rotors of two, three, and four blades are shown in Table 1.

The final blade type to be considered is constant chord zero twist. For rotors of this type there are three variables that will affect performance:

the rotor solidity, the β_0 setting, and the number of blades. The relation between rotor solidity and β_0 for maximum power, and the resulting tip speed ratio, is shown in Figure 4. These curves were generated by making a series of computer runs for a given solidity for which β_0 and X were systematically changed until a maximum power was obtained. The process was then repeated for a number of rotors of different solidities.

These results were checked to insure that they apply for a given rotor solidity regardless of whether it contains 2, 3, or 4 blades. The analysis was then repeated using NACA 4418 airfoil data in order to check for consistancy between similar profiles.

The power coefficients that can be expected from constant chord zero twist rotors with two, three, and four blades are also shown in Table 1.

Wind Tunnel Results: In an effort to experimentally verify the results of the computer simulation, a wind tunnel test program was established. Six model blades were constructed: two optimum blades and four constant chord zero twist blades. This would allow four rotor systems to be tested and a comparison to be made between several blade types, solidities, and numbers of blades. The test arrangement is shown in Figure 5. The electric generator was loaded by means of four variable resistance load banks. For any given test, the load applied to the generator was systematically varied until the combination of field excitation and resistance were such as to produce maximum power. This power was determined by measuring the voltage and amperage to the load (P=VI) and then adding to this the experimentally determined efficiency losses of the generator. (see Figure 6)

For each rotor type, a series of tests were first conducted to ascertain the β_0 setting for maximum power. That setting was then used for a series of runs at increasing wind speeds. The increase in maximum power with wind speed paralleled closely the expected cubic relationship and is shown in Figure 6. Also shown is the relationship between power and RPM as a function of applied load. Table 3 contains the power coefficients of three rotor systems for comparison with the power coefficients predicted by the computer simulation.

conclusion

Experimental verification of the computer simulation has not been completed. The differences in power coefficients listed in Table 3 are quite large with no consistent pattern discernable. Additional wind tunnel tests are planned in order to obtain a better correlation between theoretical and experimental results. Since the computer model is based on well-established aerodynamic theory, the results for comparative purposes are certainly valid.

The selection of the rotor type, i.e., optimum, LCLT, CCZT, etc., depends on the particular application but more important, depends on the method of blade manufacture and the material to be used. This is a problem of cost effectiveness and not of just rotor performance.

The problem of optimizing may be viewed differently by standardizing the power of each rotor system in terms of the required rotor diameter. This is done in the following manner. For any proposed wind generating system there will be a required power for a particular design wind speed. For the design power and rated wind speed, the required rotor diameter can be calculated from the standard power equation as $D = [8P/\pi C_p \rho V^3]^{1/2}$. The result is that

a two-bladed CCZT rotor with a diameter 5.27 percent greater than a ten-foot diameter two bladed optimum rotor will yield equal power. Therefore, the choice to be made is between a ten-foot optimum blade and a 10.53 foot CCZT blade. The decision as to which blade to use is based on which blade type would have the lowest unit production cost for the number of blades required. Table 4 indicates the per cent increase in blade diameter needed for equal power output, standardized to the optimum blade shape.

It should be stressed that the results cited apply really only to NACA 4415 airfoil profiles, although the results obtained using a NACA 4418 profile were quite similar. Other blade sections need to be analyzed before this procedure can be generalized.

It should also be kept in mind that the power coefficients found are for perfectly constructed blades. If a limited number of optimum blades were to be produced, it would be difficult to obtain the exact chord and twist distribution needed. On the other hand, better quality control might be expected for CCZT blades because of the simpler construction.

This study attempted to optimize the chord and twist distribution of four rotor types. It has been suggested that further increases in the power coefficients might be obtained by such methods as varying the airfoil profile along the blade, or by designing the blade in such a way that the C_L/C_D ratio was a function of the radial station instead of holding it at a constant C_L/C_D maximum.

TABLE 1

POWER COEFFICIENTS OF TWELVE SIMULATED ROTORS

(Listed in order of magnitude)

Type of Rotor	No. of Blades	β_o	Power Coefficient
Optimum	4	0.0	.474
Optimum	3	0.0	.463
Optimum	2	0.0	.439
LCLT	4	1.5	.460
LCLT	3	1.5	.449
LCLT	2	2.0	.428
LCZT	4	4.5	.430
LCZT	3	4.5	.423
LCZT	2	5.0	.408
CCZT	4	6.1	.425
CCZT	3	6.1	.415
CCZT	2	6.1	.396
CCZT	3	6.1	.415

TABLE 2

DIMENSIONS OF LCZT AND LCLT BLADES AS A FUNCTION OF OPTIMUM BLADE DIMENSIONS

Percent of Radius	Blade Type		
	Linear Chord Zero Twist	Linear Chord Linear Twist	
	(Chord)	(Chord)	(Twist)
100	.90 optimum	.90 optimum	1.00 optimum
10	.67 optimum	.67 optimum	.32 optimum

TABLE 3

COMPARISON BETWEEN COMPUTER SIMULATION AND WIND TUNNEL RESULTS

Case	Rotor Type	Mean Power Coefficient Wind Tunnel Tests	Power Coefficient Computer Simulation	Percentage Difference
1	2 bladed optimum	.392	.438	10.5%
2	2 bladed CCZT	.358	.391	8.4%
3	3 bladed CCZT	.391	.373	4.6%

TABLE 4

INCREASE OF BLADE DIAMETER NEEDED TO OFFSET LOSS OF EFFICIENCY DUE TO USE OF A NON-OPTIMUM BLADE

No. Blades	Rotor Type	β_o	Power Coefficient	% Increase in Diameter
2	Optimum	0.0	.439	0.00
2	LCLT	2.0	.428	1.28
2	LCZT	5.0	.408	3.73
2	CCZT	6.1	.396	5.29
3	Optimum	0.0	.463	0.00
3	LCLT	1.5	.449	1.55
3	LCZT	4.5	.423	4.62
3	CCZT	6.1	.415	5.62
4	Optimum	0.0	.474	0.00
4	LCLT	1.5	.460	1.51
4	LCZT	4.5	.430	4.99
4	CCZT	6.1	.425	5.61

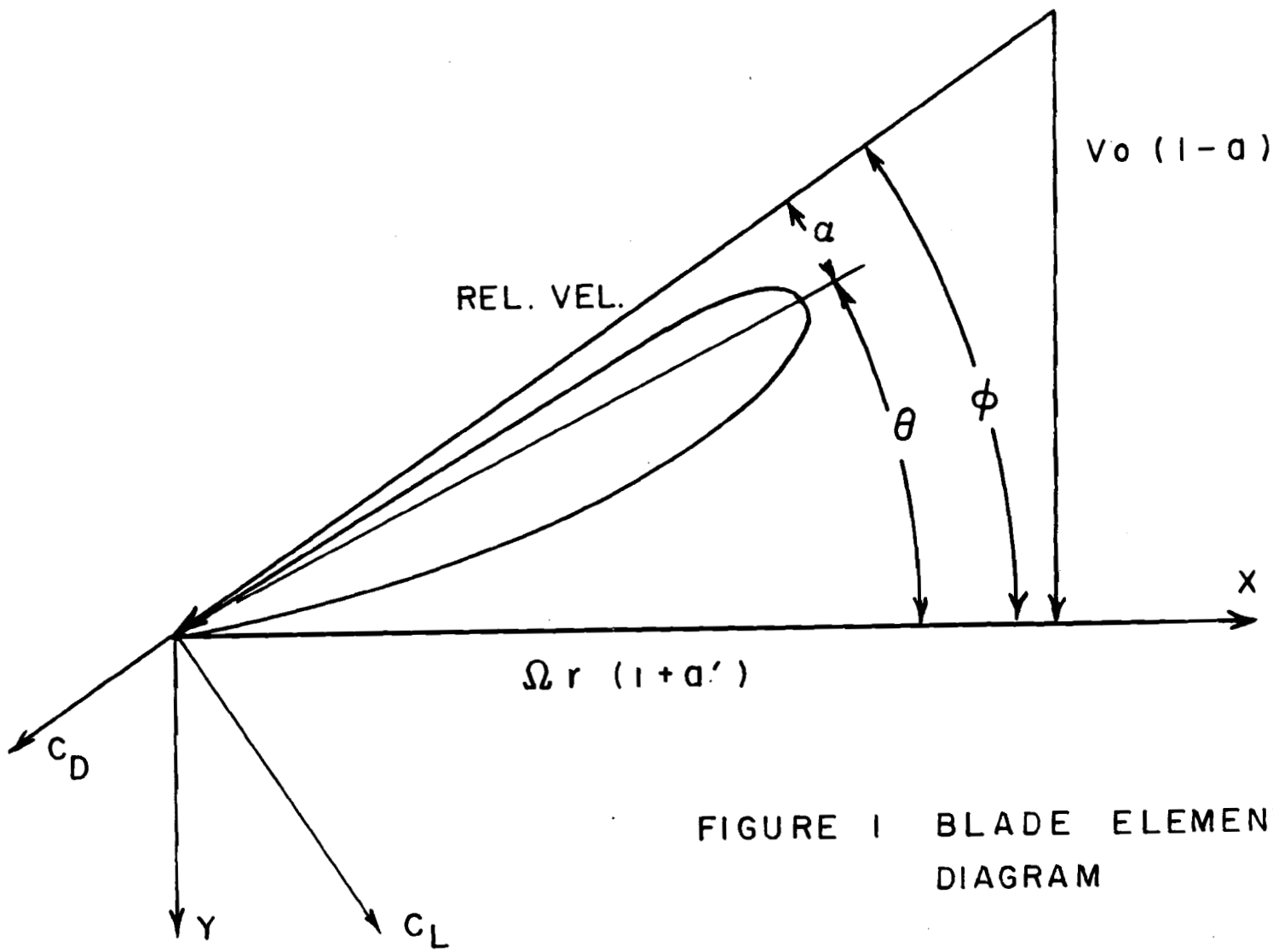

FIGURE 1 BLADE ELEMENT DIAGRAM

FIGURE 2

AXIAL AND ANGULAR INTERFERENCE FACTORS vs LOCAL SPEED RATIO

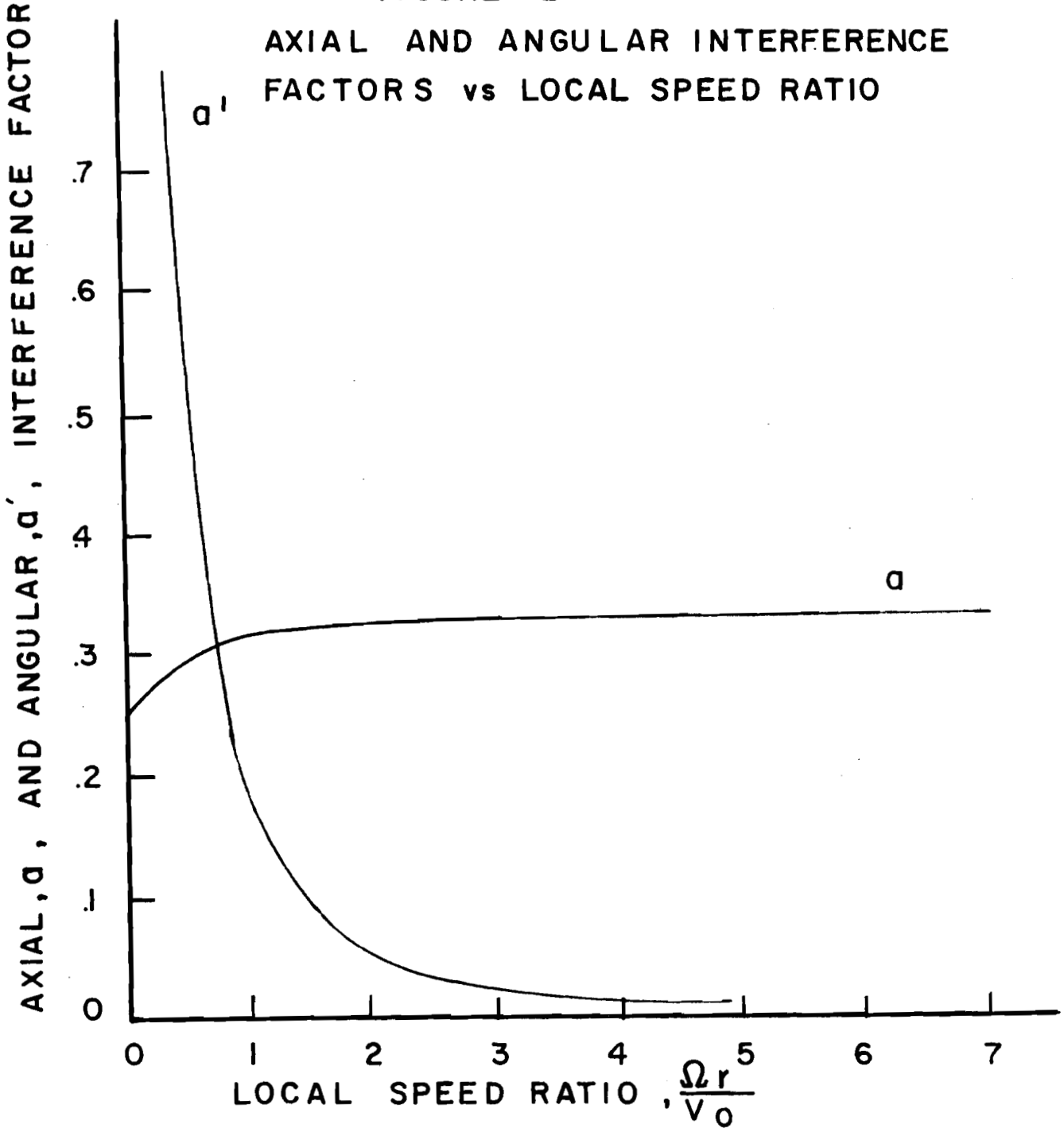

FIGURE 3

APPROXIMATIONS USED FOR THE COMPUTER SIMULATION OF THE LCZT AND LCLT BLADES

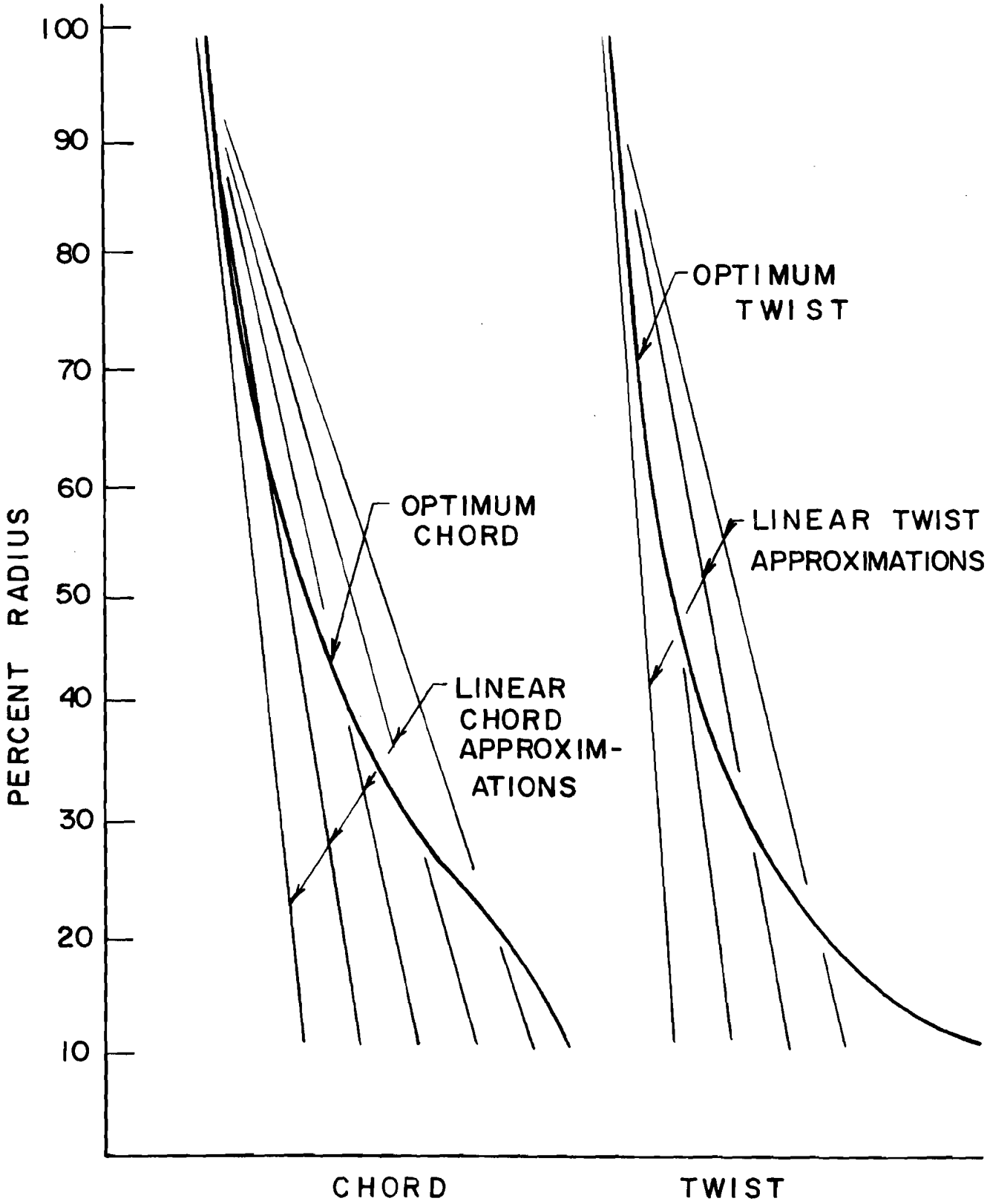

FIGURE 4

SOLIDITY vs PITCH ANGLE AND TIP SPEED RATIO FOR CONSTANT CHORD ZERO TWIST BLADES

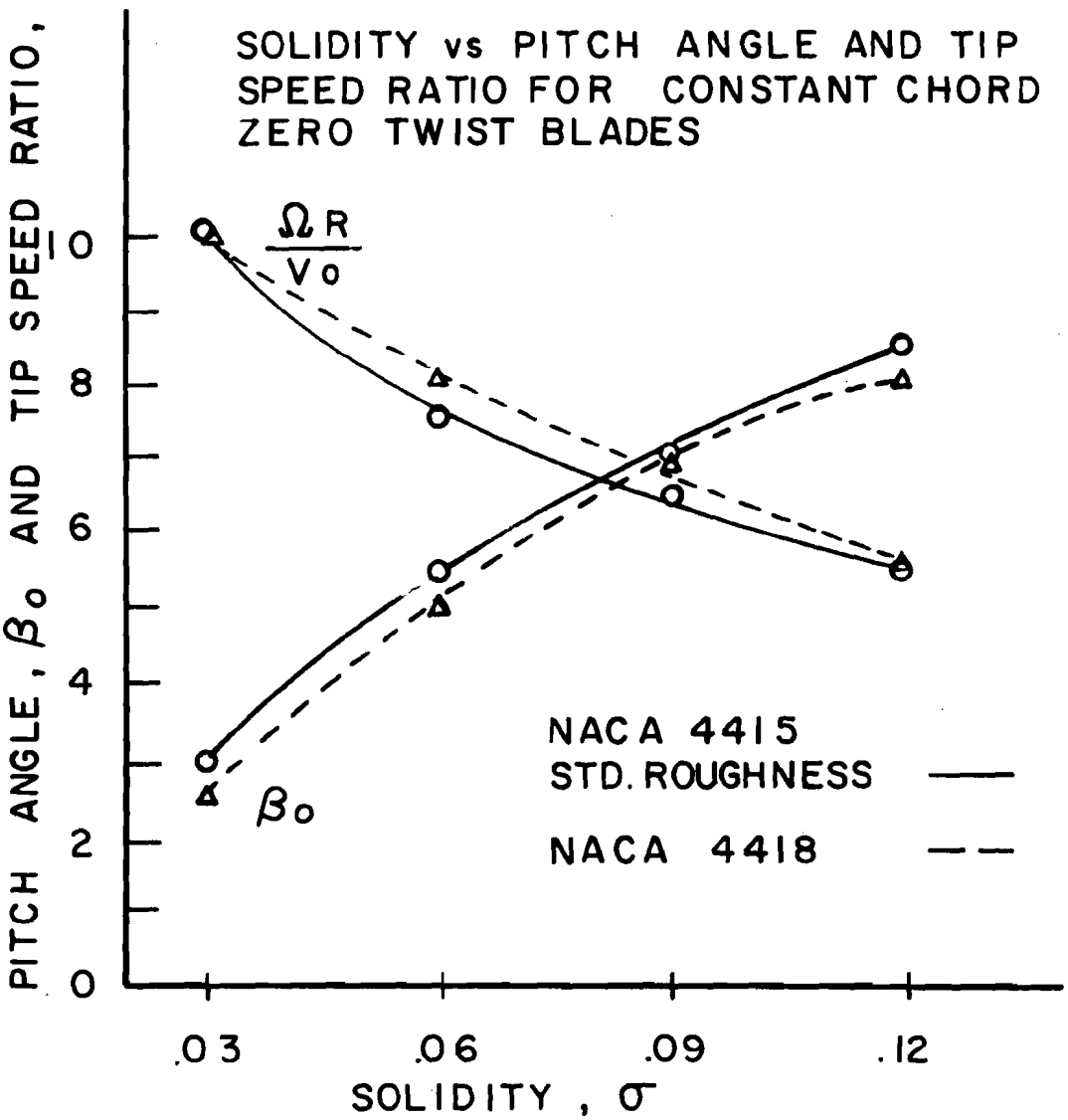

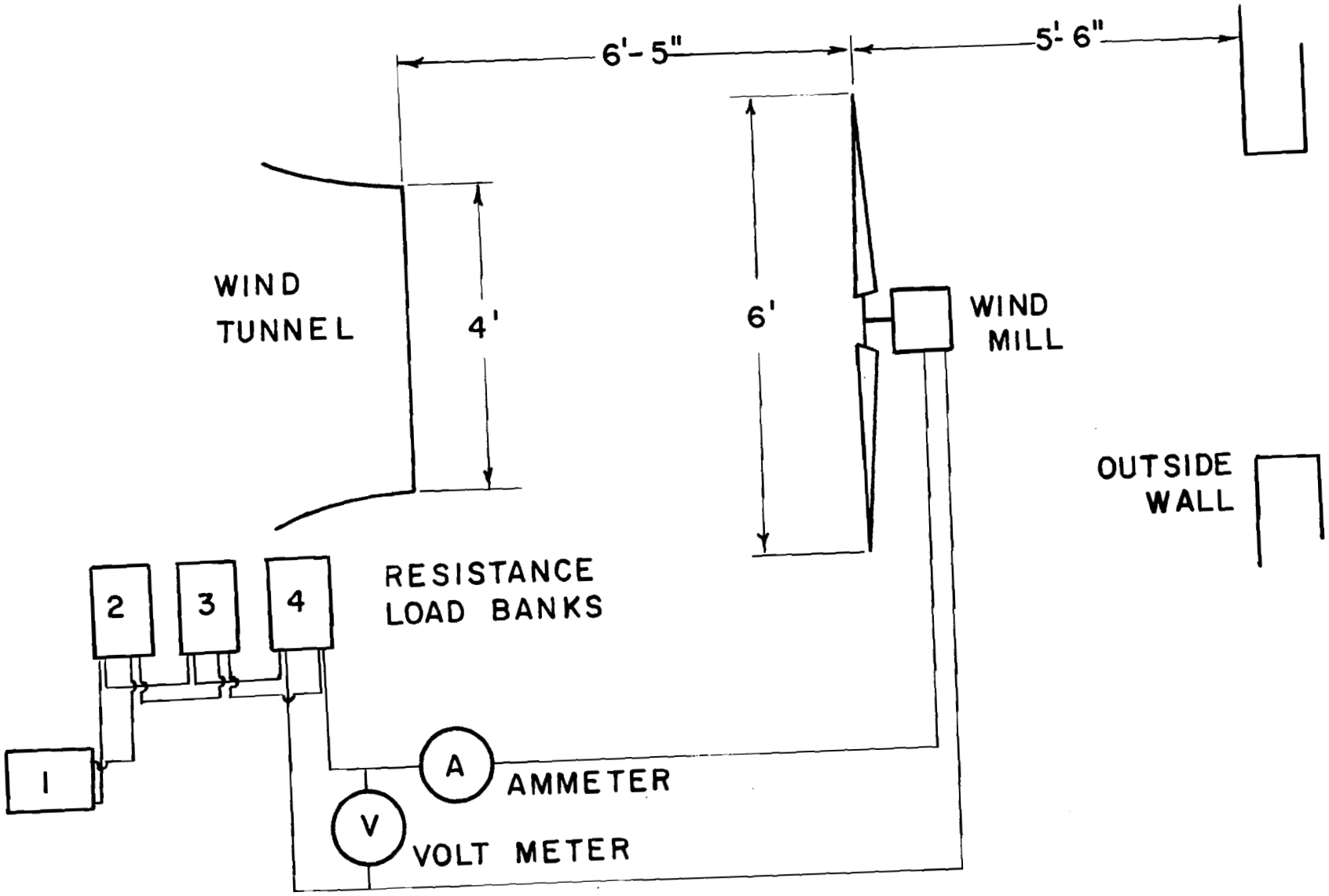

SCHEMATIC OF EXPERIMENTAL TEST SET-UP

FIGURE 5

FIGURE 6

POWER vs R.P.M. FOR 2-BLADED OPTIMUM ROTOR

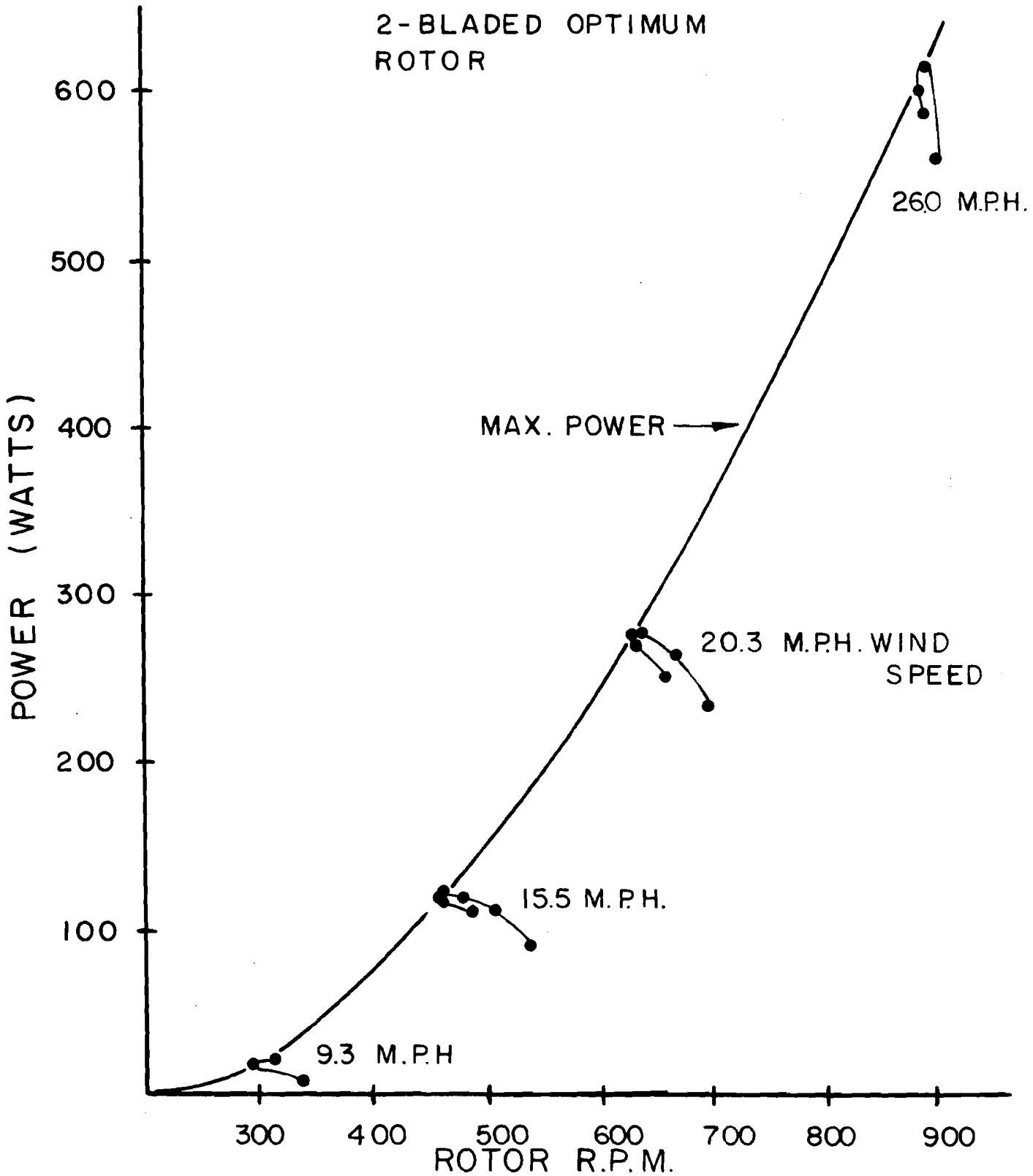

Nomenclature

a	Axial interference factor
a'	Angular interference factor
a_w	Wake axial interference factor
B	Number of blades in a given rotor
c	Local chord for a given blade
C_D	Drag coefficient
C_L	Lift coefficient
C_P	Power coefficient
C_X	Coefficient of force in the direction of rotation
C_Y	Coefficient of force normal to the plane of rotation
R	Radius of the rotor
r	Radius of a given local station
u	Axial flor velocity at the rotor
u_1	Axial flow velocity in the wake
Q_a	Torque as given by aerodynamic theory
Q_m	Torque as given by momentum theory
T_a	Thrust as given by aerodynamic theory
T_m	Thrust as given by momentum theory
Vo	Free stream velocity
Vr	The relative velocity as seen by a moving blade element
X	The tip speed ratio of the rotor devined as $\Omega R/Vo$
α	The angle between the chord of the blade element and the relative velocity
β_o	An equal angular deflection, in addition to blade twist, given to each blade element

Ω Angular velocity of the rotor

ρ Density of the fluid medium

ϕ Angle between the plane of rotation and the relative velocity

θ Angle between the plane of rotation and the chord of the blade element.

references

1. Glavert, H., Aerodynamics Theory (W. F. Durand, Editor-in-Chief), Vol. IV, Division L, Julius Springer, Berlin, 1935.
2. ibid
3. Wilson and Lissaman, "Applied Aerodynamics of Wind Power Machines," Oregon State University, July 1974.
4. Putnam, P. C., Power from the Wind, Van Nostrand Company, Inc., New York, 1948.

APPENDIX A

LNH

```
00100 PROGRAM OPT(INPUT,OUTPUT)
00105  DIMENSION CH(15)
00110 READ 1, R
00120 READ 1, B
00130 READ 1, X
00140 READ 1, CL
00150 READ 1, A
00160 1 FORMAT(F7.3)
00170 PRINT 2
00180 2 FORMAT(//5X,*RADIUS*,5X,*PC-R*,5X,*BCCLX/2PIR*,5X,*PHI*,5X,*BO*,5
00190+X,*CHORD*/)
00200 PI=3.141592654
00210 RL=0.
00220 XL=0.
00230 PER=0.
00240 P=60.
00241  DA=PI*(R**2.)
00245  H=R/10.
00250 DO 30 L=1,10
00260 XL=XL+(X/10.)
00270 P=P*PI/180.
00280 RL=RL+(R/10.)
00290 PER=PER+.1
00300 DO 5 I=1,6000
00310 P=P-(.01*PI/180.)
00320 XE=(SIN(P)*(2.*COS(P)-1.))/((1.+2.*COS(P))*(1.-COS(P)))
00330 IF(ABS(XL-XE).LT..05) GO TO 6
00332 5 CONTINUE
00334 6 DO 7 J=1,4000
00336 P=P-(.001*PI/180.)
00338 XE=(SIN(P)*(2.*COS(P)-1.))/((1.+2.*COS(P))*(1.-COS(P)))
00340 IF(ABS(XL-XE).LT..005) GO TO 10
00342 7 CONTINUE
00350 10 BCCL=(4.*SIN(P)*(2.*COS(P)-1.))/(1.+2.*COS(P))
00360 P=P*180./PI
00370 BO=P-A
00380 CH(L)=BCCL/(B*CL*X/(2.*PI*R))
00390 PRINT 20, RL,PER,BCCL,P,BO,CH(L)
00400 20 FORMAT(5X,F6.2,5X,F4.2,5X,F8.3,5X,F6.2,3X,F5.2,4X,F6.3)
00410 30 CONTINUE
00420  SUM=CH(1)+3.*CH(2)+3.*CH(3)+2.*CH(4)+3.*CH(5)+3.*CH(6)+2.*CH(7)
00421+ +3.*CH(8)+3.*CH(9)+CH(10)
00430  BAREA=((3.*H*SUM)/8.)*B
00440  SIGCL=BAREA/DA
00450  PRINT 40, BAREA
00460 40 FORMAT(//3X,*TOTAL BLADE AREA MINUS HUB OF .1R=*,F7.2,*  SQ.FT.*)
00470  PRINT 50, SIGCL
00480 50 FORMAT(//3X,*SIGMA TOTAL=*,F6.4)
00490  END
READY.
```

UNIVERSITY OF MASSACHUSETTS/AMHERST
ENERGY ALTERNATIVES PROGRAM

UNIVERSITY OF MASSACHUSETTS/AMHERST

ENERGY ALTERNATIVES PROGRAM

FIELD CONTROLLER FOR THE UMASS WIND FURNACE

by

Daniel Handmann

U.Mass Wind Furnace
Energy Alternatives Program
University of Massachusetts
Amherst, Massachusetts 01002

TR/76/5
Appendix VII

FIELD CONTROLLER FOR THE UMASS WIND FURNACE

It has been determined experimentally that maximum power output of the Lima Electric Generator can be achieved if the field current supplied to the generator for a given generator speed follows the curve shown in Figure 1. The function of the field controller is to supply field current along this I_f vs. RPM curve. To accomplish this task the field controller has five basic components; (refer to drawing #SH-I, 03.01.01 "Field Controller, Block Diagram") a tachometer, a 6 bit analog to digital converter, a 64 word by 8 bit semiconductor memory, an 8 bit digital to analog converter, and a pulse width modulated transistor switching amplifier.

The operation of the system is as follows: The tachometer is geared to the generator and has a d.c. voltage output that is linear with rpm. The output of the tachometer is converted from a voltage level to a 6 bit binary number by the analog to digital converter. The 6 bit binary number can take on integer values between 0 and 63 (base 10) which has the effect of breaking down the operating speed range of the generator into increments of 28.5 rpm. The output of the analog to digital converter is used to address one of the 64 words in memory. The contents of the addressed 8 binary bit word appear at the output of the memory. The digital to analog converter converts the word from memory into a current level between 0 and 2.6 milli-amps. This current level is the control signal for the pulse width modulated transistor switching amplifier. The switching amplifier switches a 50 volt d.c. power supply on and off at a fixed frequency (10kHz). The width of the pulse varies linearly with the control signal from the digital to analog converter. The wider the width of the pulses, the higher the average current supplied to the generator field. The switching

amplifier also monitors the amount of current being delivered to the generator field by means of a feedback loop. The feedback signal is summed into the control signal to provide current regulation necessitated by the fluctuation of the generator field's resistance with changes of field temperature.

By building the system around a memory, a certain amount of flexibility is introduced into the system. If, for example, it is determined during tests of the wind generator that a different I_f vs. RPM curve should be used, the old memory can be unplugged and replaced by a differently programmed one. For the first model of the field controller, two 32 word memories were used instead of one 64 word memory. This provides the option of changing part of the I_f vs. RPM curve at one-half the cost. The I_f vs. RPM curve can also be shifted horizontally and vertically by adjusting trimmer potentiometers included in the circuit. The actual output of the field controller is shown superimposed over the ideal I_f vs. RPM curve in Figure 2.

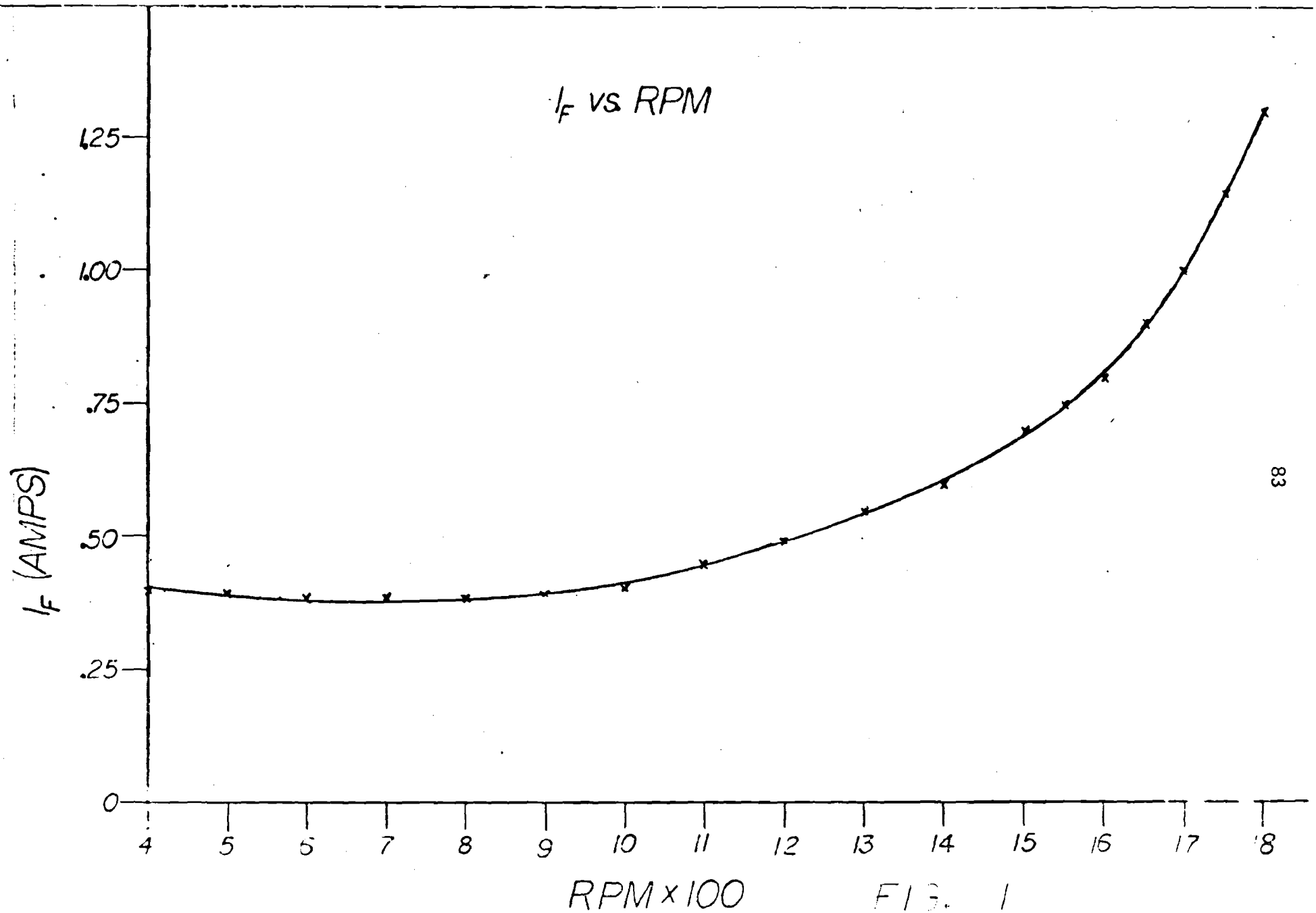
I_F vs. RPM
I_F (AMPS)
1.25
1.00
.75
.50
.25
0
4
5
6
7
8
9
10
11
12
13
14
15
16
17
18
RPM x 100

FIG. 1

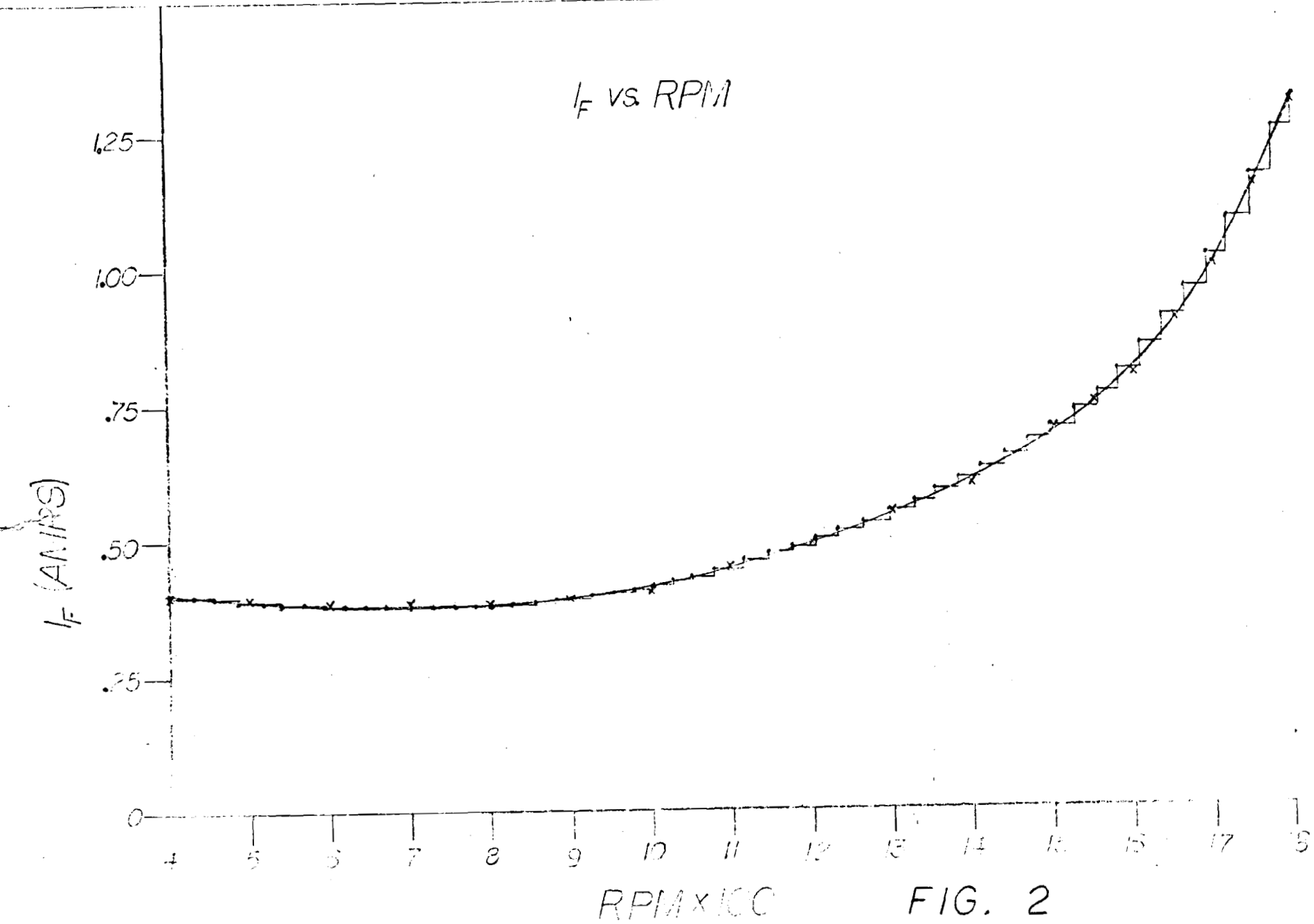
I_F vs. RPM
1.25
1.00
.75
.50
.25
0
I_F (AMPS)
4
5
6
7
8
9
10
11
12
13
14
15
17
RPM × 100

FIG. 2

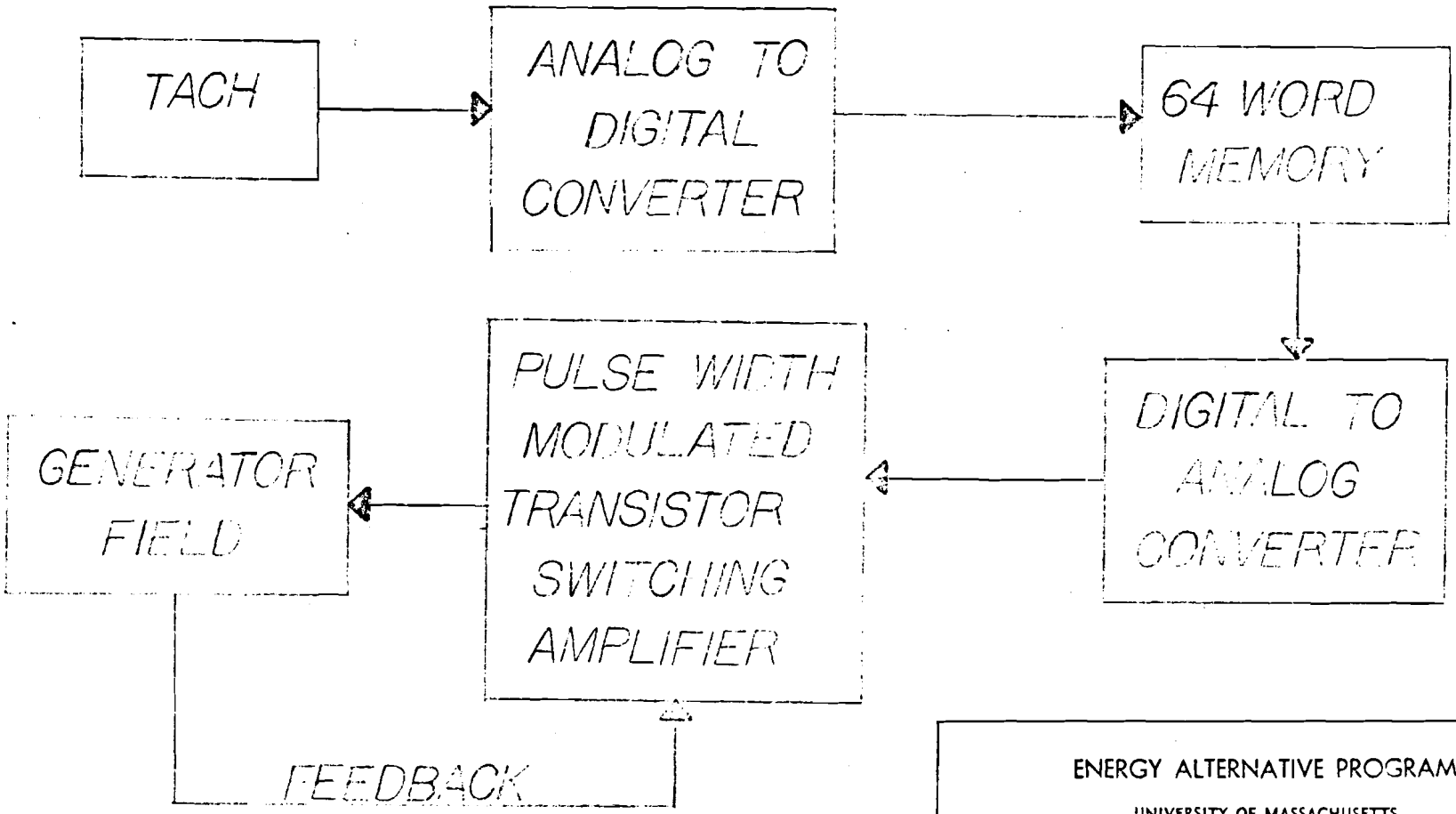

ENERGY ALTERNATIVE PROGRAM

UNIVERSITY OF MASSACHUSETTS

WIND FURNACE MARK I: FIELD CONTROLLER, BLOCK DIAGRAM

DRAWING NO. SH-1-03.01.01

DATE 3-19-76 DRN. BY D. HANEMAN

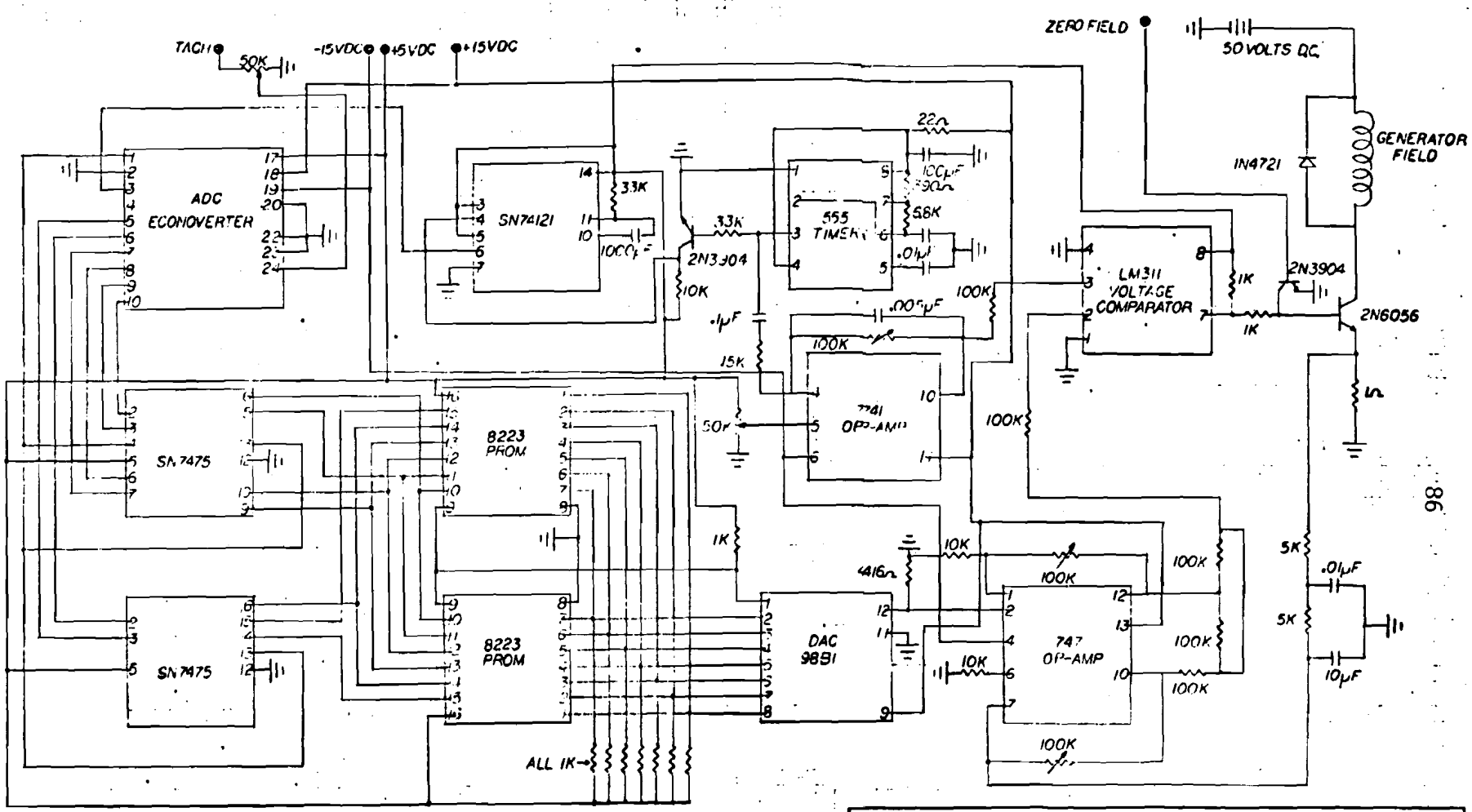

ENERGY ALTERNATIVE PROGRAM

UNIVERSITY OF MASSACHUSETTS

WIND FURNACE MARK I: FIELD CONTROLLER, SCHEMATIC

DRAWING NO. SH-I-03.0102

DATE 3-19-76 DRN. BY D. HALDIMAN

APPENDIX I: Determination of the Memory Bit Structure

In order to determine the proper bit pattern to be programmed into the memory to match the I_f vs. RPM curve, it was necessary to first determine the output current of the field controller circuit for every possible value of a memory word. Since each word contains 8 bits of information, each word can have 256 different values. To find the output current that would result for each of the 256 possible combinations of bits in a word, the following tests were run. (refer to drawing #SH-I-03.01.03, "Field Controller, Memory Simulation Test") The memories were simulated with 8 spdt switches that connected each input of the digital to analog converter to either +5 volts (logical 1) or ground (lobical 0). Then the switches were set for all of the 256 possible combinations of the 8 bits, and with an ammeter, the resulting current delivered to the generator field for each combination was recorded. Combining the results of the memory simulation test with a listing of the rpm range that each memory word would cover, and the ideal I_f vs. RPM curve, the proper memory contents to generate the desired shape for the I_f vs. rpm curve were determined. A copy of the bit structure is shown in Table 1. The memories were programmed using the Signetics 8223 Programming Procedure A, a copy of which is provided.

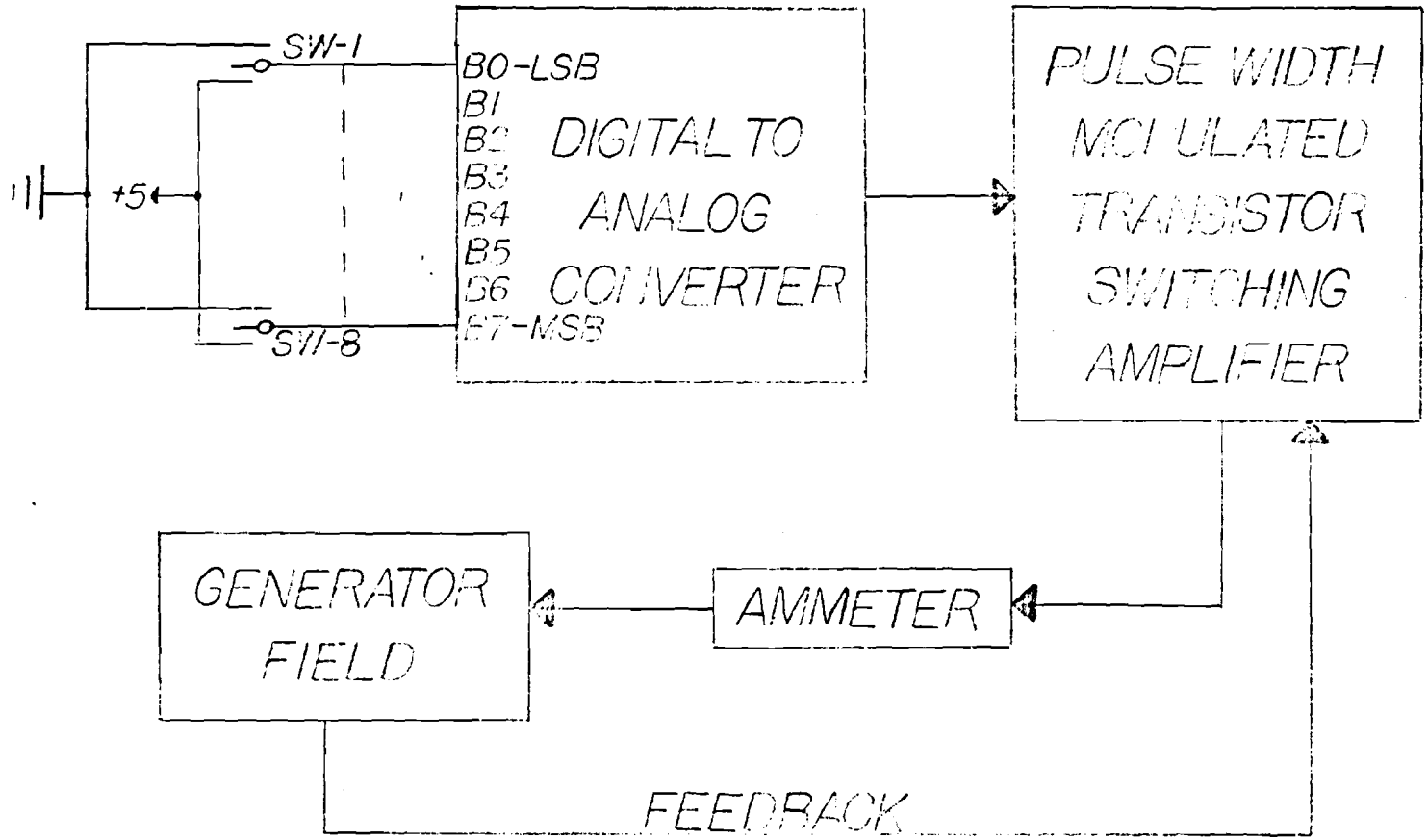

ENERGY ALTERNATIVE PROGRAM

UNIVERSITY OF MASSACHUSETTS

WIND FURNACE LINK I: FIELD CONTROLLER, MEMORY SIMULATION TEST

DRAWING NO. SH-I-03.0103

DATE 3-19-76 DRN. BY [illegible]

TABLE 1

RPM RANGE	MEMORY ADDRESS	MEMORY CONTENTS (MSB … LSB)
0-- 29	0	0 0 0 0 0 0 0 0
29-- 57	1	0 0 0 0 0 0 0 0
57-- 86	2	0 0 0 0 0 0 0 0
86-- 114	3	0 0 0 0 0 0 0 0
114-- 143	4	0 0 0 0 0 0 0 0
143-- 172	5	0 0 0 0 0 0 0 0
172-- 200	6	0 0 0 0 0 0 0 0
200-- 229	7	0 0 0 0 0 0 0 0
229-- 257	8	0 0 0 0 0 0 0 0
257-- 286	9	0 0 0 0 0 0 0 0
286-- 315	10	0 0 0 0 0 0 0 0
315-- 343	11	0 0 0 0 0 0 0 0
343-- 372	12	0 0 0 0 0 0 0 0
372-- 400	13	0 0 0 0 0 0 0 0
400-- 429	14	0 1 1 0 0 0 1 1
429-- 458	15	0 1 1 0 0 0 1 1
458-- 486	16	0 1 1 0 0 0 1 0
486-- 515	17	0 1 1 0 0 0 0 1
515-- 543	18	0 1 1 0 0 0 0 0
543-- 572	19	0 1 0 1 1 1 1 1
572-- 600	20	0 1 0 1 1 1 1 1
600-- 629	21	0 1 0 1 1 1 1 1
629-- 658	22	0 1 0 1 1 1 1 1
658-- 686	23	0 1 0 1 1 1 1 1
686-- 715	24	0 1 0 1 1 1 1 1
715-- 743	25	0 1 0 1 1 1 1 1
743-- 772	26	0 1 0 1 1 1 1 1
772-- 801	27	0 1 0 1 1 1 1 1
801-- 829	28	0 1 0 1 1 1 1 1
829-- 858	29	0 1 1 0 0 0 0 0
858-- 886	30	[illegible]

886-- 915	31	0 1 1 0 0 1 0 1
915-- 944	32	0 1 1 0 0 0 1 0
944-- 972	33	0 1 1 0 0 0 1 1
972--1001	34	0 1 1 0 0 1 0 0
1001--1029	35	0 1 1 0 0 1 0 1
1029--1058	36	0 1 1 0 0 1 1 1
1058--1087	37	0 1 1 0 1 0 0 1
1087--1115	38	0 1 1 0 1 0 1 1
1115--1144	39	0 1 1 0 1 1 0 1
1144--1172	40	0 1 1 1 0 0 0 0
1172--1201	41	0 1 1 1 0 0 1 1
1201--1230	42	0 1 1 1 0 1 0 1
1230--1258	43	0 1 1 1 1 0 0 0
1258--1287	44	0 1 1 1 1 0 1 1
1287--1315	45	0 1 1 1 1 1 1 0
1315--1344	46	1 0 0 0 0 0 0 0
1344--1373	47	1 0 0 0 0 1 0 1
1373--1401	48	1 0 0 0 1 0 0 0
1401--1430	49	1 0 0 0 1 0 1 0
1430--1458	50	1 0 0 0 1 1 1 1
1458--1487	51	1 0 0 1 0 1 0 0
1487--1515	52	1 0 0 1 1 0 0 1
1515--1544	53	1 0 0 1 1 1 1 0
1544--1573	54	1 0 1 0 0 1 0 0
1573--1601	55	1 0 1 0 1 0 1 1
1601--1630	56	1 0 1 0 1 1 1 0
1630--1658	57	1 0 1 1 0 1 1 0
1658--1687	58	1 0 1 1 1 1 1 1
1687--1716	59	1 1 0 0 0 1 1 1
1716--1744	60	1 1 0 0 1 1 1 1
1744--1773	61	1 1 1 0 0 0 1 0
1773--1801	62	1 1 1 0 1 1 [illegible]

8223 PROGRAMMING PROCEDURE

The 8223 may be programmed by using Curtis Electro Devices PR 23 Series or Spectrum Dynamics 300, 400 or 500 Series Programmers. Each performs the procedure outlined.

The 8223 Standard part is shipped with all outputs at logical "0". To write a logical "1" proceed as follows.

Programming Procedure A

Simple Programming Procedure using "bench" Equipment

1. Start with pin 8 grounded and V_{CC} removed from pin 16.
2. Remove any load from the outputs.
3. Ground the Chip Enable.
4. Address the desired location by applying ground (i.e., 0.4V maximum) for a "0", and +5.0V (i.e., +2.8V minimum) for a "1" at the address input lines.
5. Apply +12.5V to the output to be programmed through a 390 ohm ±10% resistor. Program one output at a time.
6. Apply +12.5V to V_{CC} (pin 16) for up to 1.0 second. If 1.0 second is exceeded, the duty cycle should be limited to a maximum of 25%. The V_{CC} overshoot should be limited to 1.0V maximum. If necessary, a clamping circuit should be used. The V_{CC} current requirement is 400 mA maximum at +12.5V. Several fuses can be programmed in sequence until 1.0 sec of high V_{CC} time is accumulated before imposing the duty cycle restriction.
   NOTE: Normal practice in test fixture layout should be followed. Lead lengths, particularly to the power supply, should be as short as possible. A capacitor of 10 microfarads minimum, connected from the +12.5V to ground, should be located close to the unit being programmed.
7. Remove the programming voltage from pin 16.
8. Open the output.
9. Proceed to the next output and repeat, or change address and repeat procedure.
10. Continue until the entire bit pattern is programmed into your custom 8223.

Fast Programming Procedure – Programming Procedure B

1. Remove V_{CC} (open or ground pin 16).
2. Remove any load from the output.
3. Ground CE (pin 15).
4. Address the word to be programmed by applying 5 volts of a "1" and ground for a "0" to the address lines (Solid TTL logic levels are ok, but we suggest buffer drivers or Utilogic OR/NOR gates for the addressing).
5. Apply 12.5V to the output to be programmed through 390 ohm ±10% resistor. Program one output at a time.
6. Apply +12.5V to V_{CC} (pin 16) for 25-50mS. Limit the V_{CC} overshoot to 1.0 volts max.
7. Reduce V_{CC} to ground (or open) and remove the load from the output.
8. Immediately repeat steps 5 and 6 for other outputs of the same word, or repeat 4 through 6 for a different word. Continue programming for a max of 1 second. Then remove power for 4 seconds and continue until the entire bit pattern is programmed.

After programming the 8223, the unit should be checked to insure the code is correct. If additional fuses must be opened, they may be programmed during verification.

Fast Programming Procedure – Programming Procedure C

Steps 1 through 5 are the same as in Procedure B.

6. Apply a 5mS pulse to V_{CC} (pin 16). Limit the V_{CC} overshoot.
7. Reduce V_{CC} to 5 volts for 10-15uS and verify the fuse opened (output is now a "1". If the bit programmed go on to the next bit to be programmed. If the bit did not program, then reduce V_{CC} to ground (or open) for 1-5uS and repeat step 6 and 7 until the fuse programs (1 second total time max).
8. Continue programming at this rate for 1 second. Remove all power from the device for 4 seconds then continue programming procedure.

V_{CC} Waveform

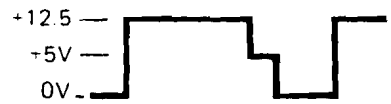

BOARD LEVEL PROGRAMMING PROCEDURE FOR THE 8223

The chip select controls which 8223 is being programmed when several PROMS are collector OR'd. To program in this manner, the only changes required are:

1. The 390 ohm resistor is reduced to $\frac{200 \text{ ohm}}{N}$ where N is the number of outputs tied together ($2 \leq N \leq 12$).
2. Reduce max fuse pulse width from 1 second max to 0.92 sec max.

MANUAL PROGRAMMER DIAGRAM

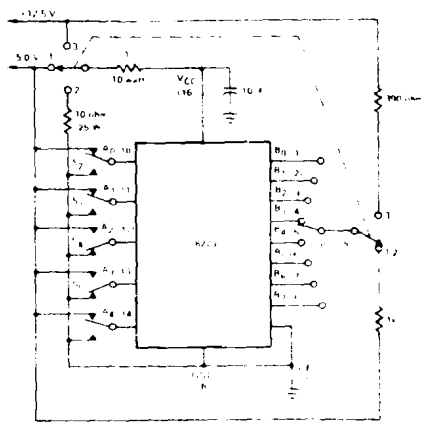

S_1 = Single pole 9 position switch

S_2 through S_6 = single pole 2 position switch

S_7 = Two pole 3 position switch with ground connected to the middle position of the section connected to V_{CC} pin 16 to go from 5 volts to 12.5V the switch will momentarily ground V_{CC}) and positions 1 and 2 of the other section connected to 5.0V to provide the needed 5 volts to the output for verification

NOTE 1 The 10μf capacitor across pin 16 to ground is required to eliminate noise from V_{CC}.

UNIVERSITY OF MASSACHUSETTS/AMHERST
ENERGY ALTERNATIVES PROGRAM

UNIVERSITY OF MASSACHUSETTS/AMHERST

ENERGY ALTERNATIVES PROGRAM

A GENERAL DESCRIPTION OF THE BLADE-PITCH CONTROLLER

by

Bruce A. Caccamo

U.Mass. Wind Furnace
Energy Alternatives Program
University of Massachusetts
Amherst, Massachusetts 01002

TR/76/ 6
Appendix VIII

A GENERAL DESCRIPTION OF THE BLADE-PITCH CONTROLLER

Abstract

The blade-pitch controller provides for maximum energy transfer between the wind and the windmill under varying wind conditions. The purpose of this paper is to define the necessary regions of control and the methods which permit stable operation through blade-pitch control.

The blade-pitch controller provides for maximum energy transfer between the wind and the windmill under varying wind conditions. In order to understand how the controller does this, we must first look at the overall structure.

The windmill is free to rotate in yaw on a platform so that the blades are always facing into the wind. Thre are three blades, which are controllable in pitch. The rotor is connected through a speed-up drive to a 25 kW generator.

Relative to windspeed there are four distinct regions of pitch control. In region 1 (0-5 mph) the pitch controller will be called upon to position the blades at an angle of attack which will provide the greatest starting torque. For these wind speeds, the pitch angle is set at minus eight degrees. In region 2, (5-26 mph) the controller will maintain the pitch angle at minus eight degrees. This will bring the generator up to speed in the shortest possible time and will deliver the maximum power at any given wind speed. In region 3 (26-45 mph) the controller maintains the generator speed at 1800 RPM. Without the controller, the generator would overspeed and trip off the line. In region 4 (above 45 mph) the controller has to feather the windmill blades. This amounts to shutting down the system to prevent destruction under high winds.

Through computer analysis, the power output curve has been related to pitch angle through the tip speed ratio (see blade-pitch schedule, Figure 1). The tip speed ratio ($\Omega R/V$) is the actual control signal used in the pitch-control circuitry to represent the desired pitch angle.

As the four control regions are transversed, the tip speed ratio will increase from 0 to 7 and then decrease to 0. As wind speed increases from 0-5 mph, the tip speed ratio increases until it reaches 7. This point represents the beginning of region 2 where generator RPM will increase with increasing windspeed. Throughout this region the blade pitch will be maintained at minus eight degrees which is equivalent to $\Omega R/V = 7$. At 26 mph the generator will reach rated RPM, and $\Omega R/V$ will start to decrease as wind speed increases. This occurs because the tachometer output is clamped at 20 volts. Thus, as wind speed increases, $\Omega R/V$ will decrease and blade-pitch will increase until reaching the feathered position at a windspeed of 45 mph. It should be noted that the controller can be commanded to feather sooner if desired (see Dwg.03. 02.01).

The pitch controller is actually a pulse-width modulated (PWM) transistor switching amplifier. (see Dwg. 03.02.01) It uses a DC power supply which the amplifier switches on and off at a fixed frequency. The wider the width of the driving pulse; the higher will be the average current delivered to the motor; and the faster the motor will turn. PWM provides a continuous fine control of the pitch angle.

Pulse-width modulation is obtained by comparing the desired pitch angle signal ($\Omega R/V$) with a triangle wave. The triangle wave is obtained by integrating a square wave. The length of time in which the voltage level of the

triangle wave is greater than that of R/V determines the width of the driving pulse (see Figure 2). A similar comparison is made between this same triangle wave and a feedback signal which represents the actual position of the blades. These two pulse-width modulated signals are then compared (they are 180 degrees out of phase with each other); thus, providing the driving signal for the motor. The motor will turn in the direction which will equate the actual angle with the desired angle.

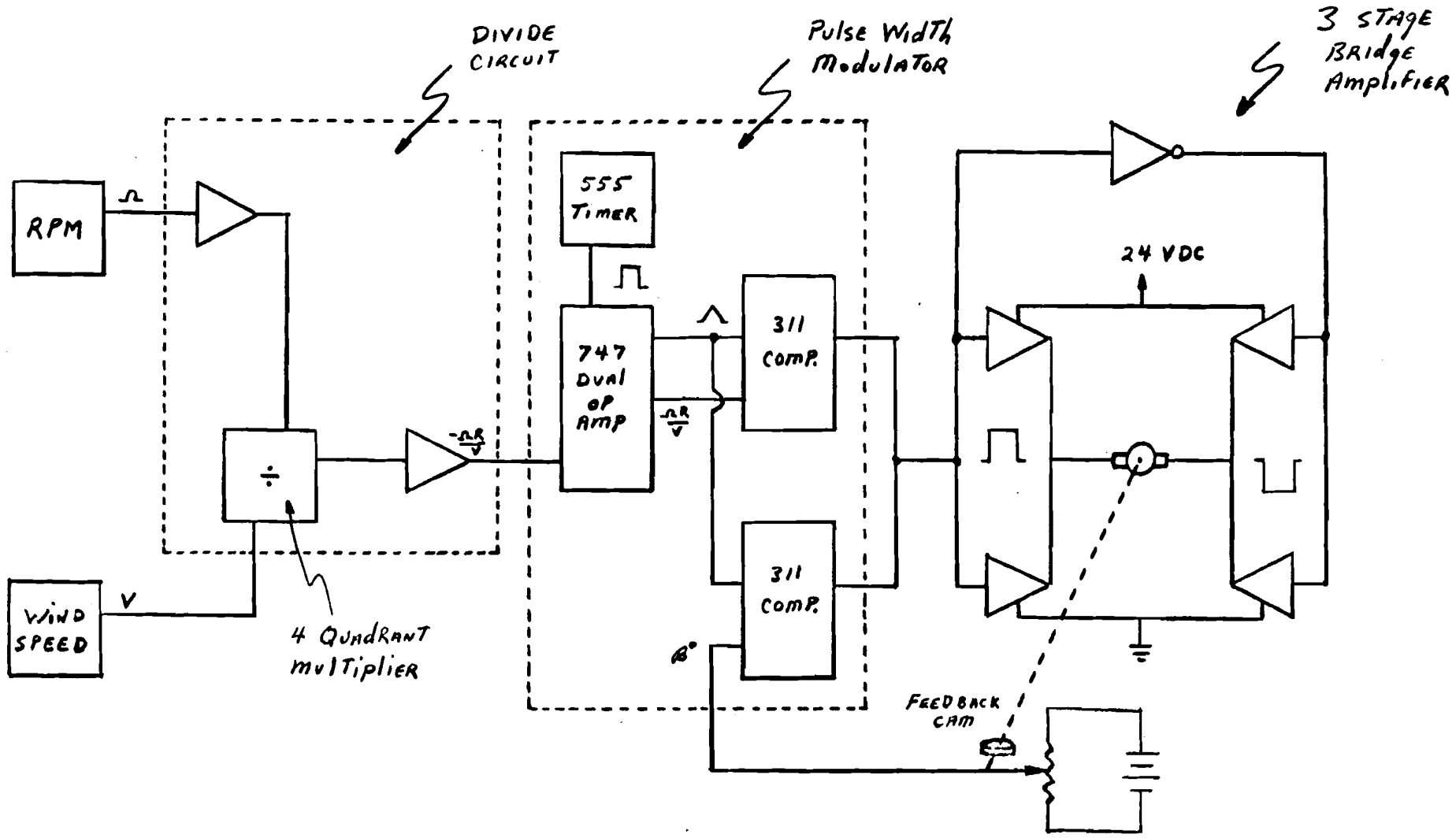

ENERGY ALTERNATIVE PROGRAM

UNIVERSITY OF MASSACHUSETTS

Blade - Pitch Controller

Block Dingram

DRAWING NO. 03.02.01

DATE 3/20/76 DRN. BY B. Cassant

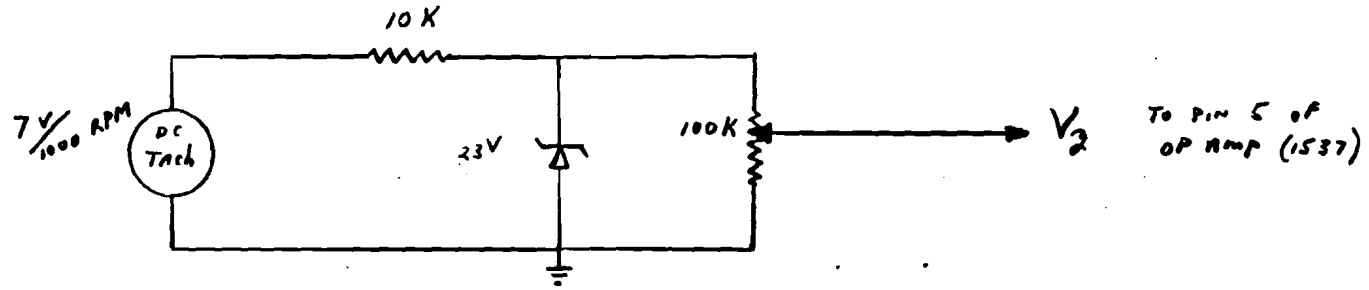

NEW RPM CIRCUIT

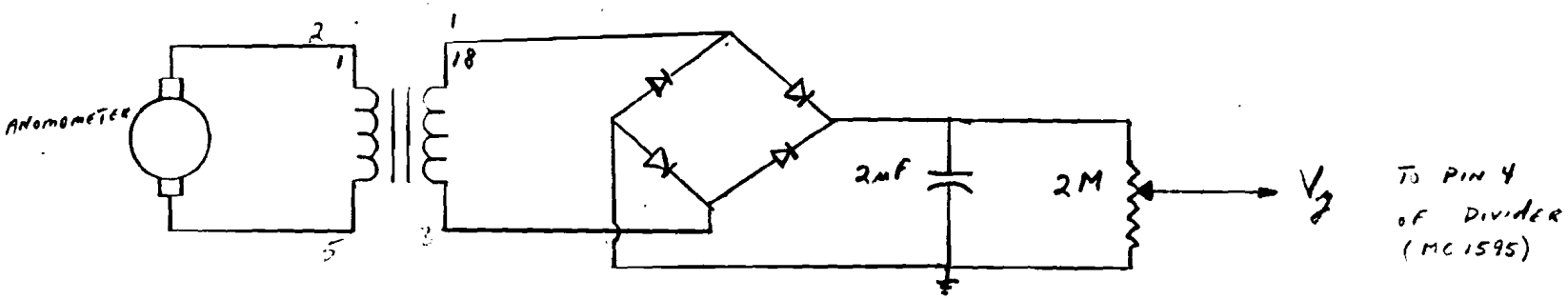

WIND SPEED CIRCUIT

ENERGY ALTERNATIVE PROGRAM

UNIVERSITY OF MASSACHUSETTS

Wind Speed + RPM Circuits

DRAWING NO. 03.02.02

DATE 3/20/76 DRN. BY B. Cascone

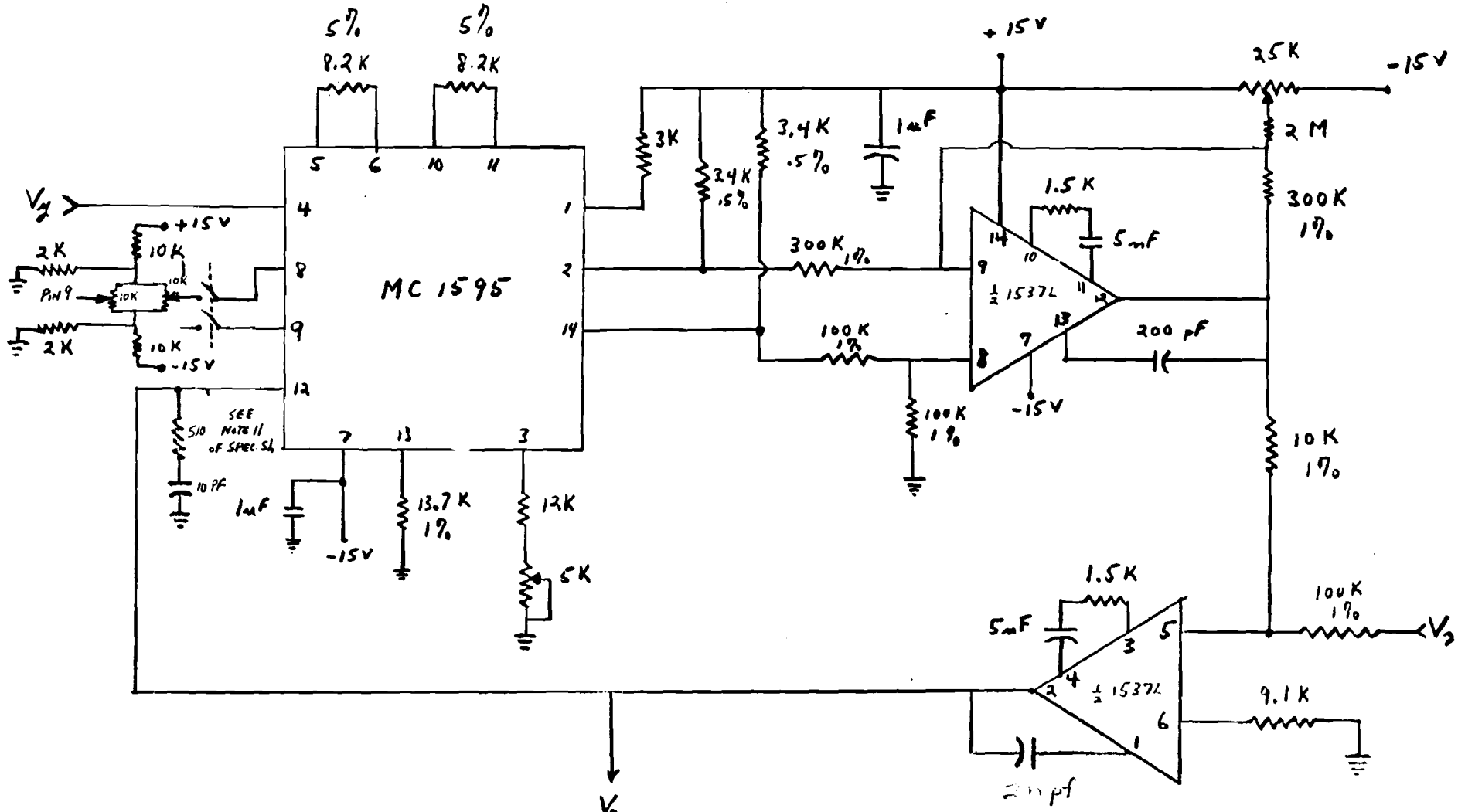

$V_o = -V_z/V_y$

$V_z = \omega R$

$V_y = V$ = wind speed

$\frac{\omega R}{V} = V_o$ = Tip speed ratio

$0 < V_z < 25v$

$0 < V_y < 5v$

ENERGY ALTERNATIVE PROGRAM

UNIVERSITY OF MASSACHUSETTS

Divider Circuit

DRAWING NO. 03.02.03

DATE 3/20/76 DRN. BY B. Cavanaugh

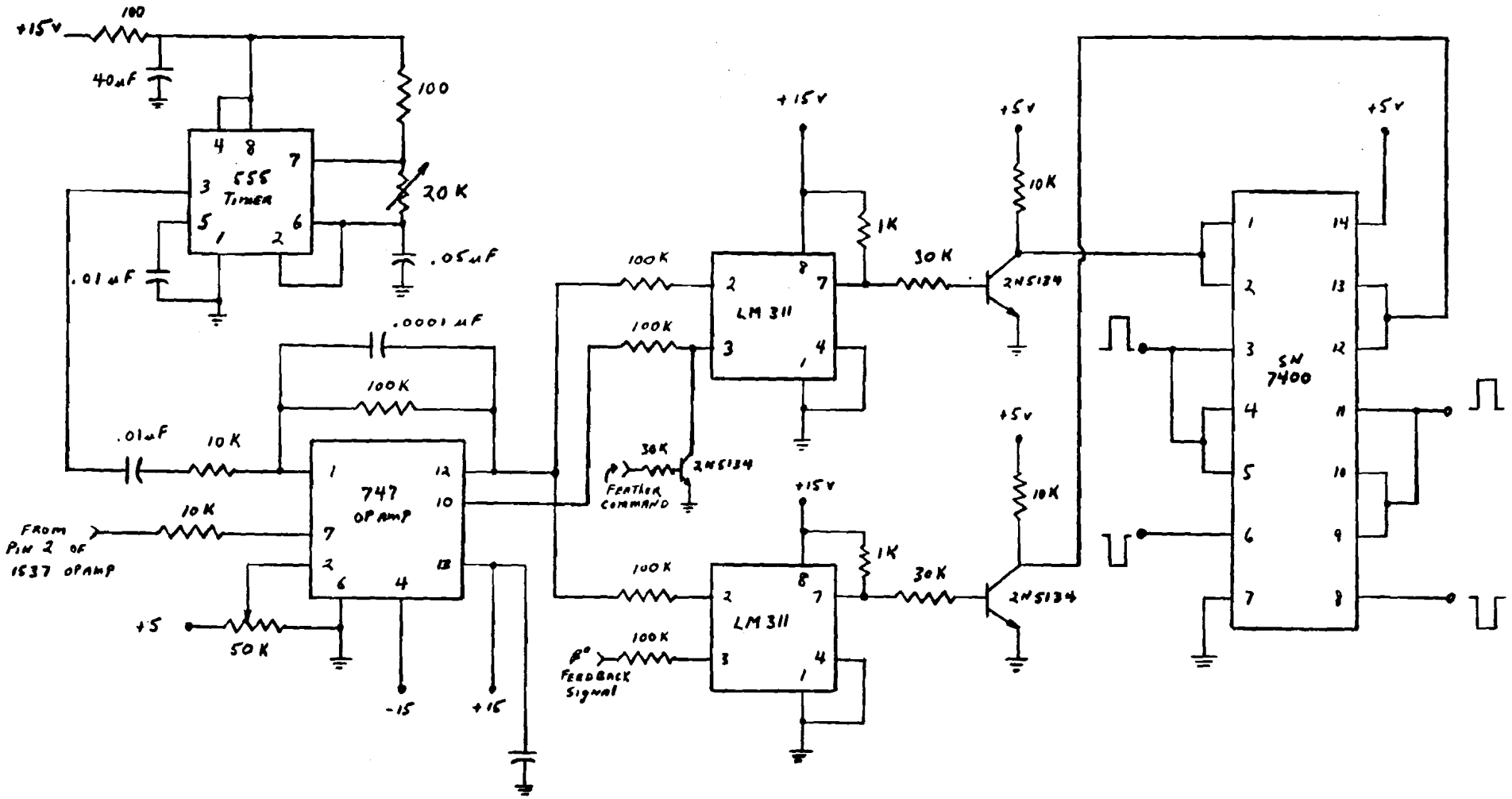

ENERGY ALTERNATIVE PROGRAM

UNIVERSITY OF MASSACHUSETTS

Pulse-Width Modulator

DRAWING NO. 03.02.04

DATE _____ DRN. BY _____

ENERGY ALTERNATIVE PROGRAM

UNIVERSITY OF MASSACHUSETTS

DRAWING NO. 03.02.05

DATE 3/20/76 DRN. BY B. Carlisle

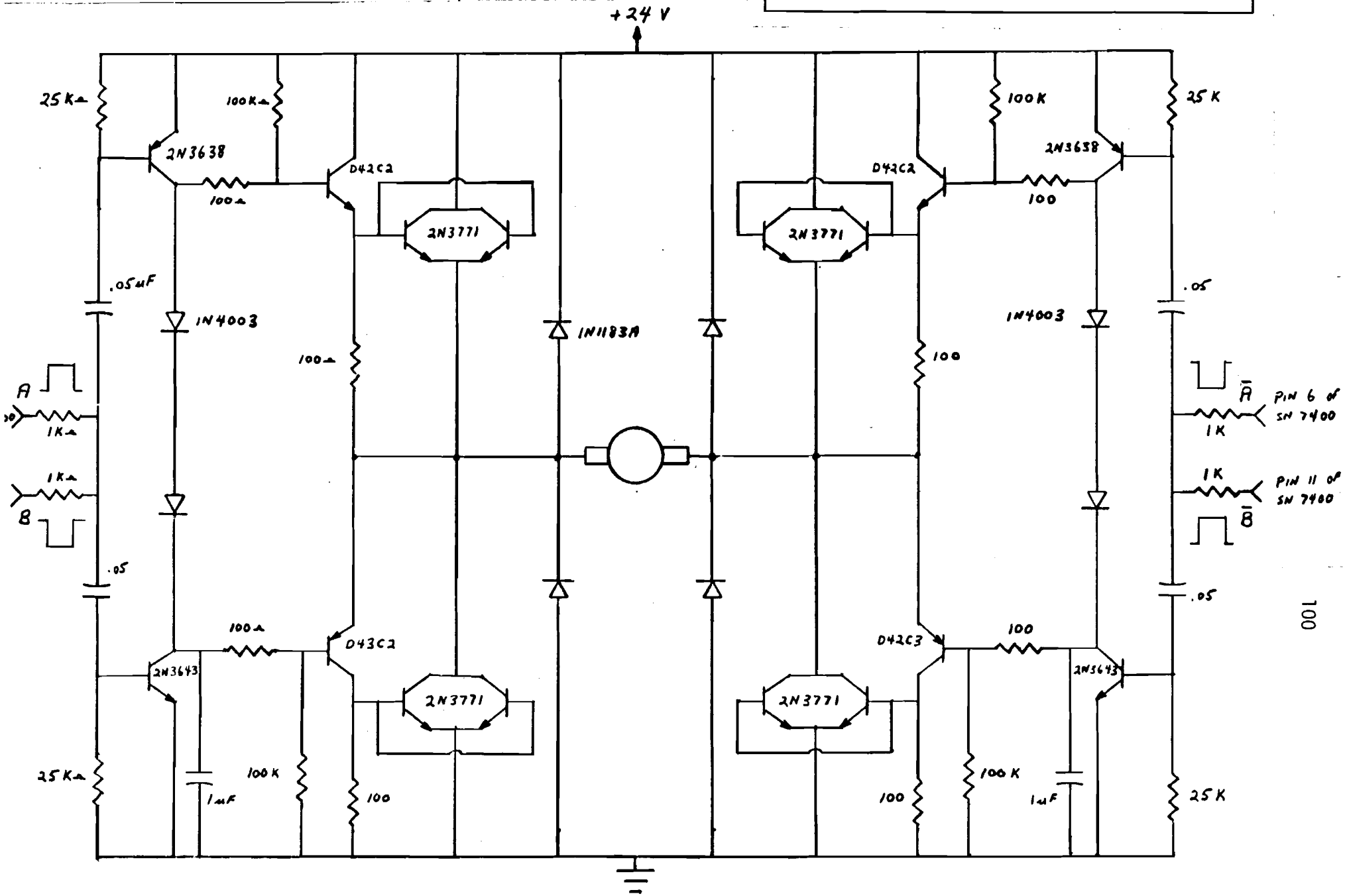

100

Power out vs Wind Speed

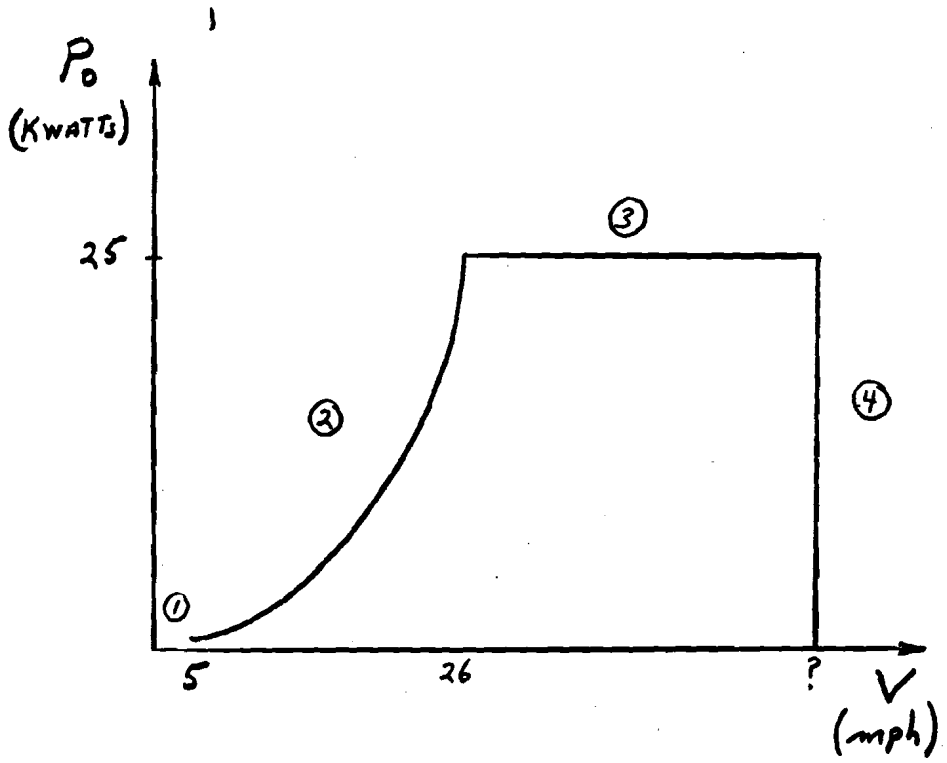

The Maximum Power Output Curve

Blade Pitch vs Tip-Speed Ratio

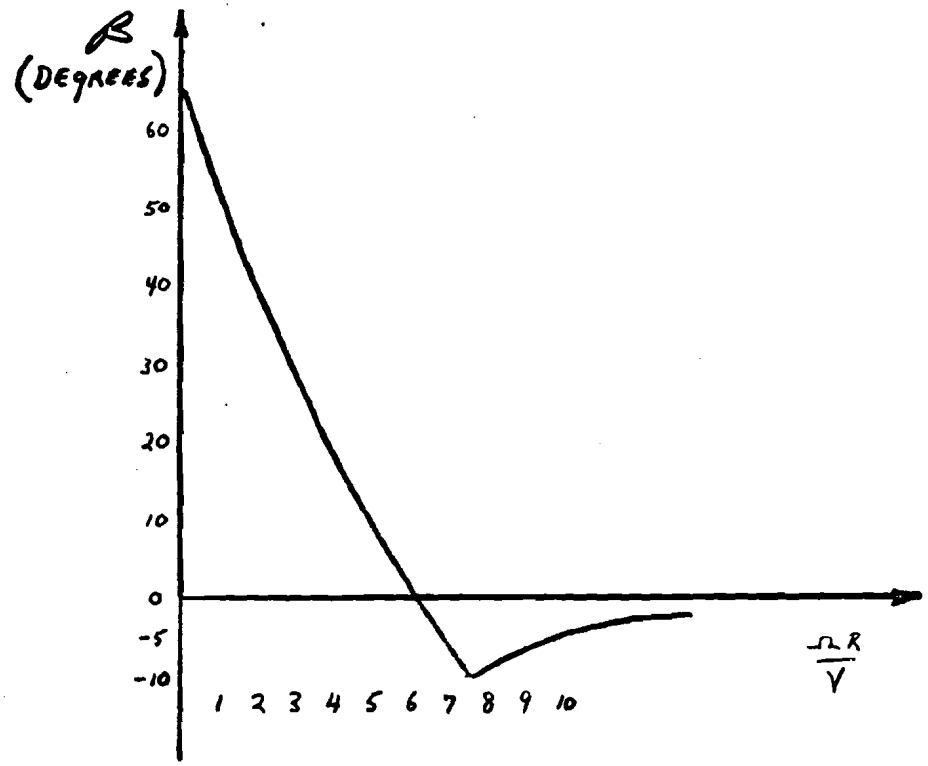

The Blade Pitch Schedule for Maximum Torque

Figure I

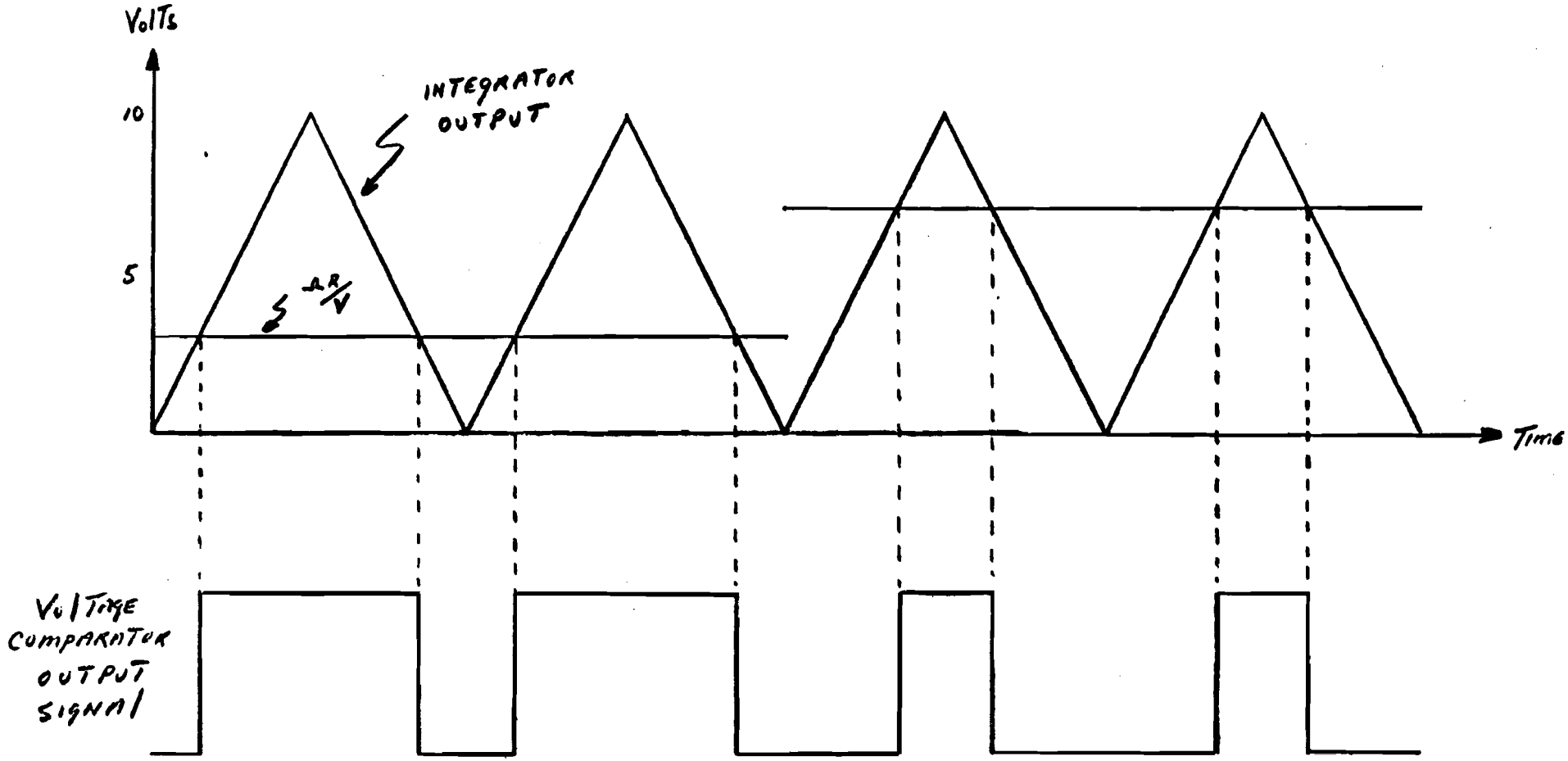

Pulse Width Modulation

Figure II

UNIVERSITY OF MASSACHUSETTS/AMHERST
ENERGY ALTERNATIVES PROGRAM

UNIVERSITY OF MASSACHUSETTS/AMHERST

ENERGY ALTERNATIVES PROGRAM

PRELIMINARY REPORT

THERMAL SYSTEMS

WIND FURNACE PROJECT

by

Jon G. McGowan
and
Ghazi Darkazalli

U.Mass. Wind Furnace

Energy Alternatives Program

University of Massachusetts

Amherst, Massachusetts 01002

April 1975

TR/76/7
Appendix IX

Work in the area of thermal systems can be divided into two categories: analytical modeling work and experimental work. The analytical modeling has formed the basis for the experimental design and a summary of its key points follows. (With the completion of the economic part of this work, a more detailed technical report on this subject will be issued.)

1. ANALYTICAL MODEL

A. Description of the Overall System Configuration

The analytical model is based on a mathematical simulation using a digital computer to determine the feasibility and performance of using wind heating systems for home heating and domestic hot water demands. Also, the possibility of combining the wind systems with a flat-plate solar collector sub-system is investigated. The basic wind energy input component for all systems is a horizontal axis wind machine.

The performance of the heating systems, for a given site and weather conditions, is studied as a function of the following key system parameters: 1) the wind generator blade diameter, 2) the wind generator tower height, 3) the size of the residential heating delivery system, 4) the size of the solar collector, and 5) the size of the thermal storage water tank. A detailed economical analysis of the total cost, for each of the systems studied will be based on the assumption of mass produced unit manufacturing. The description of the different system models follows.

(1) Model I.

Model I is the simplest windpower system (Fig. 4.1). It has no energy storage and electrical energy is delivered to the house directly from the

wind generator using electric baseboard heaters. In case there is not enough electric energy generated to keep the house at room temperature an auxiliary heating system is switched on. If at any time the electric energy generated exceeds the house heating demands, the excess energy is used for domestic hot water heating (optional).

(2) Model II.

In addition to the wind generator this system (Fig. 4.2) has a water thermal storage and a liquid to air baseboard heaters. This system's operational procedure is similar to Model I except that the electrical energy from the wind generator is transferred to the storage tank by means of resistance heaters. Heat then is delivered from the storage to the house by circulating hot water through the baseboard heaters.

(3) Model 3-A.

This system has two energy sources and one thermal storage (Fig. 4.3). A flat plate solar collector sub-system is added to the wind system described in Model II. This collector sub-system consists of a flat plate collector, a water-to-water heat exchanger and a circulating pump. Both wind and solar energy collected are delivered to the storage tank and then, using the same heat delivery system as in Model II, thermal energy is transferred to the house.

(4) Model 3-B.

This system is similar to Model 3-A except that this model uses two separate thermal storage tanks (Fig. 4.4), one for wind energy and the other for solar energy. In order to operate the collector at its highest efficiency, this model gives priority to delivering energy from the solar

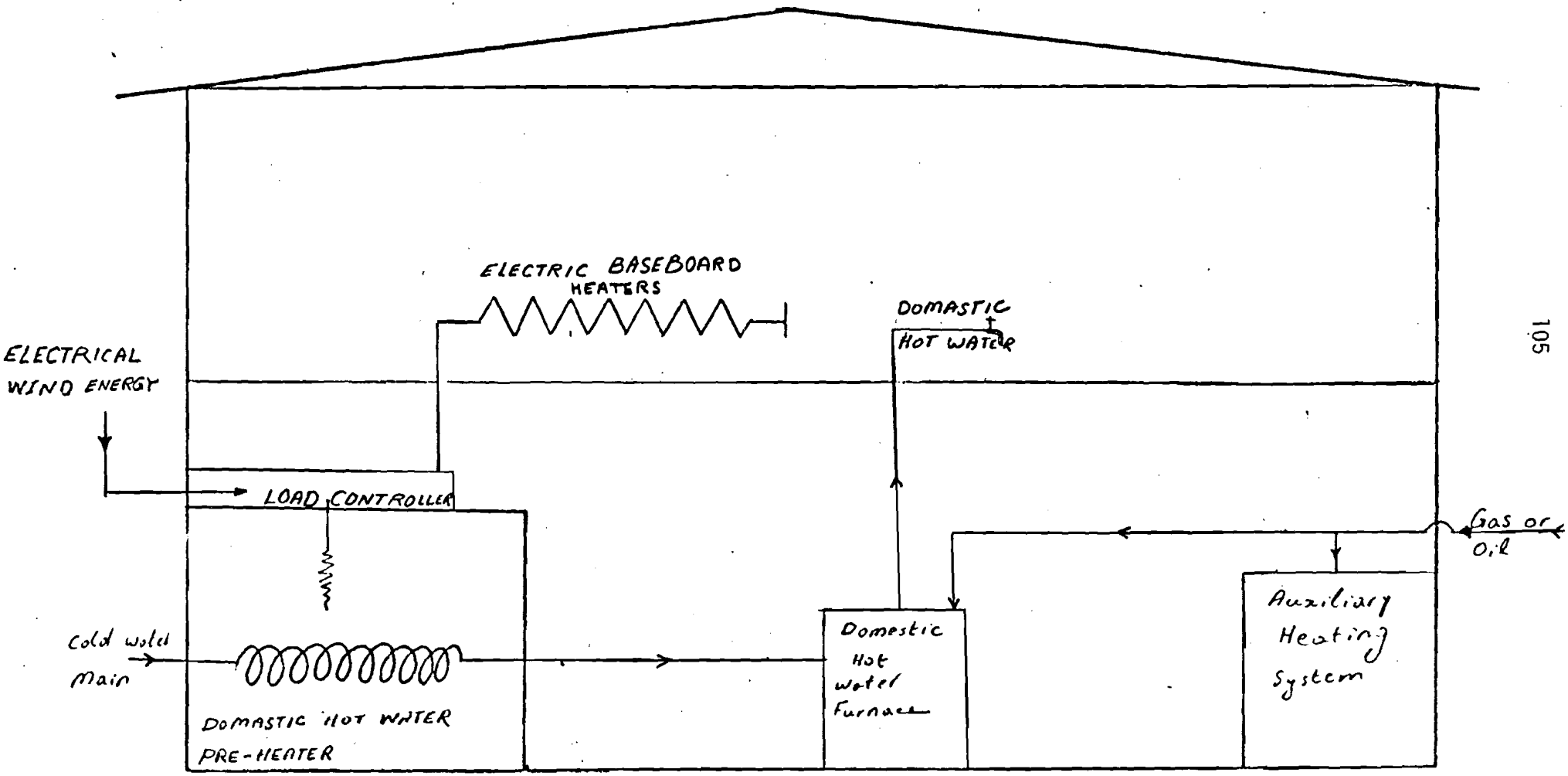

Model 1

FIG. 4.1

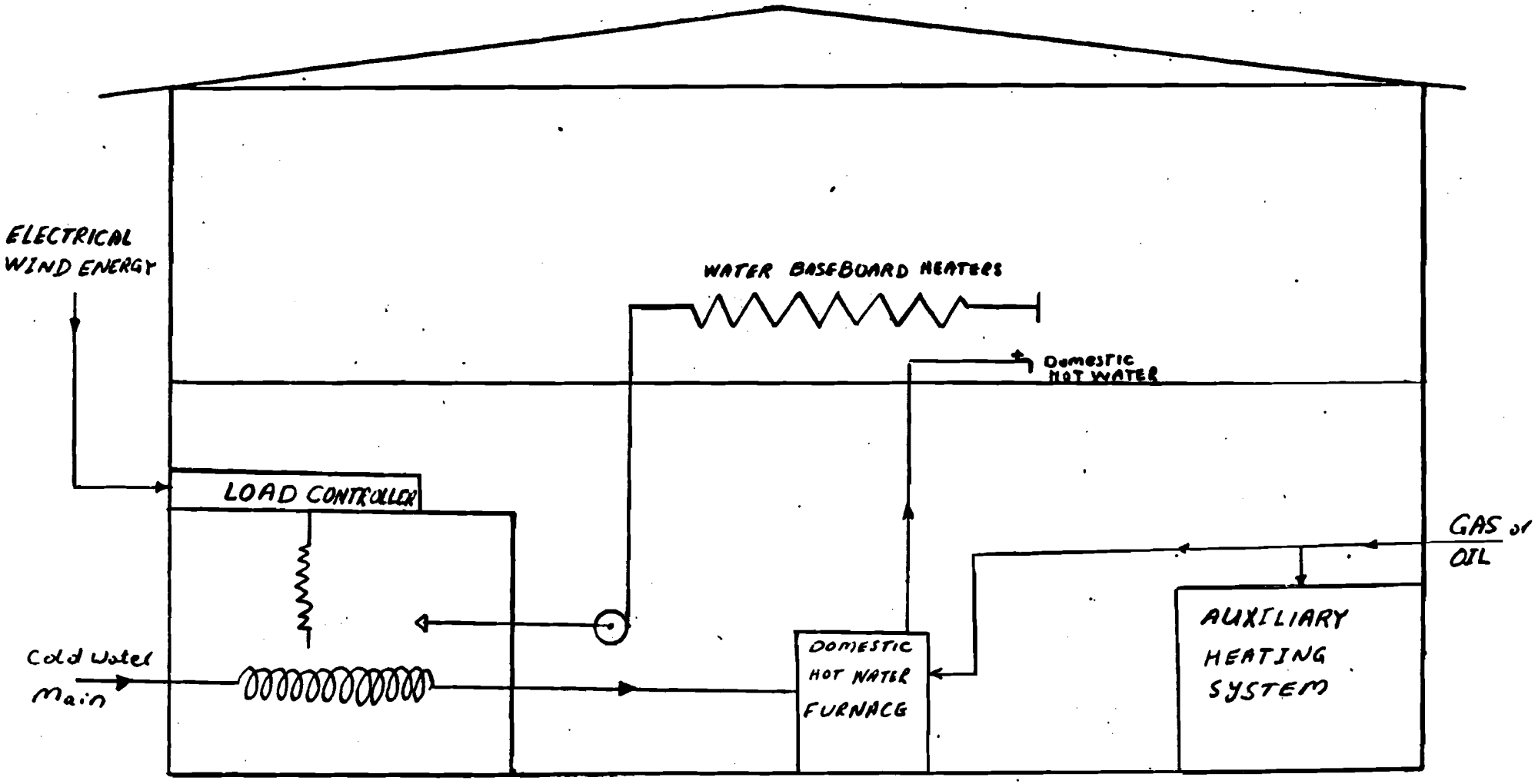

Model 2 FIG. 4.2

storage tank to the house. When the temperature of the solar storage is less than the desired lower limit, then the system will deliver energy from the wind storage tank. The two storage tanks are connected to each other via a mixing pump which is used when the temperature of one of the storage tanks is higher than the upper limit.

(5) Domestic Hot Water Model.

This model is used, in conjunction with the previous models, to investigate the possibility of using the wind and solar systems to provide the domestic hot water requirement of a residential home.

B. System Components Description

Since the overall system performance is a function of each individual component, a detailed physical model and mathematical analysis has been developed for the following basic components: the electric wind generator, the flat-plate solar collector, the thermal water storage tank, the house, and the baseboard heat exchangers. Also, it includes a derivation of the maximum windpower delivered by a wind generator as a function of the wind velocity, generator blade diameter, and generator efficiency. In addition, based on available data, the useful solar energy is determined. Also, an energy balance equation for the control volume around a storage tank is derived. The hourly heating demands are calculated using basic principles of thermodynamics and heat transfer, and standard ASHRAE practice. The amount of heat transferred to the house by the heat delivery system is calculated as a function of the size and characteristics of the internal heat exchangers.

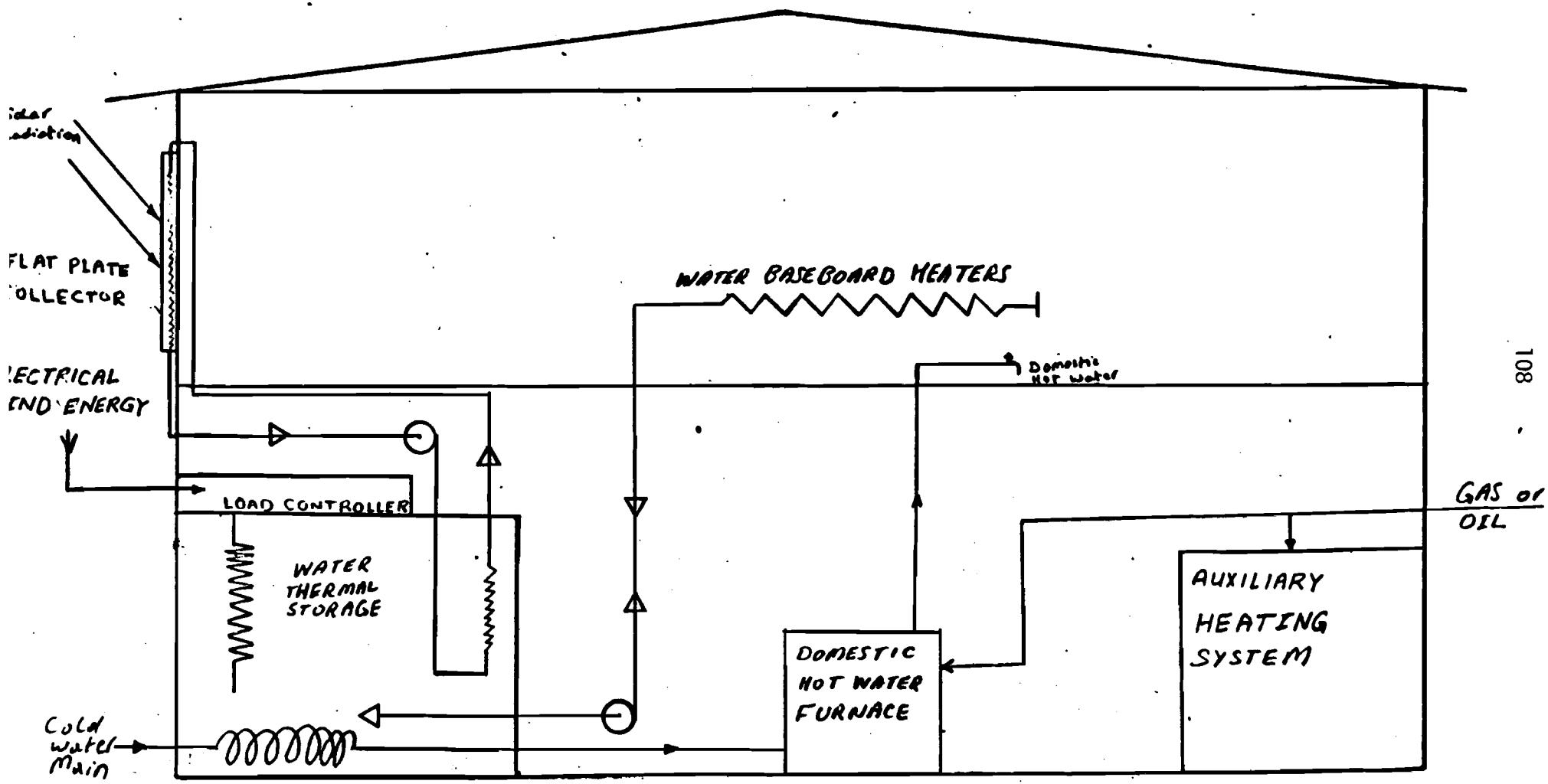

Model 3A

FIG. 4.3

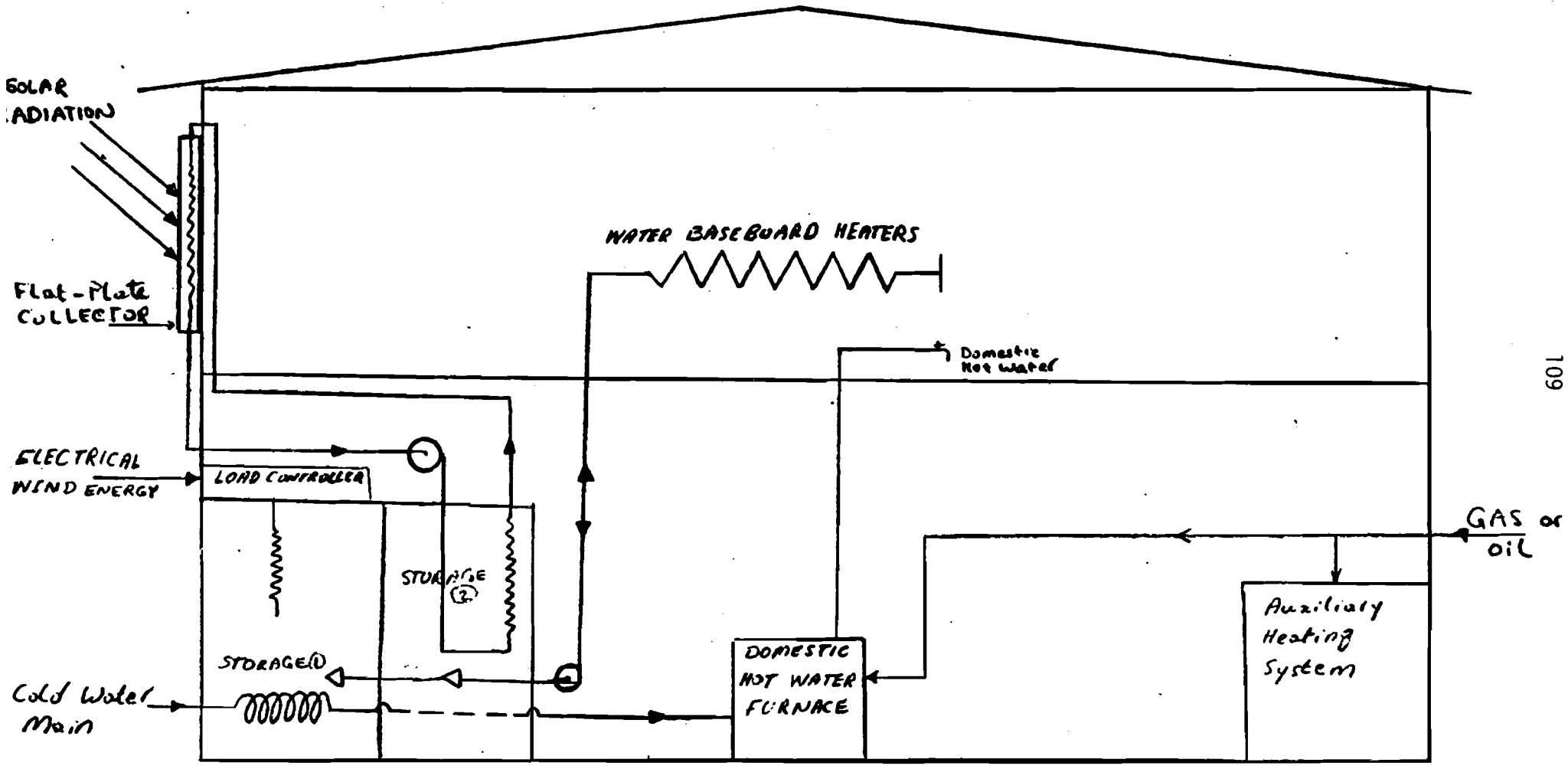

Model 3B FIG. 4.4

C. Digital Computer Analytical Models

Because of the variety of models tested and the number of different component configurations the computer models includes the following program and sub-programs: 1) a main program which specifies the model, the system configuration, and the initial conditions of the various components. Also, the program combines the other sub-programs to determine the system performance (Fig. 4.5), 2) a data sub-program which includes the weather and solar data for a given site, 3) a wind sub-program that calculates the windpower available, 4) a solar sub-program that calculates the useful solar energy available to the house, 5) a load sub-program which calculates the house heating load, 6) a heat exchanger sub-program which calculates the energy delivered by the baseboard heaters, and 7) a hot water sub-routine that determines the energy delivered by the system in a form of domestic hot water. The use of a specific sub-program depends on the system configuration of the model tested.

D. System Performance and Analtyical Results

A summary of the most important analytical results for the various models previously discussed follows. The results are based on maintaining the house inside temperature at 68°F. All systems are tested for both the average and model homes by varying key system parameters such as:

1) wind generator blade diameter
2) wind generator tower height
3) water storage tank size
4) the heat delivery system size
5) solar collector size

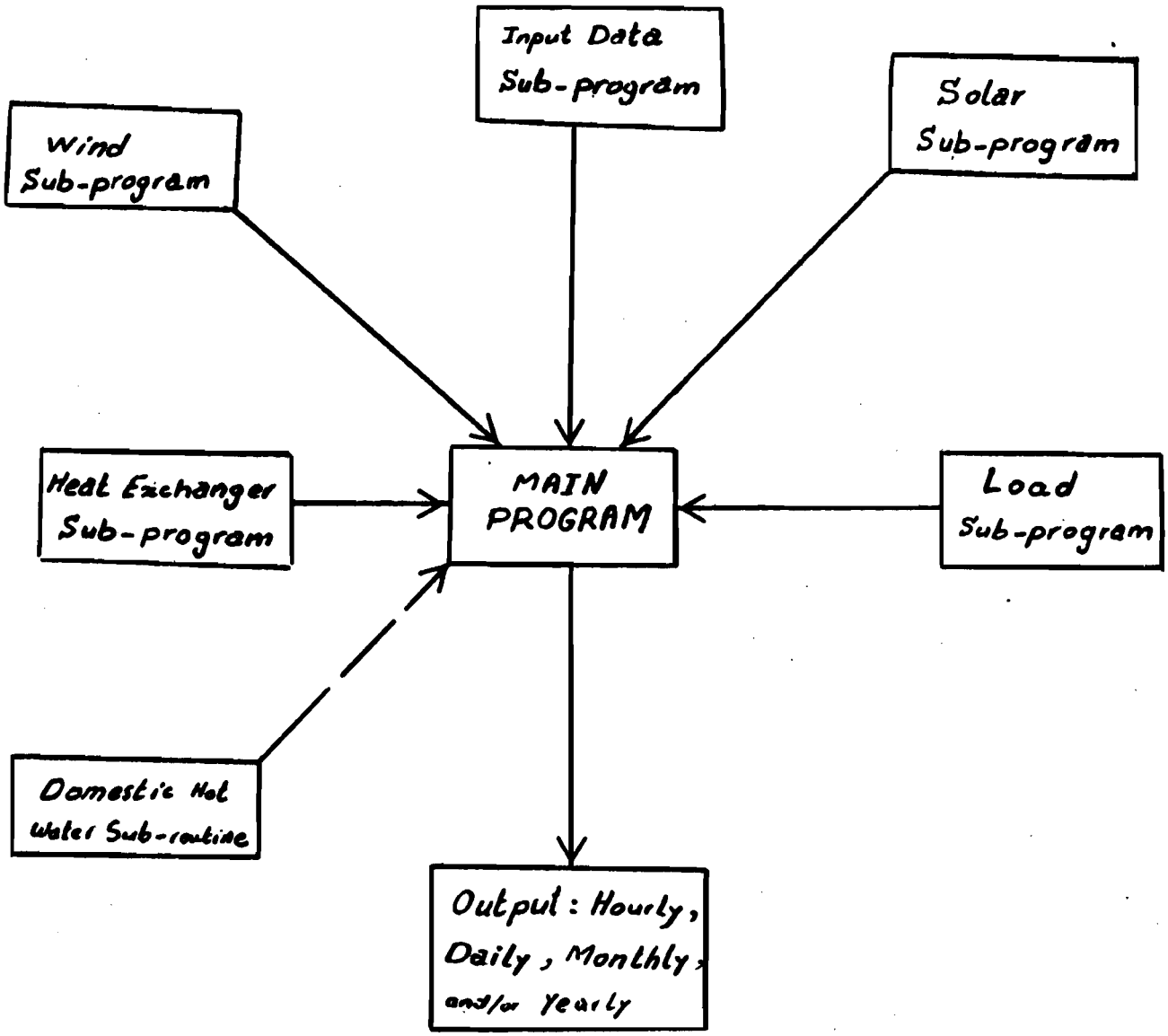

A Block Diagram of the Computer Model

FIG. 4.5

Table 4.1 represents a monthly summary of the heating load of both the average and model homes based on the weather data from Hartford, Conn. Figure 4.6 represents typical monthly values of the "average" home energy requirements and the input of the wind and solar systems. The representative windpower output shown in the figure is based on a 32.5 foot blade diameter wind generator placed on an 80 foot high tower. The solar energy input is given for a 200 square foot flat plate solar collector mounted vertically on the south wall of the house. Due to the interaction between the system components, and other losses, the amount of solar and wind energy the system delivers to the house is less than the energy inputs shown in the figure. To determine the exact amount of useful energy delivered by the system an hour-by-hour analysis is performed using the analytical model described previously.

To determine and compare the performance of the previously described models, a parameter (Q_{aux}/Q_{total}) is defined as the ratio of the energy delivered to the house from an auxiliary source to the total house heating energy requirements. Throughout the past year, a large number of computer runs for the Hartford wind data and Blue Hills, Mass. solar data were performed. This parameter serves to measure the energy performance of the various systems, and as a major input to future system economic studies. Figure 4.7 shows performance for the wind generator system without storage (Model 1) as a function of wind generator blade diameter and tower height (lower lines of each band represent 100 ft. tower heights). The performance of the windpower heating system with water thermal storage is summarized for varying storage sizes and blade diameters in Figures 4.8 and 4.9.

Month	Model House* (No Basement)	Average House* (SH-1) (Model with Basement)
SEPTEMBER	308.7	721.6
OCTOBER	826.1	1850.6
NOVEMBER	1841.1	3503.8
DECEMBER	2295.5	4829.3
JANUARY	3018.6	6272.1
FEBRUARY	2265.9	4746.1
MARCH	2172.8	4581.6
APRIL	1481.8	3186.2
MAY	817.9	1822.2
Total load for Heating Season	15028.4 kWhr	31913. kWhr

Table 4.1 - Residential Heating Requirements (for 6600 Degree Day Climate)

* These numbers might be changed slightly when the final house description is added to the program.

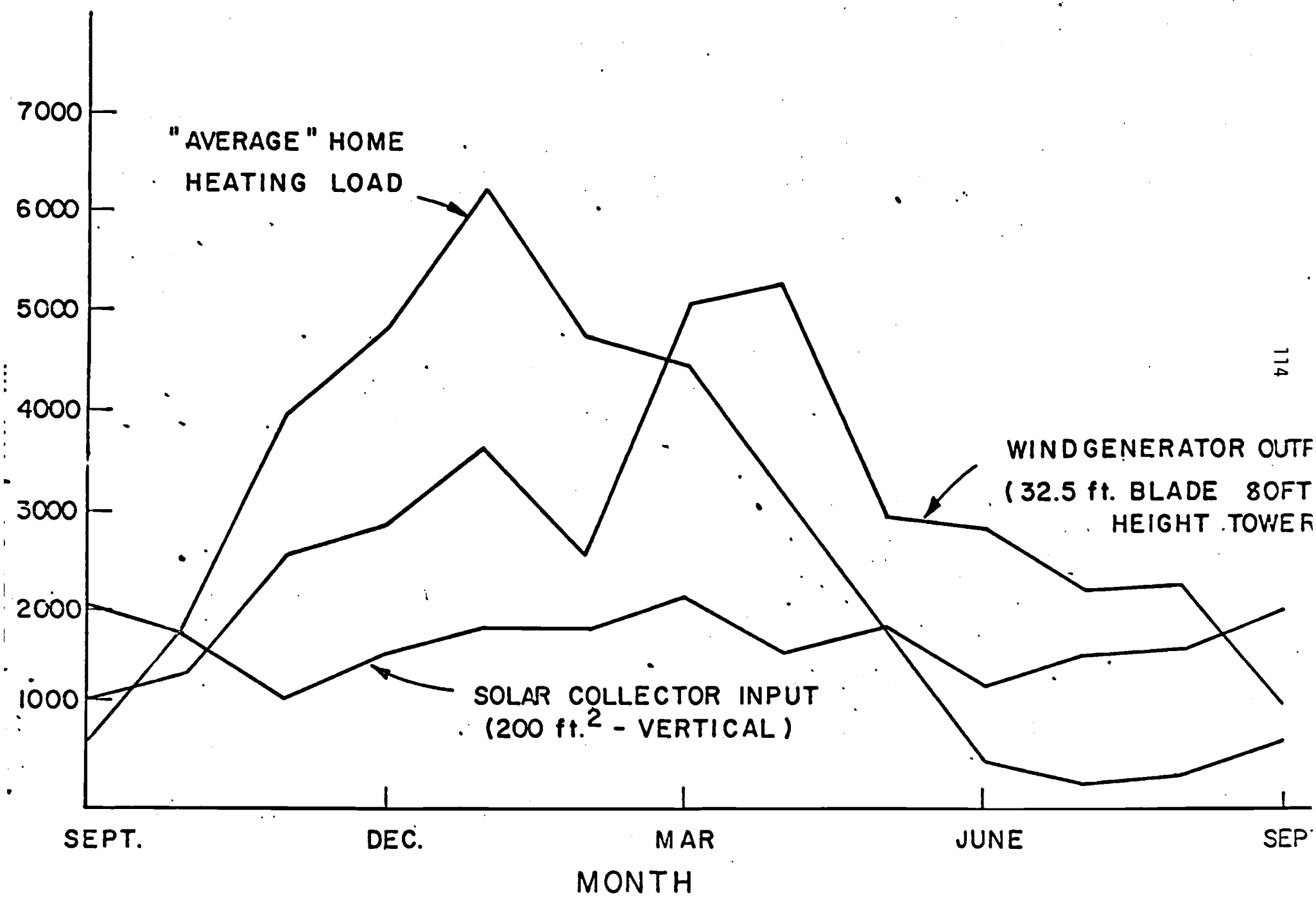
7000
6000
5000
4000
3000
2000
1000
"AVERAGE" HOME
HEATING LOAD
WINDGENERATOR OUTF
(32.5 ft. BLADE 80FT
HEIGHT TOWER
SOLAR COLLECTOR INPUT
(200 ft.^{2} - VERTICAL)
SEPT.
DEC.
MAR
JUNE
SEP
MONTH

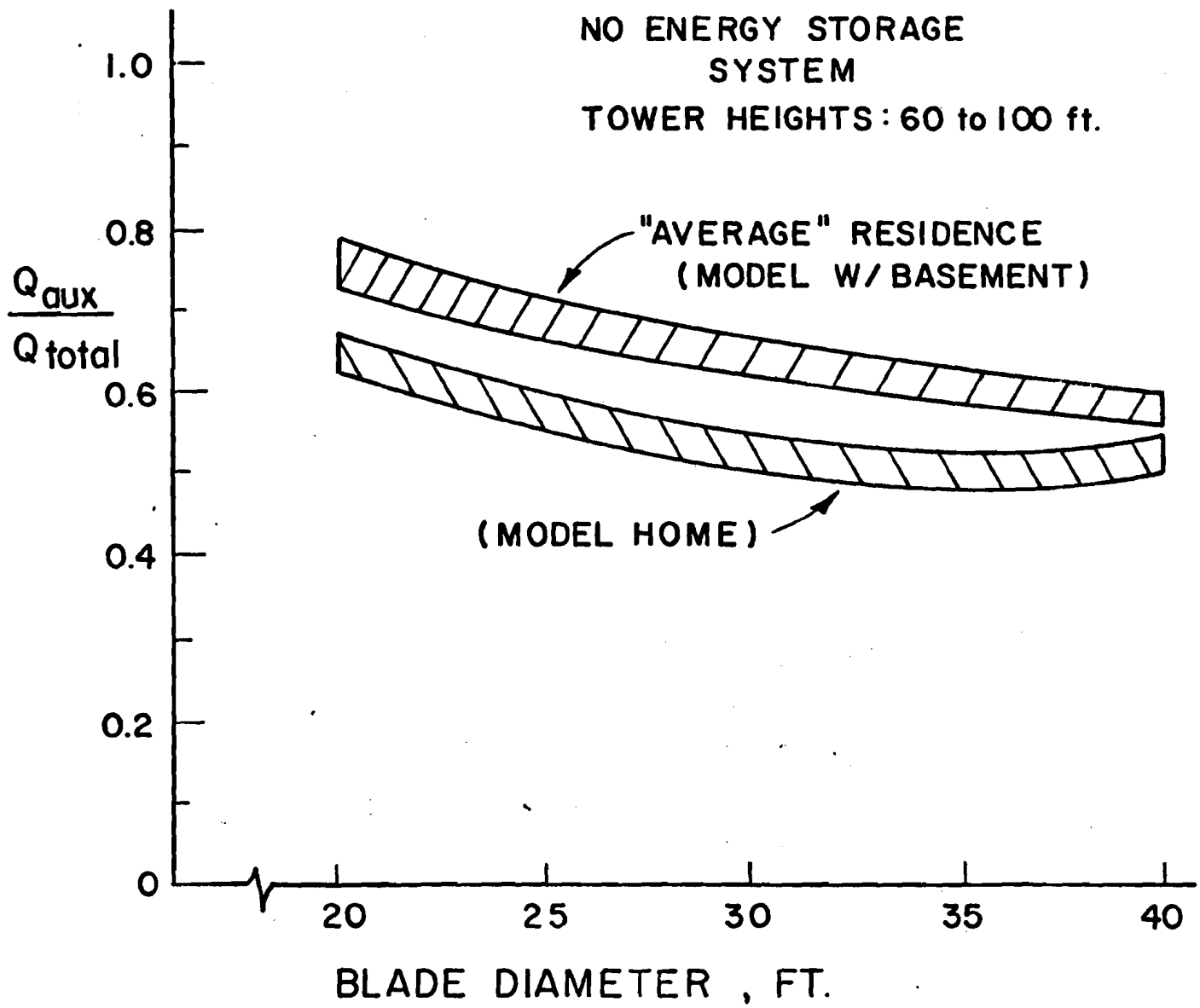
NO ENERGY STORAGE SYSTEM
TOWER HEIGHTS: 60 to 100 ft.
"AVERAGE" RESIDENCE (MODEL W/ BASEMENT)
(MODEL HOME)
Q aux / Q total
1.0
0.8
0.6
0.4
0.2
0
20
25
30
35
40
BLADE DIAMETER , FT.

FIG. 4.7

The modelling of the combined wind and solar heating system obviously opens up the possibility of varying more system parameters, thus it takes more graphs to show this system's performance. Figures 4.10 to 4.17 summarize a series of runs for this system. Figure 4.10 gives results for three house heating loads and varying collector size, with the system also supplying 50 gallons of hot water per day. Figure 4.11 shows the effect of storage size and blade diameter on system performance. Figures 4.12 to 4.14 present results for 3 different tower heights varying blade diameter and collector area. Figures 4.15 to 4.17 represent another way of showing these results.

The two tank storage system (Model 3B0 performance is shown in Figures 4.18 to 4.20. Figure 4.18 also shows the performance of solar-only and wind-only heating systems. From these series of analytical runs it is apparent that the added cost of the two tank system is not justified by a large corresponding increase in system performance.

With the increased availability of more wind and solar data at the end of the 1975-76 heating season, it is anticipated that a series of analytical runs using this new data will be carried out.

D. The Systems Economics Model

A detailed cost analysis of the various systems under consideration is presently in progress. This model includes a detailed cost analysis (present and future prices) of all the system component and installation costs. The total cost of the wind or wind and solar heating systems will include the acquisition costs of all systems components, and the cost of operation and maintenance. It is planned to optimize system cost, varying

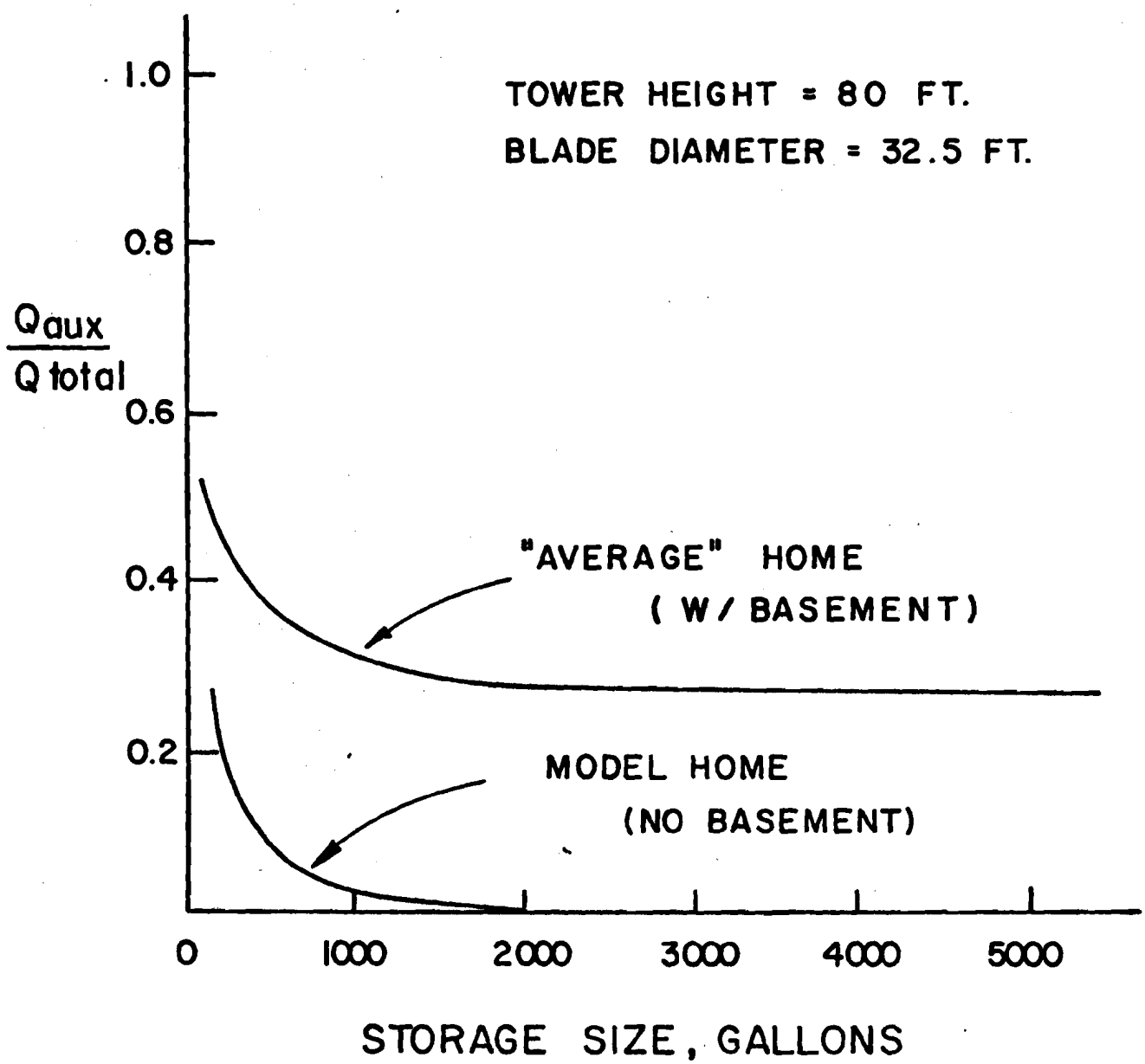
TOWER HEIGHT = 80 FT.
BLADE DIAMETER = 32.5 FT.
Qaux / Q total
1.0
0.8
0.6
0.4
0.2
"AVERAGE" HOME
(W/ BASEMENT)
MODEL HOME
(NO BASEMENT)
0
1000
2000
3000
4000
5000
STORAGE SIZE, GALLONS

FIG. 4.8

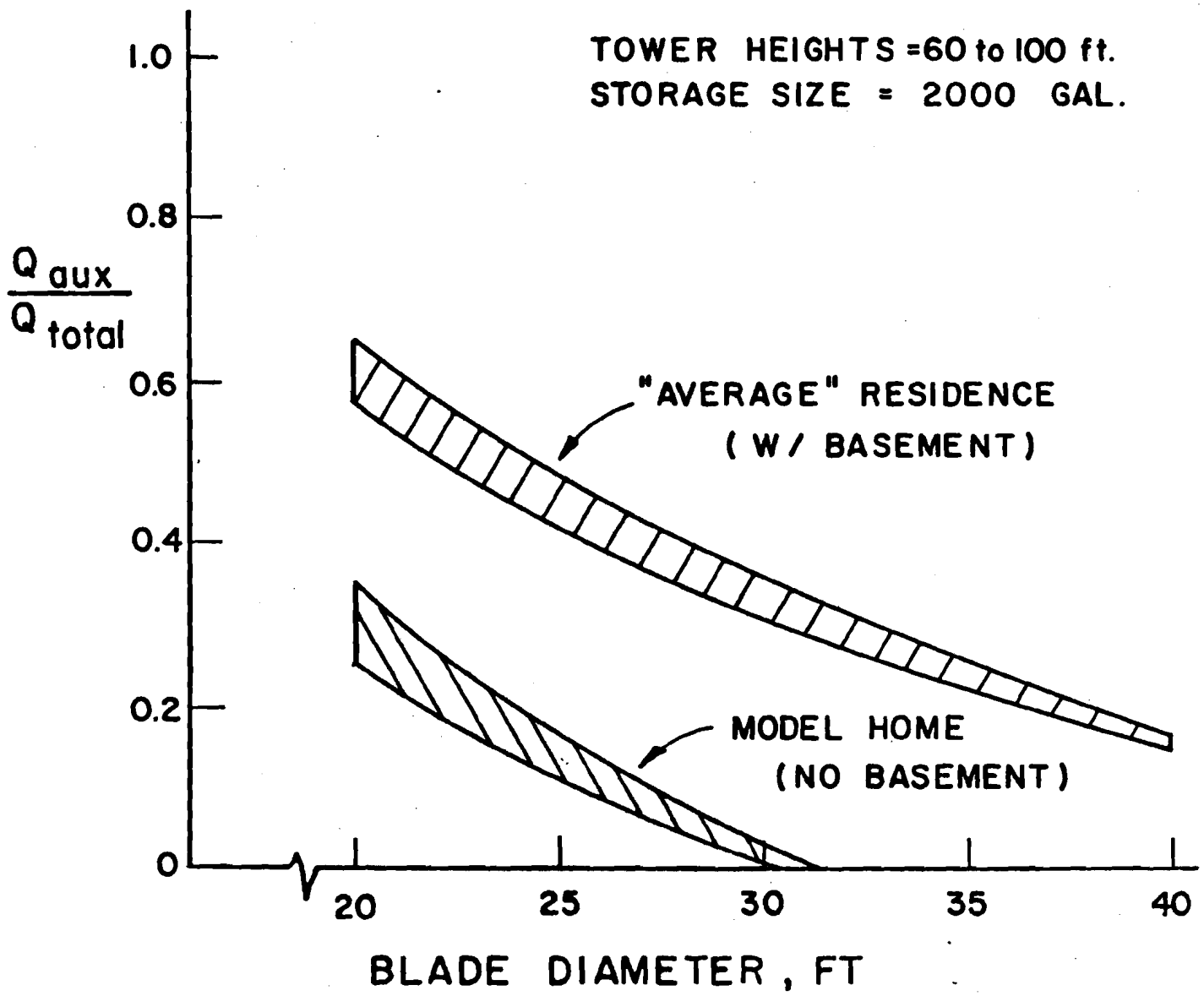
TOWER HEIGHTS =60 to 100 ft.
STORAGE SIZE = 2000 GAL.
1.0
0.8
0.6
0.4
0.2
0
Q aux / Q total
"AVERAGE" RESIDENCE
(W/ BASEMENT)
MODEL HOME
(NO BASEMENT)
20
25
30
35
40
BLADE DIAMETER, FT

FIG. 4.9

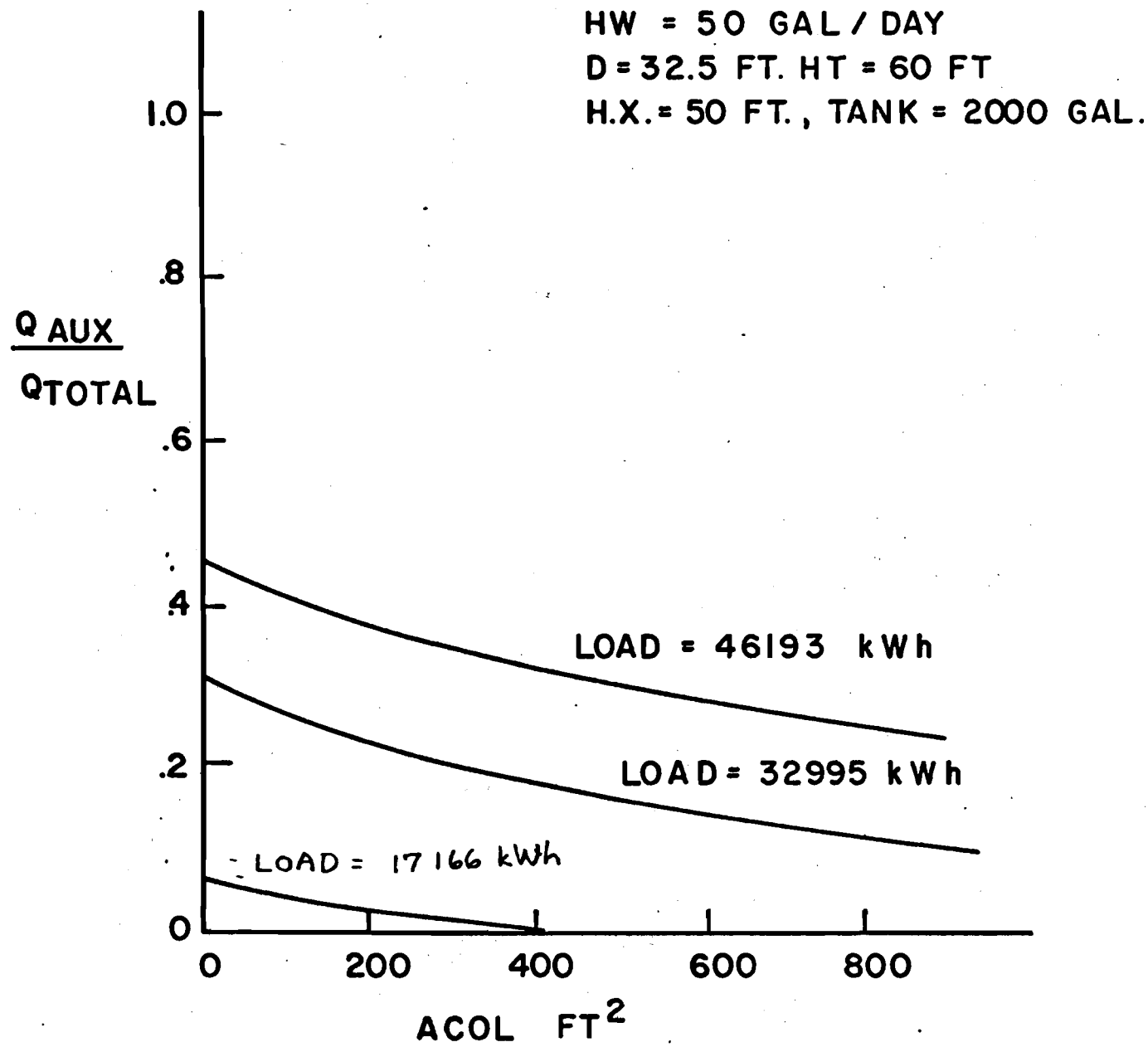
HW = 50 GAL / DAY
D = 32.5 FT. HT = 60 FT
H.X. = 50 FT., TANK = 2000 GAL.
1.0
.8
.6
.4
.2
0
Q AUX / QTOTAL
LOAD = 46193 kWh
LOAD = 32995 kWh
LOAD = 17166 kWh
0
200
400
600
800
ACOL FT²

FIG. 4.10

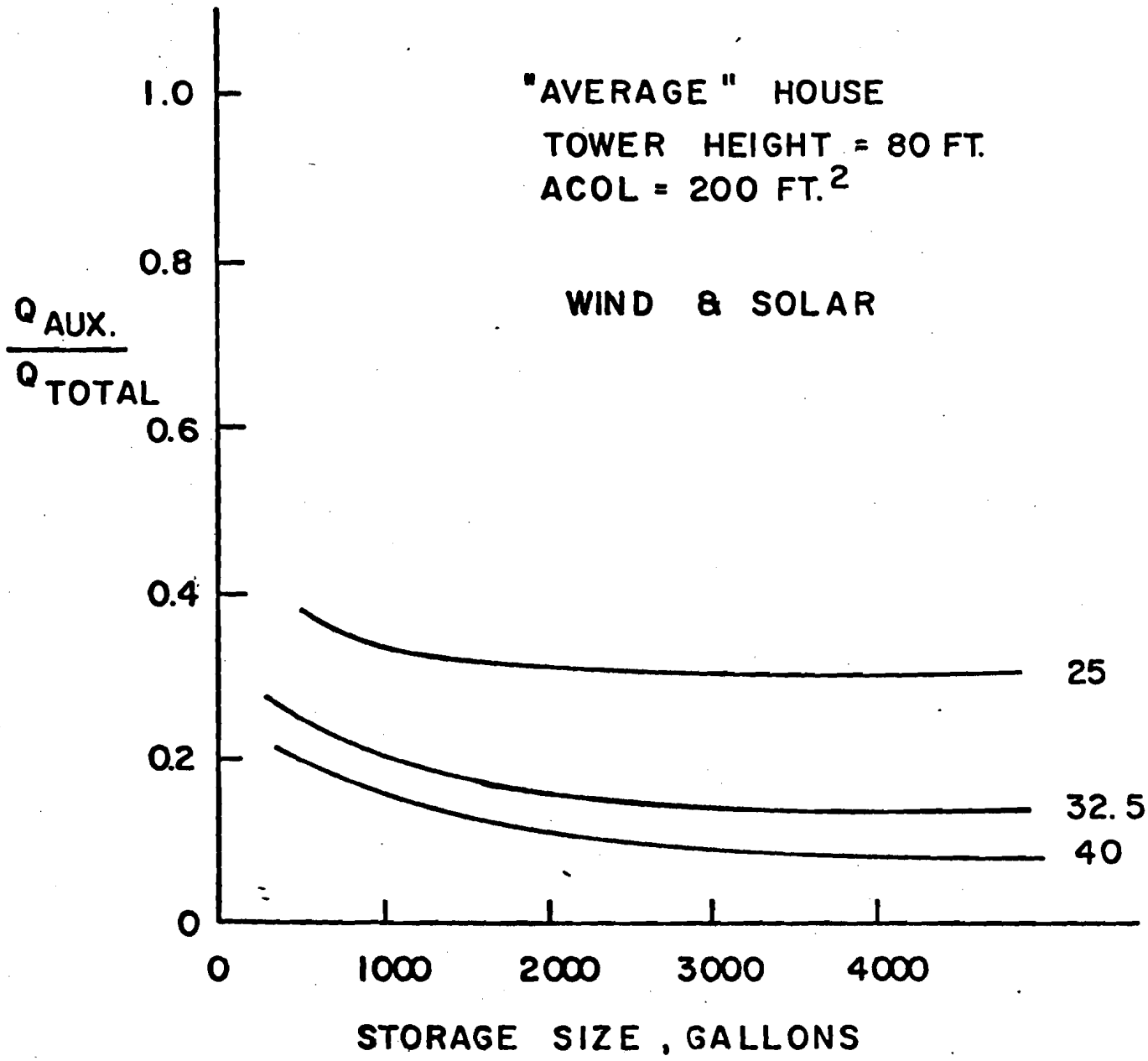
"AVERAGE" HOUSE
TOWER HEIGHT = 80 FT.
ACOL = 200 FT.2
WIND & SOLAR
Q AUX. / Q TOTAL
1.0
0.8
0.6
0.4
0.2
0
25
32.5
40
0
1000
2000
3000
4000
STORAGE SIZE, GALLONS

FIG. 4.11

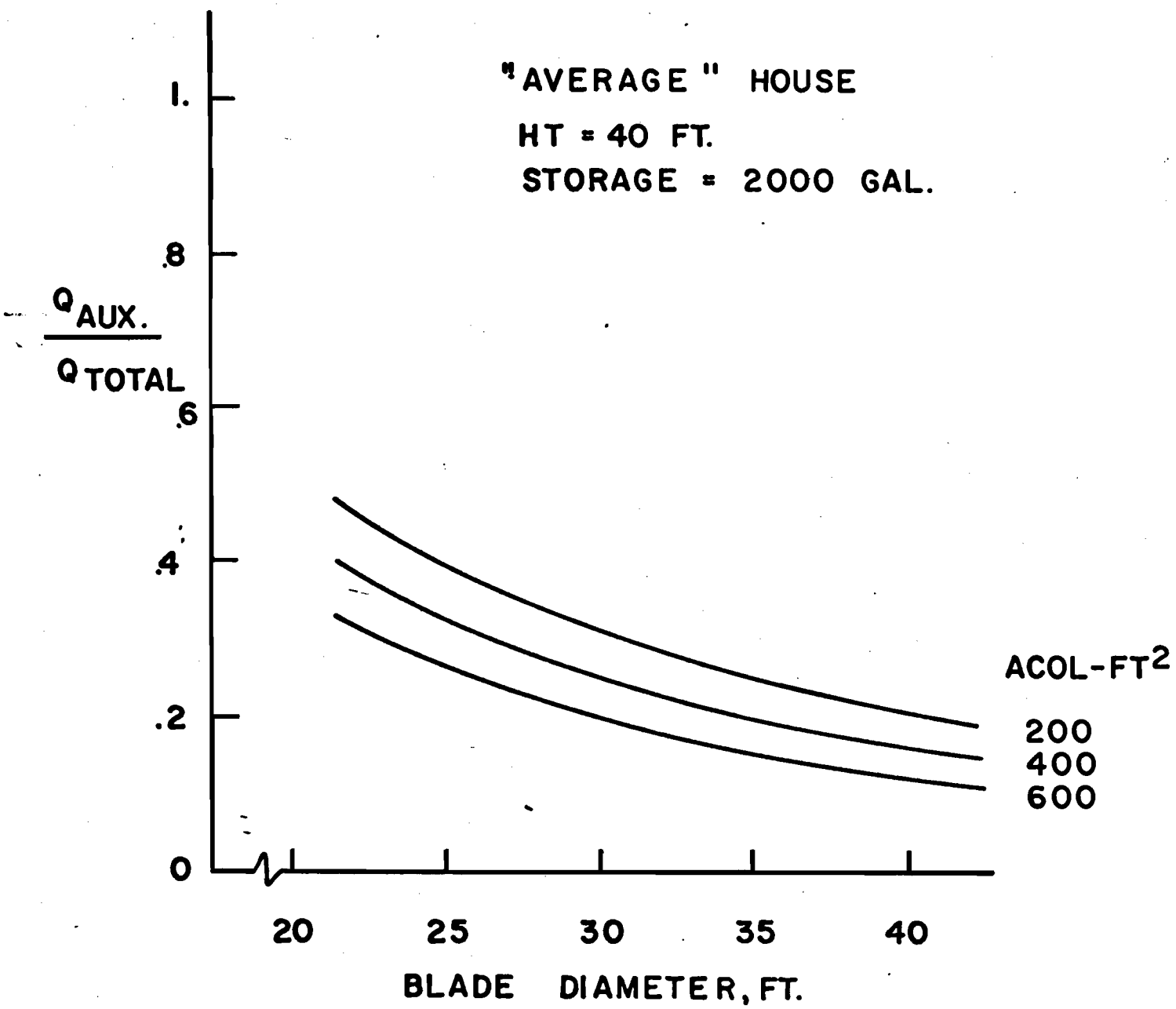
"AVERAGE" HOUSE
HT = 40 FT.
STORAGE = 2000 GAL.
Q AUX. / Q TOTAL
1.
.8
.6
.4
.2
0
ACOL-FT2
200
400
600
20
25
30
35
40
BLADE DIAMETER, FT.

FIG. 4.12

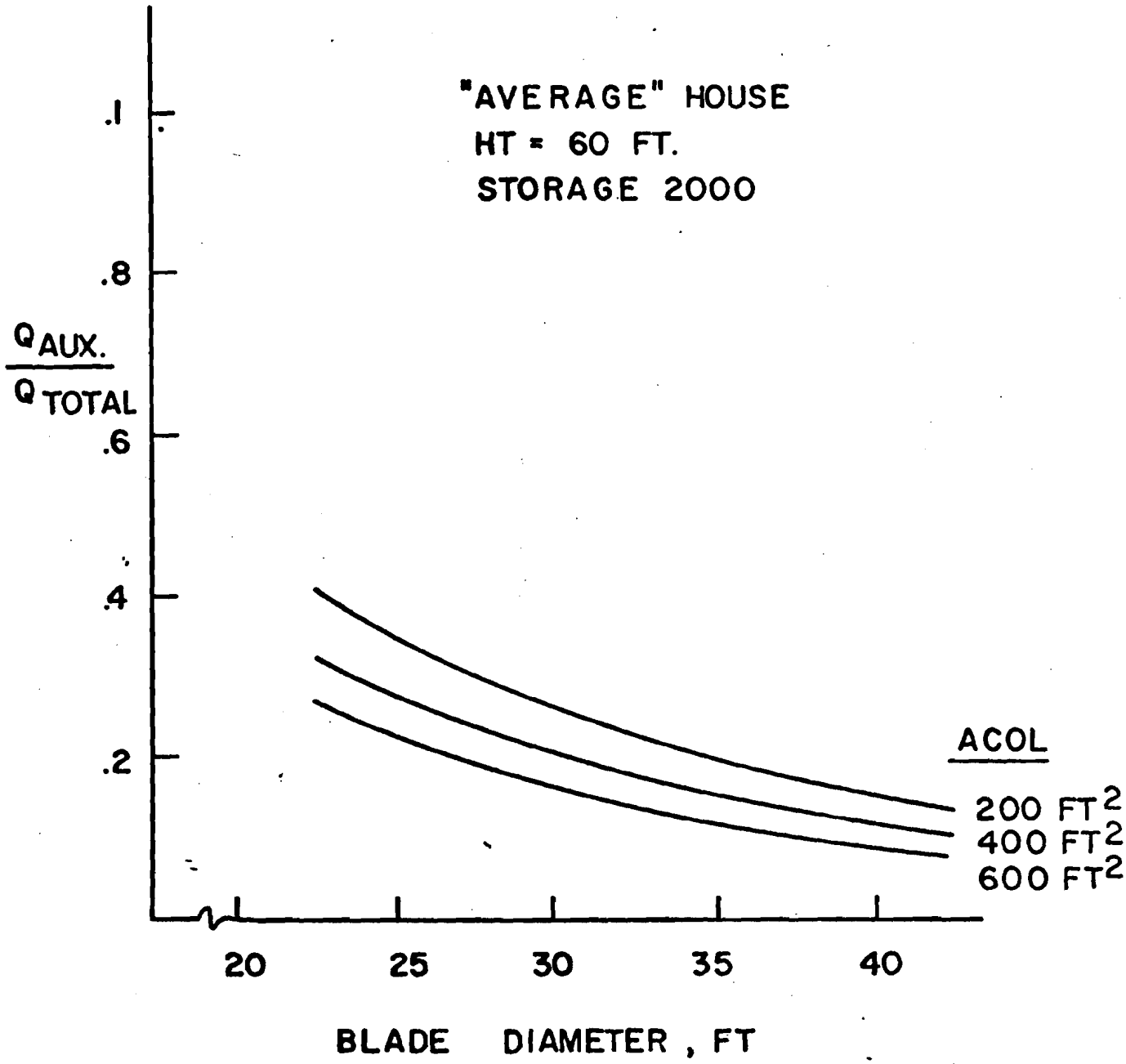
"AVERAGE" HOUSE
HT = 60 FT.
STORAGE 2000
.1
.8
.6
.4
.2
Q AUX. / Q TOTAL
ACOL
200 FT2
400 FT2
600 FT2
20
25
30
35
40
BLADE DIAMETER, FT

FIG. 4-13

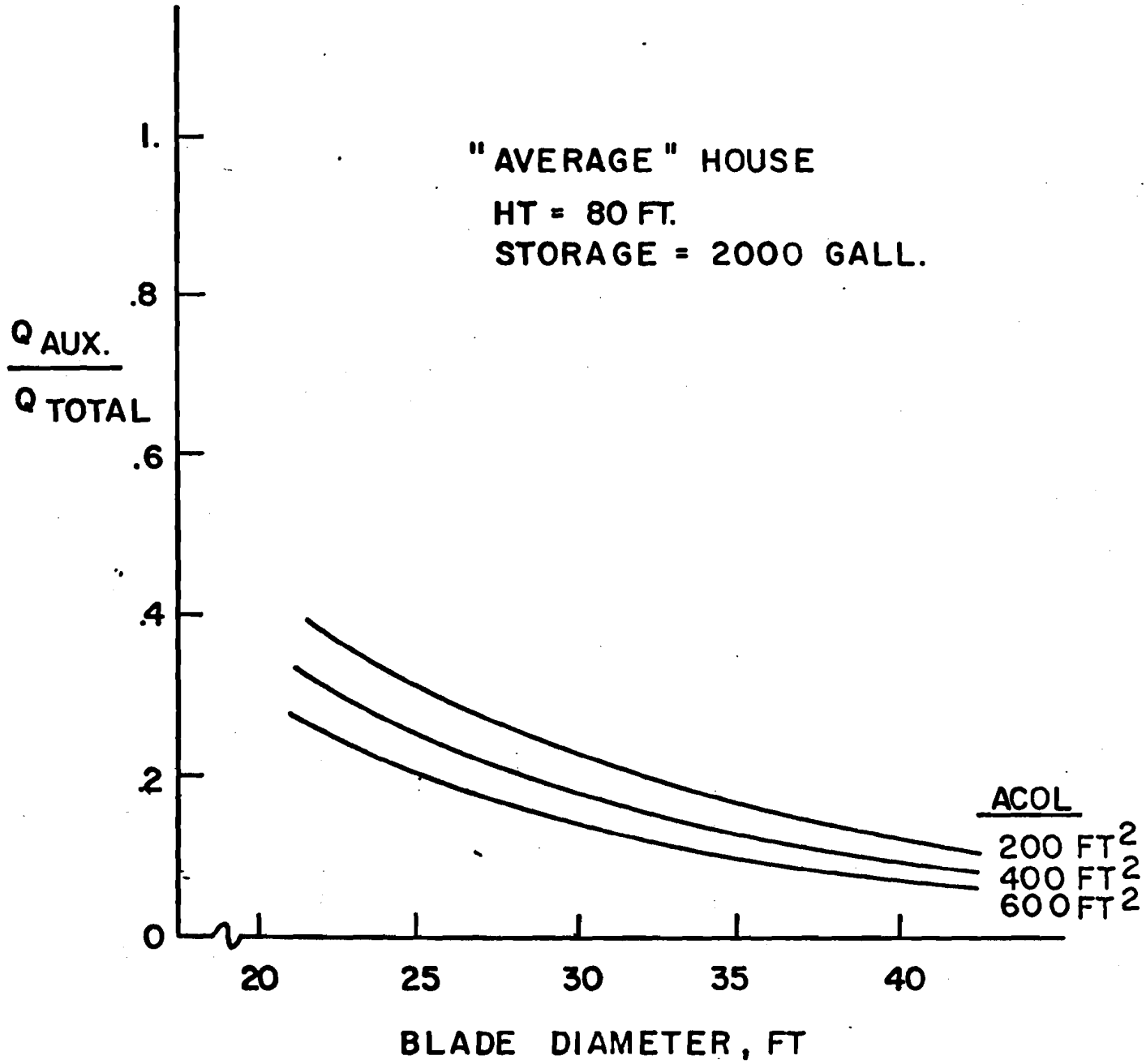
"AVERAGE" HOUSE
HT = 80 FT.
STORAGE = 2000 GALL.
Q AUX. / Q TOTAL
1.
.8
.6
.4
.2
0
20
25
30
35
40
BLADE DIAMETER, FT
ACOL
200 FT2
400 FT2
600 FT2

FIG. 4.14

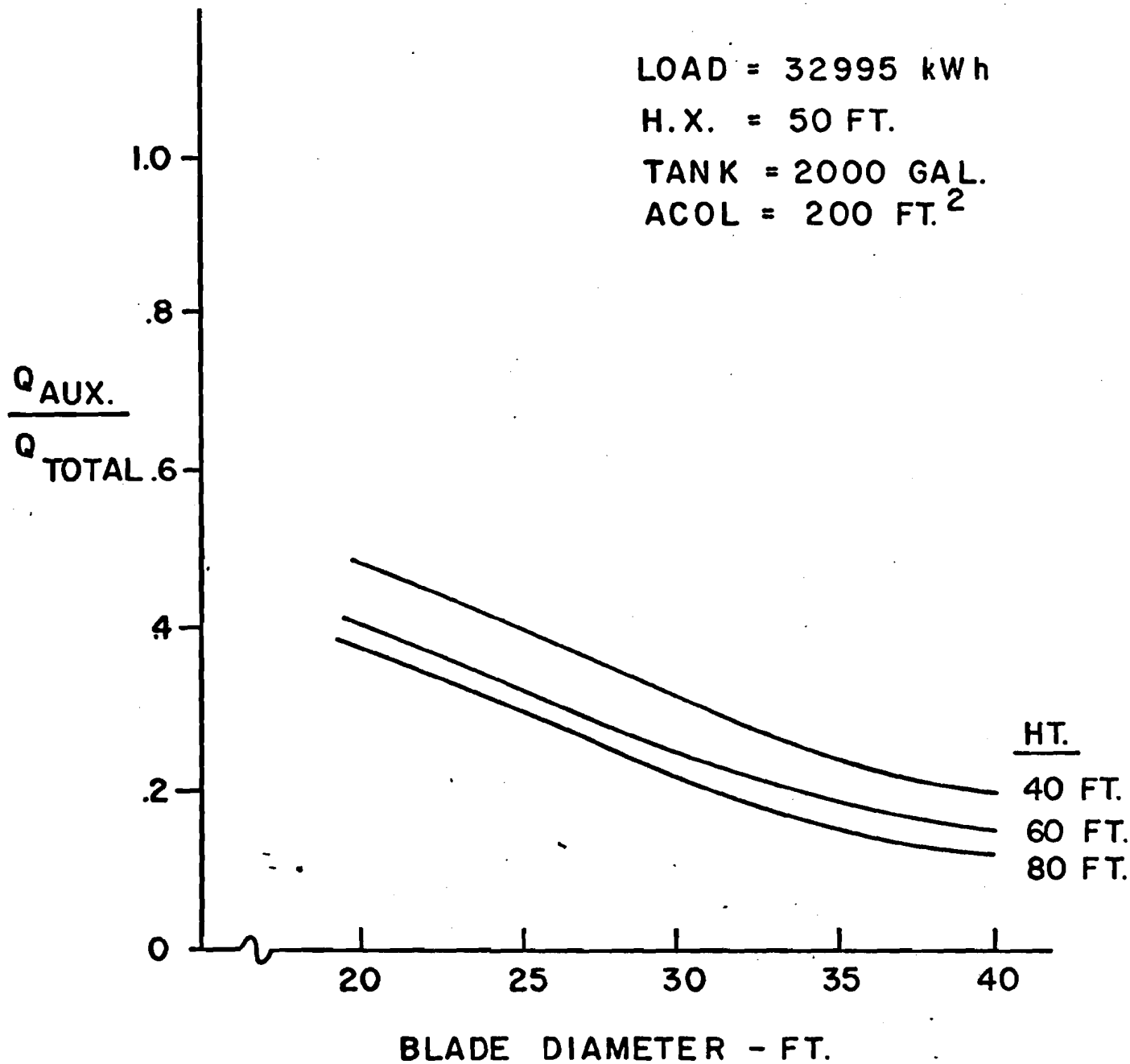
LOAD = 32995 kWh
H.X. = 50 FT.
TANK = 2000 GAL.
ACOL = 200 FT.2
1.0
.8
.6
.4
.2
0
Q AUX. / Q TOTAL
20
25
30
35
40
BLADE DIAMETER - FT.
HT.
40 FT.
60 FT.
80 FT.

FIG. 4.15

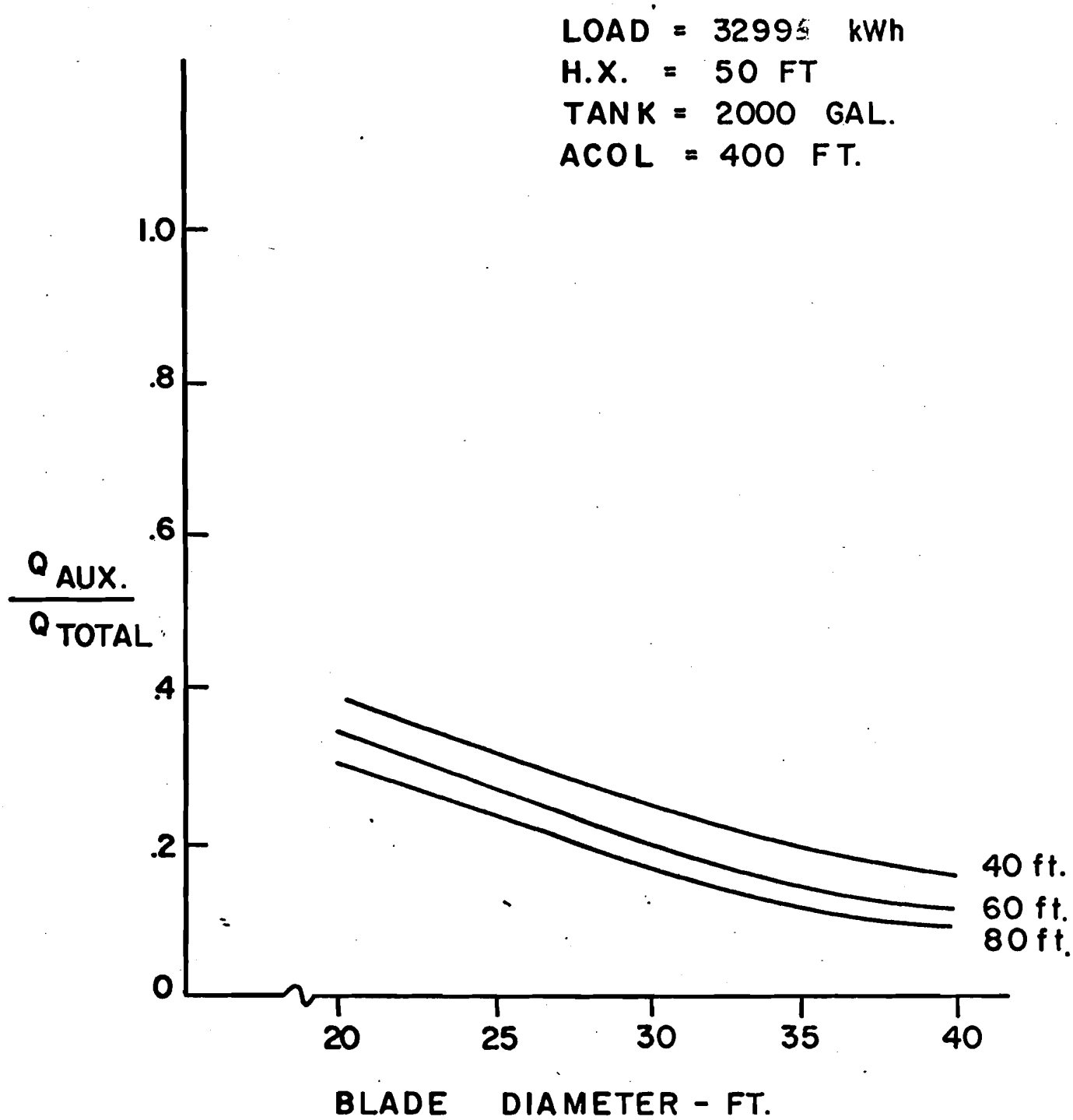
LOAD = 32995 kWh
H.X. = 50 FT
TANK = 2000 GAL.
ACOL = 400 FT.
1.0
.8
.6
.4
.2
0
Q AUX. / Q TOTAL
40 ft.
60 ft.
80 ft.
20
25
30
35
40
BLADE DIAMETER - FT.

FIG. 4.16

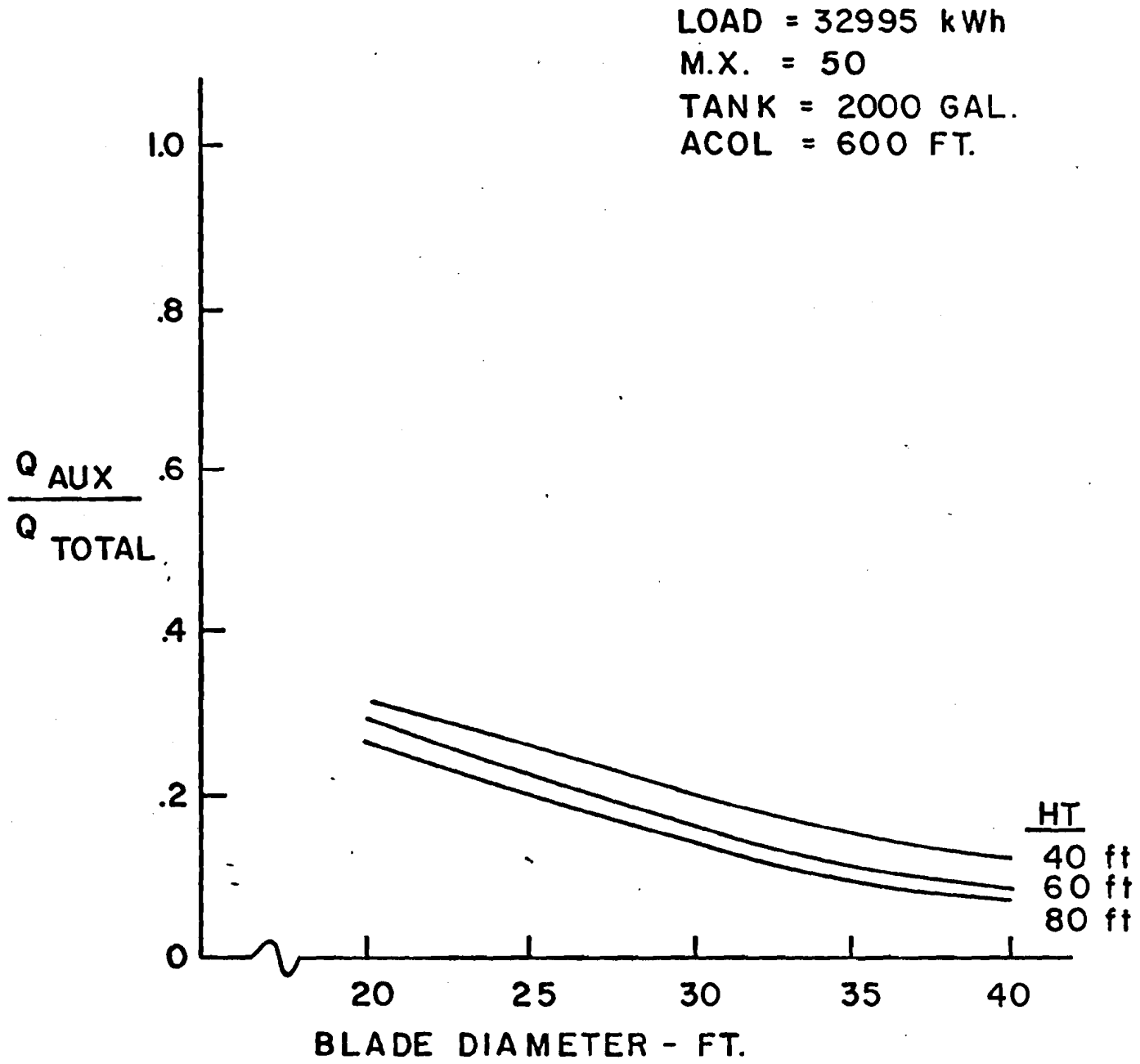
LOAD = 32995 kWh
M.X. = 50
TANK = 2000 GAL.
ACOL = 600 FT.
1.0
.8
.6
.4
.2
0
Q AUX / Q TOTAL
HT
40 ft
60 ft
80 ft
20
25
30
35
40
BLADE DIAMETER - FT.

Fig. 4.17

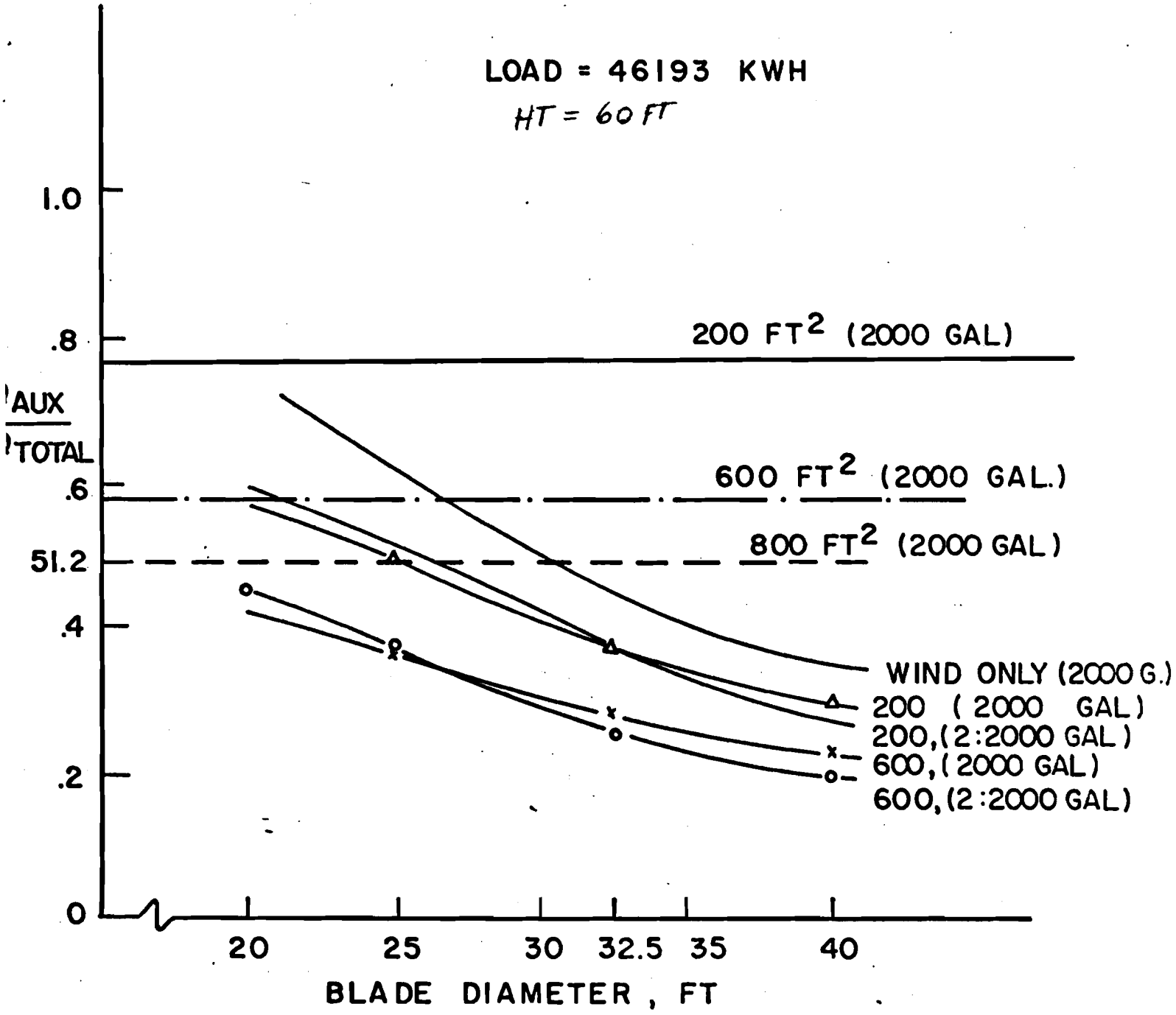
LOAD = 46193 KWH
HT = 60 FT
1.0
.8
.6
51.2
.4
.2
0
AUX / TOTAL
200 FT2 (2000 GAL)
600 FT2 (2000 GAL.)
800 FT2 (2000 GAL)
WIND ONLY (2000 G.)
200 (2000 GAL)
200,(2:2000 GAL)
600,(2000 GAL)
600,(2:2000 GAL)
20
25
30
32.5
35
40
BLADE DIAMETER, FT

FIG. 4.18

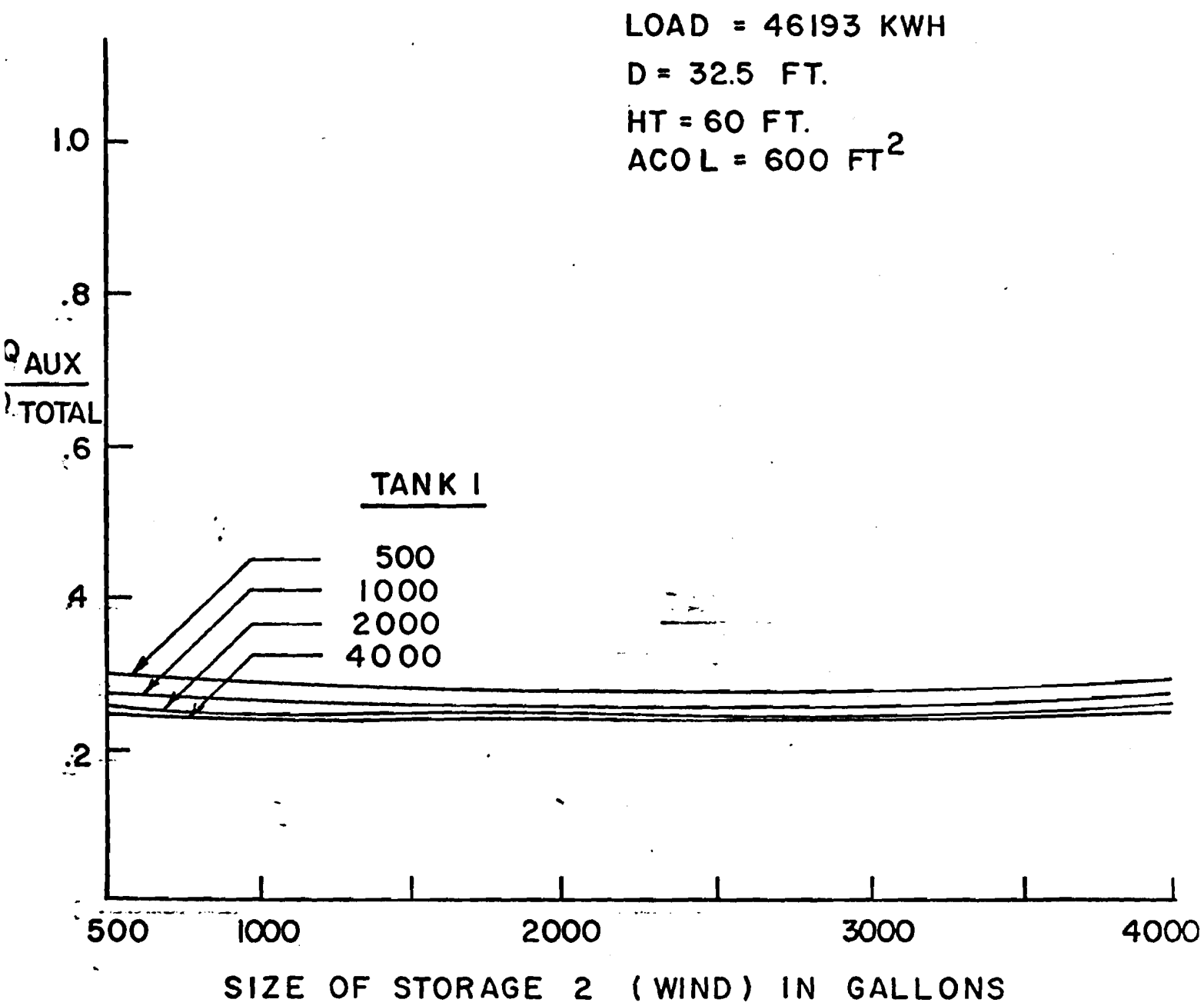
LOAD = 46193 KWH
D = 32.5 FT.
HT = 60 FT.
ACOL = 600 FT2
1.0
.8
.6
.4
.2
QAUX / QTOTAL
TANK I
500
1000
2000
4000
500
1000
2000
3000
4000
SIZE OF STORAGE 2 (WIND) IN GALLONS

FIG. 4.19

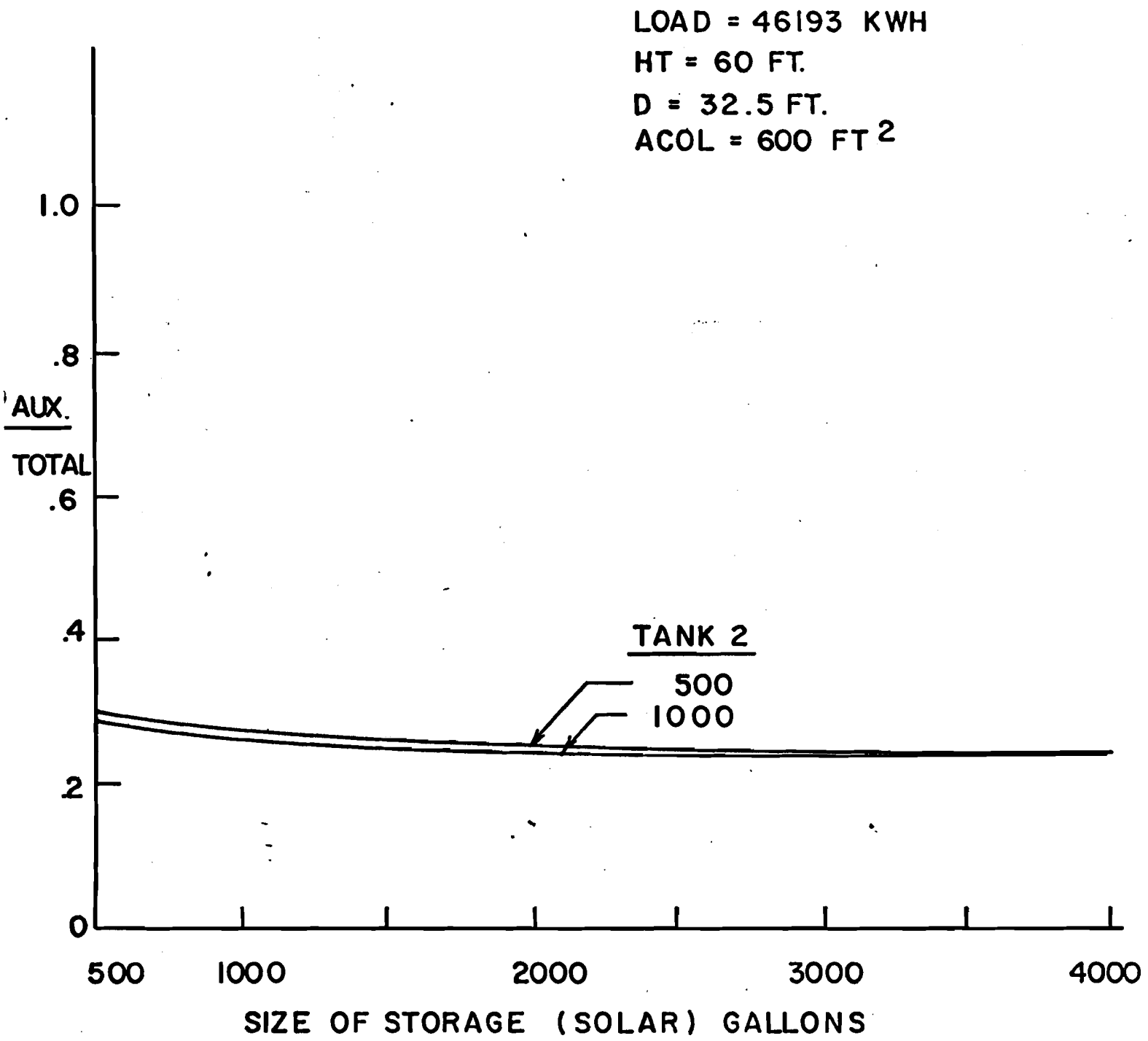
LOAD = 46193 KWH
HT = 60 FT.
D = 32.5 FT.
ACOL = 600 FT 2
1.0
.8
AUX.
TOTAL
.6
.4
.2
0
TANK 2
500
1000
500
1000
2000
3000
4000
SIZE OF STORAGE (SOLAR) GALLONS

FIG. 4.20

the important parameters that affect overall performance.

2. EXPERIMENTAL SYSTEM

Under this task of the work, the thermal systems group has designed and purchased all the components necessary for the simulation of systems 1-3 in SH-1. Previous quarterly reports have dealt with the details of the experimental system and will not be repeated here. During the summer of 1976, a complete technical report describing the background and final details of the experimental system will be completed.

At the present time, due to the shifting of available technicians to other phases of the project, the thermal subsystems (such as solar collectors, storage tanks, baseboard heaters, etc.) have not been completely installed (and tested) in SH-1. However, all the necessary equipment and preliminary instrumentation has been obtained and is expected to be in operation (for experimental testing) by June of 1976.

UNIVERSITY OF MASSACHUSETTS/AMHERST
ENERGY ALTERNATIVES PROGRAM

UNIVERSITY OF MASSACHUSETTS/AMHERST

ENERGY ALTERNATIVES PROGRAM

Preliminary Report

WIND DATA COLLECTION AND ANALYSIS

WIND FURNACE PROJECT

by

Frank C. Kaminsky

U.Mass. Wind Furnace
Energy Alternatives Program
University of Massachusetts
Amherst, Massachusetts 01002

TR76/8
Appendix X

Wind Data Collection and Analysis

The overall objective of this portion of the research effort is the development of statistical models and computer software that can be used in estimating the productivity of alternative types of wind-driven generators proposed for a given location. These models and computer programs are being developed and tested using wind data from the New England area and design data from several sources: The UMass wind-driven generators being constructed and proposed as part of the total research effort in the development of a wind furnace; alternative wind-driven generators being constructed and proposed by NASA; and commercially available generating systems from Dunlite, Australia, Elecktro, Switzerland and Aero Power, U.S.A. The work in this portion of the research effort is progressing on schedule and is summarized below in two parts. The first describes the data collection sites that have been established and the second describes the effort that has been directed toward the development of statistical models and computer software.

Part I: Data Collection Sites

Using equipment funds from the wind furnace grant and additional funds from other sources, four data collection sites have been established in the vicinity of the University of Massachusetts/Amherst. These sites have been operating continuously since the Summer of 1975 and will provide hourly wind speed data that serves as input to computer simulation programs for evaluating the performance of the wind furnace. These sites are located in the towns of Leyden, Northfield, Shelburne and

Amherst, Massachusetts. Except for the Amherst site, continuous chart-paper recording systems have been installed with anemometer amps located on towers and/or telescopic masts. At the Amherst site, average wind speed is recorded at half-hour intervals using a transmission line and a mechanical paper punch. The result is a paper tape that can be input to the time sharing system at the University. Since the anemometer cups for this system are located at the site of the home which is being constructed as part of this research effort, this input will provide a means of evaluating and comparing the simulated performance of the wind furnace to the actual performance.

Four other data sites have been established through a cooperative effort between the research team and private individuals also concerned with the development of windpower systems. These individuals, Mr. R. Blazej, Grassy Brook Village, Newfane, Vermont; Mr. D. Lawrence, Barnstable Harbor, Barnstable, Massachusetts; Mr. F. Harvey, Mt. Equinox, Sky Line Drive, Vermont; and Mr. G. Leary, Holyoke Gas and Electric, have provided funds and, with assistance from the research team at the University of Massachusetts, have established data collection sites. These sites have been operating continuously since the Fall of 1975 and will provide additional data for evaluating the performance of the wind furnace.

In addition to the eight sites mentioned above, additional data has been secured through the generosity of Brookhaven National Labs, Long Island, New York. This data, hourly wind speed taken simultaneously at six different heights (from 37 ft. to 400 ft.) for two years, will provide the basis for several statistical studies that are being conducted.

Through the effort of several undergraduate students at UMass, the data from all sites is being analyzed on a monthly basis. A solid data

base will be available, eventually, to evaluate the performance of alternative designs for the wind furnace in different contexts, namely, hilltop locations, coastal areas and valley location.

Part II: Statistical Models and Computer Software

Several computer programs have been developed to assist in the analysis of wind data. Although these programs will be used primarily in the evaluation of wind-driven generators under construction and being proposed by researchers at UMass/Amherst, every attempt has been made to make all computer programs sufficiently general for widespread use. Since many of the computer programs are lengthy, they will not be included as part of this progress report. Only a description of the program will be provided. All programs have been written in the Fortran language and are currently being processed using the Control Data Cyber 70-4 at UMass/Amherst. The automatic plotter associated with this system is used extensively to save time and effort. Each computer program is described briefly below.

Program I

This program produces a velocity-duration curve for input data in the form of hourly wind speed or in the form of a histogram of hourly wind speed.

Program II

This program produces both a velocity-duration curve and a power-duration curve for either hourly wind speed data or a histogram of hourly wind speed data. The user of this program specifies the power output curve of the wind-driven generator under consideration in either a functional form or as a series of piecewise linear approximation.

Program III

This program provides the user with estimates of the parameters of three probability density functions that can be used to model average hourly wind speed over a specified period of time. The gamma, log-normal and the Weibull density functions are used as probability models. The program then produces a velocity duration curve of the input data and displays the "goodness of fit" of each model. This program provides the basis for production of power-duration curves using the three mathematical models.

Program IV

This program provides an interactive time sharing simulator for evaluating different wind-driven generators in a specified wind field. In a manner similar to that used in Program II, the user describes the power output curve of the wind-driven generator in either functional form or by a series of piecewise linear approximations. The program then operates the wind generator hour-by-hour using a data file created by the user. The energy produced on a daily basis is then provided along with a monthly summary. With this program, the performance of numerous wind-driven generators can be evaluated rapidly for a specific location.

In addition to the development of computer software for the analysis and processing of wind data statistical studies are being conducted in three areas:

1. Development of confidence intervals for power duration curves.
2. Analysis of appropriate probability density functions for describing the length of calm periods, productive periods, and furling periods.
3. Development of mathematical procedures for producing velocity-duration curves at specified heights using a histogram of wind

data that is mixed. Mixed data occurs where a portion of the frequencies were recorded at one height and another at a second height, etc.

A paper describing the results obtained in the third area described above is currently in process and will be available shortly. The first two areas described above are under examination and results will be described as they become available.

UNIVERSITY OF MASSACHUSETTS/AMHERST
ENERGY ALTERNATIVES PROGRAM

UNIVERSITY OF MASSACHUSETTS/AMHERST

ENERGY ALTERNATIVES PROGRAM

DYNAMICS OF NEW ENGLAND WIND FURNACE

by

Merit P. White

U.Mass. Wind Furnace
Energy Alternatives Program
University of Massachusetts
Amherst, Massachusetts 01002

TR/76/9
Appendix XI

DYNAMICS OF NEW ENGLAND WIND FURNACE

The frequencies and shapes of the lower modes of vibration of the structure and generator system have been calculated. The principal dynamic loads have been analyzed and their interactions with the vibration modes estimated. The result can be represented diagramatically as a matrix of columns (modes of response) and rows (loadings).

General remarks

The extent to which a particular mode of vibration will be excited by a particular loading system depends primarily on the following factors:

1. Load magnitude
2. Degree of coupling between the exciting mechanism and the modal response. Basically, the exciting force must be capable of doing positive work during a cycle of motion. For example, an external force acting on a point of the structure which has a component of motion parallel to the force does work and can add energy to the system while the system moves.
3. Resonance: in the case of a periodic force the relation between its frequency and that of the modal response is important, the closer the agreement the greater is the rate of doing work on the system.
4. System damping or the ability to dissipate vibrational energy compared to the rate at which energy is supplied. A steady state constant amplitude condition is reached when the two rates are equal - work done per unit time equals mechanical energy lost per unit time.

The structural system of the Windpower Furnace as currently designed does not contain any significant damping or energy dissipating capability. If it turns out to be necessary, such mechanisms (damping devices) can be installed in appropriate locations. This should be avoided if possible because of costs of such units and also the necessity of maintaining them over the life of the system. A better solution for undesirable vibrations is to avoid resonances between loadings and system vibrations, perhaps by changing stiffnesses or weights of components.

Modes of Vibration Considered

1. Vertical displacement: The foot of the 10" steel pipe tower maintains contact with its base support due to the weight of the whole system combined with the vertical component of the 3000-lb force in each of the four steel-rope guys. The steel pipe and the generator unit have a combined weight of 4900 lbs. Thus the total base compression is about 16,000 lbs and this is the maximum value of a vertical dynamic oscillation force that will not cause uplift. A more severe vibration will produce uplift and the result will be a large energy dissipation due to repeated impacts at the base. A vertical vibration mode can be produced by a vertical dynamic loading, for example due to blade unbalance. The extreme case occurs if a blade is lost during rotation. The centrifugal force in that situation is

$$F = W r \omega^2/g$$

where W = blade weight, r = distance of its center of gravity from the spin axis, ω the angular velocity in radians/second, and g = gravity acceleration. At the maximum expected RPM, W = 77 lb, r = 4', ω = 17.5

and g = 32.2. Then,

$$F = 3000 \text{ lb}$$

F has a period T = 0.36 sec. At lower speeds the dynamic force is reduced and the period lengthened.

2A-2B. Axial (horizontal) displacement of the generator unit combined with pitching about a horizontal transverse axis: This mode causes flexure of the supporting pipe and changes of length of the guys. Two modes have been calculated: the lower is primarily translation with small pitching angles and has a period of 0.7 second. The second is primarily pitching with small translations and has a period of 0.05 seconds.

3A-3B. Lateral translation combined with rocking about the longitudinal axis: There are two modes calculated, the first is primarily translation with a period of 0.7 seconds, the second is primarily rocking with a period of 0.03 seconds.

4A-4B. Torsional (about a vertical axis coinciding with the support axis): Two conditions have been considered: in the first, the base of the supporting pipe is not restrained in torsion and the only torsional restraint in the system is furnished by the guys. This mode has a period of 1.66 seconds. If the base of the support is restrained in torsion the period becomes 0.12-0.15 seconds. In each case, the generator unit is assumed to be rigidly fixed by a brake to the supporting mast. Of course, during operation the generator unit is not so restrained and there is no torsional or rotational mode of vibration.

5. Airfoil flexure: Time dependent airfoil loads will cause the airfoil to deflect, mainly in its weakest direction which is roughly parallel to the spin axis of the system. This is an important design

consideration since it determines how much clearance between the airfoil disc and the support system - steel pipe and guys - has to be left for this bending deformation. The smaller the flexure allowance of the airfoil blades the higher can be the point of attachment of the guys to the supporting pipe. The higher that attachment the stiffer and stronger is the system as a whole, which is advantageous. The flexural frequency of each blade is estimated, from measurements on a simply supported blade, to be about 3 - 4 cycles per second when cantilevered at the hub.

Dynamic Loads

1. Blade unbalance: Differences in weight or geometry of individual blades can give rise to unbalanced centrifugal forces normal to the rotating shaft acting at the hub. This force vector rotates with the turning shaft. Besides producing bending stresses in the shaft this force can also initiate oscillation in Modes 1, 2B, 3A, 3B, 4A (or 4B). The extreme case is, of course, that in which a blade is lost.

2. Wind gradient and tower shadow: During a rotation each blade passes through a cycle of different wind velocities. The wind gradient results from the ground drag which normally results in increasing wind speeds with elevation. Tower shadow is due to interference of the supporting pipe with the airflow. The resulting lift force on each blade is a periodic force so that the combined loading due to all three blades acted on by the wind is a periodic force more or less parallel to the spin axis and a periodic couple about a horizontal axis normal to the spin axis. Both have the same frequency, three times the rotational frequency of the shaft. The effect of this loading is to cause horizontal

oscillations parallel to the spin axis and angular oscillations about a horizontal axis through the mass center and normal to the spin axis.

3. Gusts and turbulence: These give rise to non-periodic forces acting on the blades more or less parallel to the spin axis. There would also be some loading of the generator unit. The blades and tower have to be designed for peak gust loads. There is unlikely to be any periodic response of the system.

4. Gyroscopic-Coriolis Forces: These result from simultaneous rotations about two perpendicular axes, in this case the spin ω of the shaft, rotor, and blade assembly on the one hand, coinciding with a rotation Ω of the entire system about its vertical axis, due to a change of wind direction. For an ω corresponding to 167 rpm and a reasonable value of Ω, for example 1 rpm (= 0.1 rad/sec), the Coriolis acceleration at the tip of a blade is small, about 2g. The gyroscopic couple of the whole rotor, shaft, etc. is

$$C = I\omega\Omega$$

where I is the mass moment of inertia about the shaft axis.

For all periodic loadings the periods or ranges of periods have been calculated. There has been no attempt to predict modal responses caused by the expected loads since the result of any such calculation is expected to be highly undependable. When the system is in operation, observations will indicate which of the modes are excited and to what extent. If curative measures are needed, they will be facilitated by knowing which of the dynamic loadings may be causing the trouble.

The following table shows (horizontally) the various modes of response and (vertically) the several dynamic loading mechanisms - both with their

periods or frequencies. The squares with + correspond to a possible model excitement by a particular load. An ++ indicates a probable state of excitation.

MODAL RESPONSES OF NEWF

DYNAMIC LOADS	1 Vertical (Z) T=0.025 f=40	2A Axial Translation (X) + Pitching (Y) T=0.7 f=1.5	2B Pitching (Y) + Translation (X) T=0.05 f=20	3A Lateral Translation (Y) + Rocking (X) T=0.7 f=1.5	3B Rocking (X) + Lateral Translation (Y) T=0.03 f=30	4A Rotation (Z) Base of Mast free T=1.66 f=0.6	4B Rotation (Z) Base of Mast fixed T=0.12 f=8	5 Flexure of Blade f ~ 3-4
Blade out of balance (or lost) f=rps $\leq$ 3 T $\geq$ 0.33	+		+	+		+	+	
Wind Velocity Gradient or Mast Shadow f=3xrps $\leq$ 9 T $\geq$ 0.1		++	+	++	+			+
Gusts and turbulence		++	+	+	+			+
Gyroscopic and Coriolia forces f <<		+	+					+

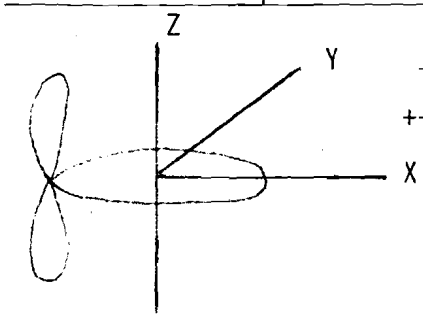

+ = Possible Excitation

++ = Probable Excitation